Title
Exploring Self-Assembly and Photomechanical Switching Properties of Molecules at Surfaces

Author
Cho, Jongweon

Publication Date
2010

Peer reviewed|Thesis/dissertation

Exploring Self-Assembly and Photomechanical Switching Properties of Molecules at Surfaces

by

Jongweon Cho

A dissertation submitted in partial satisfaction of the

requirements for the degree of

Doctor of Philosophy

in

Physics

in the

Graduate Division

of the

University of California, Berkeley

Committee in charge:

Professor Michael F. Crommie, Chair
Professor Zi Qiang Qiu
Professor Peidong Yang

Spring 2010

Exploring Self-Assembly and Photomechanical Switching Properties of Molecules at Surfaces

by

Jongweon Cho

Abstract

Exploring Self-Assembly and Photomechanical Switching Properties of Molecules at Surfaces

by

Jongweon Cho

Doctor of Philosophy in Physics

University of California, Berkeley

Professor Michael F. Crommie, Chair

The possible reduction of functional devices to molecular length scales provides many exciting possibilities for enhanced speed, device density, and new functionality. Optical actuation of nanomechanical systems through the conversion of light to mechanical motion is particularly desirable because it promises reversible, ultra-fast, remote operation. Past studies in this area have mainly focused on solution-based molecular machine ensembles, but surface-bound photomechanical molecules are expected to be important for future applications in molecular machines, molecular electronics, and functional surfaces. Cryogenic ultra-high-vacuum scanning tunneling microscopy has been employed to study the surface-based photomechanical switching properties of a promising class of photomechanical molecule called azobenzene.

In the case of tetra-*tert*-butyl-functionalized azobenzene (TTB-AB) molecules adsorbed on Au(111) reversible switching by means of ultraviolet and visible excitation is experimentally observed at the single-molecule level. The presence of the metallic surface leads to a significant change of the molecular photoswitching properties: (i) photoswitching cross section is significantly reduced compared to the molecules in solution environment, (ii) photoswitching directionality is strongly affected. (iii) correlation between molecular ordering, electronic structure, and photoswitching capability is observed. (iv) new photoswitching dynamical mechanisms become operative.

The results presented in this thesis provide insight into our understanding of photoswitching and adsorption properties of surface-bound molecules and elucidate the important role of molecule-surface interactions and molecule-molecule interactions.

Contents

List of Figures

List of Tables

Acknowledgements

First and foremost, I would like to express my profound gratitude to my advisor, Professor Mike Crommie. The creativity, enthusiasm, and scientific intensity that he demonstrates made graduate work at Berkeley the rewarding experience it was. I would also like to thank Professors Zi Qiang Qiu and Peidong Yang for serving on my Dissertation Committee.

The Crommie group, past and present, has always provided a great diversity of individuals to work. In particular I would like to thank those who I closely worked with, postdoctoral fellows Luis Berbil-Batista, Armen Kirakosian, grad students Matt Comstock, Niv Levy, Ivan Pechenezhskiy for numerous helpful discussions. I would also like to acknowledge some other members in the Crommie group, Victor Brar, Sarah Burke, Yen-Chia Chen, Régis Decker, Lorenzo Flores, Mike Grobis, Xinghua Lu, Kacey Meaker, Giang Nguyen, Melissa Panlasigui, Chenggang Tao, Andre Wachowiak, Yang Wang, Yayu Wang, Daniel Wegner, Ryan Yamachika, Yossi Yayon, Travis Zack, Xiaowei Zhang, and Yuanbo Zhang for the memorable time that we spent together at Berkeley.

I am thankful to the members of the Fréchet group, the Louie group, the Grossman group, and the Vollhardt group for many stimulating conversations and refreshing perspectives: Daniel Poulsen, Frank Lauterwasser, Carine Edder, David Strubbe, Emmanouil Kioupakis, Yosuke Kanai, Varadharajan Srinivasan, and Steven Meier.

Last but not least, I would like to thank my family and friends for their love and support during these years. In particular I would like to thank my lovely wife Soomi, my cute baby Eunsoo (Justin), my father Youngchun, my father-in-law Hojeong, my mother-in-law Yangsoon, and my brother Junwon. None of the presented works would have been possible without them. Special thanks to Pauline Iliff and Jenny White, who made my days at Berkeley enjoyable.

This dissertation is dedicated to my late mother Oklang, who had shown her everlasting support through my life.

Part I

Introduction

Chapter 1

Surface-bound Molecular Photomechanical Coupling

1.1 Light-driven Nanomechanical Devices on the Molecular Level

The miniaturization of components in functional devices in industry is currently pursued by top-down fabrication. Future miniaturization will soon advance into regimes where the bulk properties no longer dominate but rather surface and quantum effects become more important [1]. In response to this, much current research attention has focused on the bottom-up approach. One promising avenue here is to use molecules to build up nanoscale devices and machines at the molecular level [2, 3, 4, 5]. A molecular machine is defined as an assembly of molecules (or even a single molecule) that perform mechanical (machine-like) movement (output) as a result of external stimuli (input) [4].

Using external stimuli to control functional molecular properties via conformational changes is a fundamental concept in nature. In many biological systems specific functions are based on the cooperation of individual molecular units which are enabled and controlled by well-defined changes in molecular geometry. One example is the light-induced *cis*-to-*trans* isomerization of retinal chromophore in rhodopsin, which plays an important role in the human vision process [6].

Such switching processes between different molecular conformational states provide exciting opportunities for possible practical applications in the field of molecular electronics, molecular machines, and functional surfaces. The possibility to design molecules with specific functional properties opens the door for utilization of molecules as building blocks for integrated functional nanoscale devices [7]. However, for future applications it is essential to control molecular switching and to connect molecular systems to non-molecular bulk materials. The central challenge is coupling external excitations efficiently to surface-bound molecules without losing their inherent functionality. This requires understanding structural and electronic properties including the interaction with solid interfaces and controlling the

switching between different molecular conformations by external stimuli.

Various external stimuli, such as temperature, electrons, light, and electric field, can be applied to induce molecular switching [8]. In particular, using light to control molecular conformational states offers great possibilities of reversible, remote, and ultrafast operation of molecular devices.

Photochromic switches form an elegant example of molecules with an intrinsic switching mechanism. Photochromism is the reversible structural transformation of a chemical species between two different geometries, where two forms have different absorption properties [9]. The different electronic and optical properties of the two isomers may enable the control of the molecular conformation by means of photoirradiation. The photochromic phenomenon is observed in several classes of molecular systems including azobenzenes, spiropyrans, fulgides, and diarylethenes [10]. In particular, azobenzene is promising because of its simple structure and reversible photoisomerization properties, and will be discussed at length in this thesis.

1.2 Introduction to Azobenzene

Azobenzene is a simple photoswitchable organic molecule that consists of two phenyl rings joined by two double-bonded nitrogen atoms, as shown in figure 1.1(a). Azobenzene has two isomeric configurations: nearly planar *trans* ("E" form) and non-planar *cis* ("Z" form). The ground electronic state of the azobenzene is the *trans* isomer, and the *cis* isomer is 0.6 eV higher in energy than *trans*. The energy barrier from *trans* to *cis* is found experimentally to be about 1.6 eV [11], and the activation barrier from *cis* to *trans* is ∼1 eV.

Azobenzene can be reversibly actuated between two conformational states in solution under UV (≈365 nm; 3.4 eV) and blue light (≈420 nm; 2.95 eV) exposure, so-called *cis-trans*

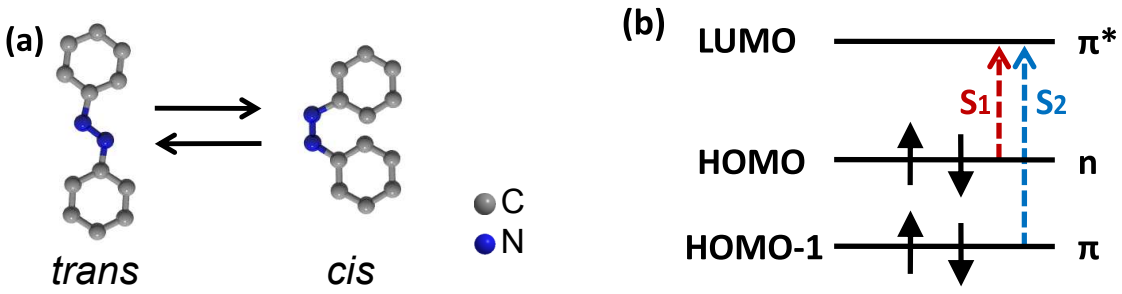

Figure 1.1: (a) Azobenzene *cis-trans* photoisomerization and (b) electronic structure. Electron spin configuration (black arrows) denotes the electronic ground state (S_0). Red and blue arrows denote the electronic excitation from S_0 to S_1 (first excited state) and to S_2 (second excited state), respectively.

photoisomerization. The two isomers exhibit different absorption spectra in solution. The *trans*-azobenzene typically shows an intense absorption band in the near-UV region and a weak band in the visible region. In conversion to the *cis*-azobenzene, the UV absorption resonance shifts to shorter wavelengths, and the intensity of visible absorption resonance increases noticeably.

The UV and visible optical absorption resonances of *trans*- and *cis*-azobenzene corresponds to the excitation of an electron from the azobenzene electronic ground state S_0 to either the first excited state (S_1) or second excited state (S_2), as shown in figure 1.1(b). The S_1 excited state, also referred to as the (n,π) state, results from an electronic transition from an occupied non-bonding nitrogen atom lone pair (n) to an unoccupied N-N anti-bonding π orbital (π^*). The S_2 excited state, also referred to as the (π,π^*) state, results from an electronic transition from an occupied N-N bonding π orbital (π) to an unoccupied N-N anti-bonding π orbital (π^*). Therefore, azobenzene is characterized by a low-lying S_1 (n,π^*)-state and a large energy gap between this and the next higher S_2 (π,π^*)-state [12].

Photoisomerization of azobenzene, where the molecule absorbs a photon and changes its conformation, is an important example of the coupling between electronic excitation by light and mechanical degrees of freedom of the molecule. The "electromechanical coupling" between the electronic structures of the molecule and molecular vibrations triggered by a photon absorption leads to a certain floppiness of the molecular structure allowing large scale molecular distortions. Upon photoisomerization, azobenzene exhibits a considerable length change from *trans* to *cis* by 30% of the *trans* length (2.5 Å, measured from the 4-4' positions of a single azobenzene molecule) [13]. This length change can be amplified from one derivative to another by different functionalization of the azobenzene unit.

Azobenzene derivatives have been used to construct photoswitchable devices in various molecular systems and environments for many years. Here a few important examples are illustrated: Hugel *et al.* showed that a nanoscale optomechanical device based on the conformation change of the azobenzene polymer can be designed [13]. Ichimura *et al.* reported that azobenzene photoisomerization can be used to produce light-driven motion of macroscopic liquid droplets on a flat solid surface [14]. Banghart *et al.* showed azobenzene-regulated ion channels can be controlled by light [15].

While azobenzene molecules undergo reversible photoisomerization in solution, this does not necessarily mean that the same reaction will take place when the molecules are adsorbed onto a surface. In the next section we will discuss how the presence of a surface influences azobenzene photoisomerization.

1.3 Proximity of a Surface on Azobenzene Photoswitching

While free molecules have discrete energy levels, the adsorption of molecules on a surface involves the formation of a molecule-surface bond. The molecule is then no longer free, and consequently its electronic and vibrational states may change. The molecular levels are

pinned to the surface electronic structure due to hybridization and charge transfer, resulting in substantial broadening of the molecular resonances. The modified electronic structure of the molecules results in a change in the optical absorption spectrum of the molecule.

Photochemistry of azobenzene molecules adsorbed at metallic surfaces is expected to be different from its counterpart in the gas phase and solution environment. Two fundamental aspects that have to be taken into account for the photochemistry of surface-bound molecules are (i) quenching and (ii) steric hindrance. The metal provides a continuum spectrum of excitations based on the creation of electron-hole pairs or excitation of phonons. These serve as a dominant channel for absorbing the energy of the molecular excitation, resulting in quenching of the excited state inhibiting the photoswitching process. At metal surfaces, electronic quenching is expected to lead to greatly reduced excited state lifetimes. In addition, since azobenzene undergoes a relatively large conformational change upon photoisomerization, the photoswitching process may be mechanically hindered due to geometrical confinement to the the surface (this can also alter the potential energy landscape of the excited state).

Since the metallic surface can absorb the photons and create electron-hole pairs, the surface may participate in electronic excitation and relaxation pathways. It may lead to effective quenching of electronic excitations [16] or open up new reaction pathways such as coupling to photoexcited surface charge carriers. The direct electronic excitation mechanism, the most commonly believed mechanism for molecules in the gas phase and solution, may not be operative for adsorbed molecules due to much smaller cross sections [17].

In the next two sections we will discuss the excitation mechanism and dynamics associated with azobenzene photoisomerization.

1.4 Azobenzene Photoisomerization: Excitation Mechanism

When it comes to the photoisomerization of the azobenzene derivatives in solution, the photoswitching excitation mechanism is well understood based on the inherent molecular optical absorption properties.

The situation changes when the molecules are attached to a surface. When light is irradiated onto molecules adsorbed to a metallic surface, three conceptually different excitation mechanisms can be considered, separately or in concert [17]: (i) direct intramolecular excitation, (ii) surface excitation, (iii) thermal excitation.

In direct intramolecular excitation, the photon absorption occurs within the adsorbed molecule via a direct optical transition between the highest occupied (HOMO) and the lowest unoccupied molecular orbital (LUMO). The electronically excited states of the molecule involved in this excitation mechanism follow Franck-Condon transition rules. Once excited, the molecule then evolves in the excited state, prior to de-excitation to the ground state via a downward Franck-Condon transition. If the excited state lifetime is sufficiently long, then photoswitching takes place (assuming no other constraints such as steric hindrance

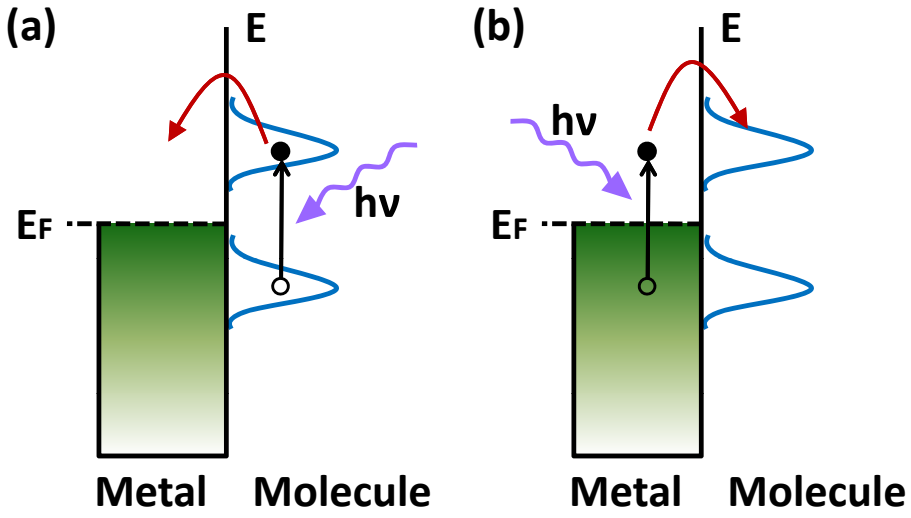

Figure 1.2: Schematic view of the energy diagram for the surface photochemistry. The metal Fermi level is denoted E_{F}which lies between HOMO and LUMO of the molecule. (a) Direct intramolecular excitation followed by quenching of the excited state due to the coupling between the molecule and surface; (b) Surface excitation leads to the photo-excited charge carrier transfer from the surface to the adsorbed molecule.

exist). Note that this mechanism is operative in the photoswitching of free molecules. Figure 1.2(a) depicts direct excitation followed by quenching of the excited state due to the molecule-surface interaction.

In surface excitation, the photon absorption occurs in the surface. The electronically excited state is reached via charge transfer of the photo-excited charge carriers to the molecules or energy transfer during resonant electron scattering processes. The excited state lifetime and the steric hindrance play important roles here in order for the photoswitching to occur. Figure 1.2(b) shows schematic diagram of surface excitation followed by charge transfer of photoexcited charge carriers to the adsorbed molecule.

In either direct or surface excitation, relaxation of of the light energy results in surface heating and causes thermally-induced chemistry. This excitation mechanism involves only the ground electronic state due to the low energies associated with multiple scatterings of phonons generated by heating the surface.

Recently, the Wolf and Tegeder group proposed that photoisomerization of tetra-*tert*-butyl-functionalized azobenzene molecules on Au(111) is induced by a surface-mediated charge transfer process [18, 19]. In their picture, based on wavelength-dependent threshold behavior, photoexcited hot holes in the gold first relax to the top of the Au d-band followed by their transfer to the HOMO of the molecule, resulting in the photoswitching process.

Different mechanisms involving STM-tip-induced isomerization, such as resonant inelas-

tic electron tunneling [20, 21] and applied electric field [22], have been proposed.

1.5 Azobenzene Photoisomerization: Dynamical Mechanism

One of the most interesting issues of azobenzene photoisomerization is the question of the dynamical mechanism of isomerization. The dynamics associated with azobenzene photoswitching can be described in terms of the ground and excited state potential energy surface (PES). There are two pathways by which isomerization is commonly considered to take place: the rotation pathway and the inversion pathway. Upon electronic excitation to the π^* orbital, the equilibrium molecular geometry in the electronically excited state differs from that in the ground state. As a result, the excited state molecule feels transient forces on its external and internal coordinates. There are two important reaction coordinates: the out-of-plane CNNC dihedral angle associated with the rotation pathway and the in-plane inversion of one NNC angle associated with the inversion pathway. Another isomerization pathway has been proposed by Diau, concerted inversion, where both NNC bond angles bend at the same time [24].

An interesting and puzzling aspect of the azobenzene photoisomerization is the difference in quantum efficiency, switching probability per single photon absorption, upon excitation to the S_1 state and S_2 state [23]. Table 1.1 summarizes the experimental values [12]. While the S_0 to S_1 transition of *trans* isomer is symmetry-forbidden, it is approximately twice the quantum efficiency of the S_0 to S_2 transition.

In order to elucidate the dynamical mechanism associated with azobenzene photoisomerization, the details of the PES landscape should be thoroughly inspected. Due to the difficulty of the experimental techniques involved, theoretical calculations have so far been the primary tools to investigate this issue [24, 25, 23]. The key factors are the existence of an energy barrier and the PES curve crossings (conical intersection) along the relaxation pathway. The presence of the barrier should lower the quantum yield to the photoisomerization direction. A branch in the relaxation processes occurs at the conical intersection and thus the photoswitching probabilities depend on the ground and excited PES landscape.

Figure 1.3 shows how the excited state evolves as the reaction coordinate changes, according to the recent theoretical work in Ref. [23], where the *trans*-to-*cis* quantum efficiency discrepancy is explained. Their conclusion is that excitation to the S_1 state leads to isomerization via the rotation mechanism and excitation to the S_2 state leads to isomerization via concerted inversion mechanism.

While these intensive theoretical efforts have been made, direct determination of the azobenzene dynamical pathway has never been experimentally observed until now, to the best of our knowledge.

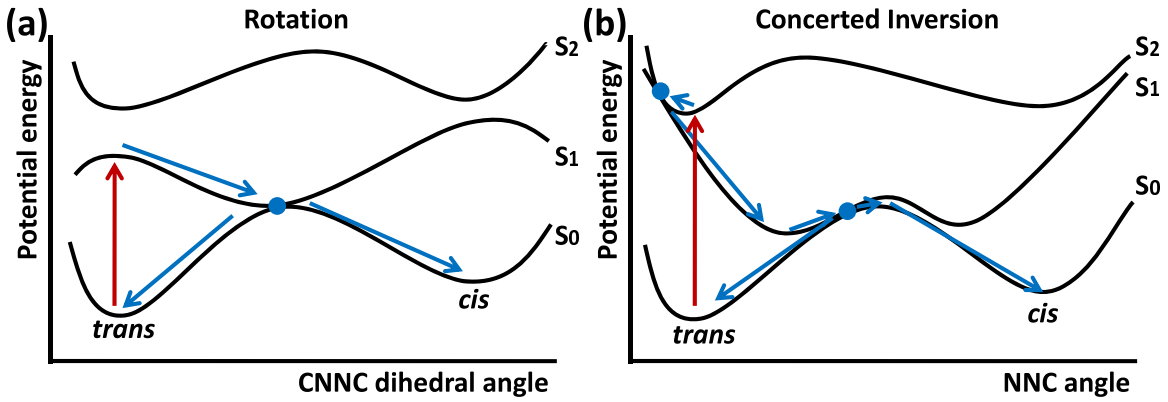

Figure 1.3: Schematic diagram of *trans* →*cis* photoisomerization of azobenzene. The ground state (S_0), first excited state (S_1), and second excited state (S_2) are denoted. (a) after S_0 →S_1 excitation. (b) after S_0 →S_2 excitation. The red arrows denote photoinduced electronic excitation via an upward Franck-Condon transition. The circles represent potential energy curve crossings (conical intersection). Adapted from Ref. [23].

Table 1.1: Quantum efficiency for azobenzene photoisomerization in solution (n-hexane), adapted from [12].

	ϕ_T (*trans* to *cis*)	ϕ_C (*cis* to *trans*)
$S_0 \rightarrow S_1$	0.24 ± 0.03	0.60 ± 0.12
$S_0 \rightarrow S_2$	0.10 ± 0.01	0.40 ± 0.06

1.6 Summary of Thesis Contents

This thesis is aimed at presenting our exploration of self-assembly and photoswitching properties of azobenzene derivatives at metallic and semiconducting surfaces.

This thesis is divided into two primary parts: Part I is an introduction and Part II describes our STM study of azobenzene derivatives at surfaces.

The first part of this thesis consists of three chapters. Chapter 1 introduces the background and significance of our investigation of molecular photoswitching on surfaces. Chapter 2 describes the principles of scanning tunneling microscopy. Chapter 3 includes experimental technique and instrumentation employed in the work presented in this thesis.

The second part of this thesis consists of nine chapters: The majority of these chapters are organized into a series of chapters that have either been published or whose manuscripts are in preparation. Chapter 4 describes the self-assembly property of unfunctionalized azobenzene molecules on a Au(111) surface. Chapter 5 describes the STM manipulation of the unfunctionalized azobenzene molecules on Au(111). Chapter 6 describes the reversible

photoswitching of azobenzene derivative, 3,3'-5,5'-tetra-*tert*-butyl-azobenzene (TTB-AB) molecules on Au(111). Chapter 7 describes the measurement of photoswitching rates of TTB-AB molecules on Au(111) under different wavelengths of light. Chapter 8 describes the influence of structural phases on the photoswitching of TTB-AB molecules on Au(111). Chapter 9 describes investigations of photoisomerization dynamical mechanisms of TTB-AB molecules on Au(111) based on surface molecule chirality. Chapter 10 describes the surface anchoring and dynamical properties of azobenzene derivatives functionalized with a thiol-group. Chapter 11 describes the adsorption and switching capabilities of azobenzene derivatives functionalized with different ligands on Au(111). Chapter 12 describes our preliminary investigations of TTB-AB molecules on the GaAs(110) surface.

Chapter 2

Scanning Tunneling Microscopy

Since its invention in 1982 by Gerd Binnig and Heinrich Rohrer [26], the scanning tunneling microscope (STM) has been used to produce images of metallic and semiconducting surfaces with unprecedented spatial resolution. The STM has revolutionized surface science by providing a means not only to image atomic-scale real-space structure, but also to determine atomic-scale electronic structure as well [27]. In addition, it has developed into a tool capable of the manipulation of individual atoms and molecules on surfaces. [28, 29, 30].

2.1 Quantum Mechanical Tunneling

Scanning tunneling microscopy and spectroscopy allows us to gain insight into structural and electronic properties of surfaces and interfaces at an atomic scale. The working principle of STM is based on the quantum mechanical tunneling effect: When an atomically sharp metallic tip approaches an electrically conducting sample at a certain bias voltage, a current starts to flow (typically at a distance of 5 to 10 Å) even before the tip mechanically crashes into the sample.

A simple one-dimensional potential barrier problem that junior undergrads encounter in quantum mechanics class captures the essential principle of how STM works. In classical mechanics, an electron with energy E moving in a potential $V(z)$ can overcome a potential barrier V_0 only if $E > V_0$ - otherwise it is reflected. In quantum mechanics, however, the electron is described by a wave function $\Psi(z)$ and has a nonzero probability of tunneling through a potential barrier as long as $V_0 < \infty$ for an electron approaching a potential barrier of height V_0 and width d. As a simple model, the potential $V(z)$ here is assumed to be constant within each of the three regions:

$$\begin{array}{lll} \text{region I} & \text{z} < 0, & V(z) = 0, \\ \text{region II} & 0 \leq \text{z} \leq \text{d}, & V(z) = V_0, \\ \text{region III} & \text{d} < \text{z}, & V(z) = 0, \end{array}$$

In each regions the quantum mechanical wave function describing the electron satisfies the time-independent Schrödinger equation,

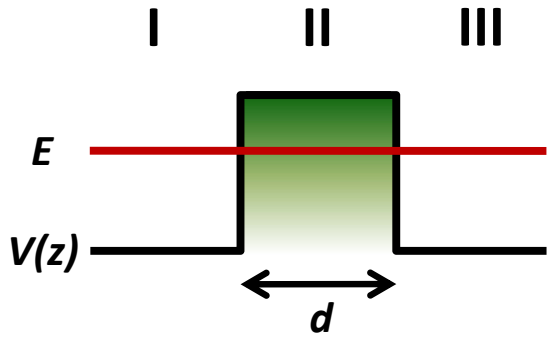

Figure 2.1: In quantum mechanics, the electron is described as a wave function $\Psi(z)$ that has a probability to tunnel across the potential barrier. I, II, III represents three different regions that the wave function should meet the boundary conditions.

$$\left(-\frac{\hbar^2}{2m_e}\frac{d^2}{dz^2}+V(z)\right)\Psi(z)=E\Psi(z). \tag{2.1}$$

where m_e and $\hbar$ represent the electron mass and Planck's constant divided by 2π. The respective solutions for the different regions are:

$$\begin{array}{ll} \text{region I} & \Psi_1 = e^{ikz} + Ae^{-ikz} \\ \text{region II} & \Psi_2 = Be^{-\kappa z} + Ce^{\kappa z} \\ \text{region III} & \Psi_3 = De^{ikz}, \end{array}$$

where $k^2 = 2m_eE/\hbar^2$ and $\kappa^2 = 2m_e(V_0 - E)/\hbar^2$. The incident current density j_i and the transmitted current density j_t can be described by

$$j_i = \frac{\hbar k}{m_e} \tag{2.2}$$

$$j_t = -\frac{i\hbar}{2m_e}\left[\Psi_3^*(z)\frac{d\Psi_3(z)}{dz} - \Psi_3(z)\frac{d\Psi_3^*(z)}{dz}\right] = \frac{\hbar k}{m_e}|D|^2 \tag{2.3}$$

and the transmission coefficient T is given by the transmitted current density divided by the incident current density:

$$T = \frac{j_i}{j_t} = |D|^2 \tag{2.4}$$

Fulfilling the boundary conditions of the wave function at the discontinuities of the potential, the wave function at each regions is obtained. The transmission coefficient, which is of importance in this model, is then given by

$$T = |D|^2 = \frac{1}{1 + \frac{(k^2+\kappa^2)^2}{4k^2\kappa^2}\sinh(\kappa d)}. \tag{2.5}$$

In the limit of $\kappa d \gg 1$, the transmission coefficient can be approximated by

$$T \approx \frac{16k^2\kappa^2}{(k^2+\kappa^2)^2}\exp(-2\kappa d). \tag{2.6}$$

where $\kappa = \frac{\sqrt{2m_e(V_0-E)}}{\hbar}$.

As T is dominated by the exponential factor $\exp(-2\kappa d)$, tunneling in this model depends exponentially on the barrier width d times the square root of the effective barrier height $V_0 - E$. A good rule of thumb is that the tunneling current increases by about an order of magnitude by decreasing the tip-sample distance by about an Å. This explains the very high spatial resolution of the STM measurements.

2.2 STM Topography: Surface Structure

Although the simple model introduced in the previous section captures the inherent exponential dependence of the tunneling current on the tip-sample distance, it fails to explain any dependence of the current on the electronic structure of tip or sample.

To explain the electron tunneling between two weakly coupled electrodes, Bardeen used first-order time-independent perturbation theory [31]. Tersoff and Hamann applied Bardeen's formalism to the STM geomety in order to appropriately describe the tunneling process in STM configuration [32, 33]. In their work, the tip is approximated by a sphere, and only s-type wave functions contribute to the tunneling matrix elements. The tunneling geometry in the Tersoff-Hamann model is shown in Fig. 2.2, where R stands for the effective tip radius, r_0 the center of curvature of the tip, and d the tip-sample distance. At low temperatures and small bias voltages V, the current can be described by

$$I \propto V \cdot \rho_t(E_F) \cdot \exp(-2\kappa d) \cdot \sum_\mu |\Psi_\mu(\vec{r}_0)|^2 \cdot \delta(E_\mu - E_F) \tag{2.7}$$

where E_F is the Fermi energy and $\rho_t(E_F)$ is the density of states at the Fermi level of the tip. The bias across the tunnel junction refers to the voltage of the sample with respect to the tip. The decay rate κ is proportional to the effective local potential barrier height ϕ, which is to a good approximation equal to the average of the tip and sample work functions. The quantity

$$\rho_s = \sum_\mu |\Psi_\mu(\vec{r}_0)|^2 \cdot \delta(E_\mu - E_F) \tag{2.8}$$

can be identified with the surface local density of states (LDOS) at the Fermi level, evaluated at $\vec{r}_0$. The tip wave function Ψ_μ decay exponentially into the vacuum - hence, the current

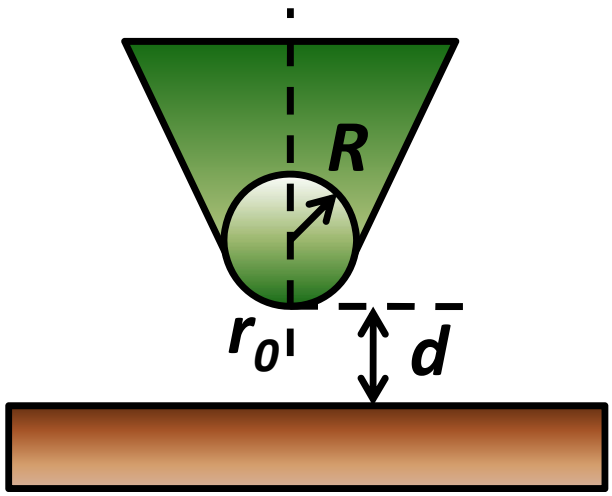

Figure 2.2: Schematic diagram of the tunneling configuration in Tersoff-Hamann model: d represents the tip-sample distance, R the effective tip radius, and r_0 the center of the tip.

has exponential dependence on the tip-sample distance:

$$I \propto \exp(-2\kappa d). \tag{2.9}$$

Following the described approximations the STM topographic images are interpreted as a contour of constant local density of states in the vicinity of the Fermi edge. According to Eq. 2.7, the area $z(x,y)|_{I=\text{const.}}$ is a trace of constant LDOS at E_F above the sample at the tip location. In this simple model, the LDOS follows the topography to a good approximation and the constant current images can be interpreted as the topography of the surface.

Figure 2.3 shows the typical STM topographic images of gold surface in (111) crystallographic direction [Fig. 2.3(a)] and atomic resolution of the surface gold atoms [Fig. 2.3(b)]. To acquire such STM images, the z-component of the tip position is adjusted by a feedback loop to keep a constant tunnel current between the tip and the surface while a raster scan generator moves the tip across the surface. In this "topography imaging mode", the z component of the tip position is recorded as a function of surface coordinates of (x, y) and thereby provides a measure of the surface contours. Color coding the $z(x, y)$ signal often helps to visualize the sample surface topography.

Care must be taken in the interpretation of the observed features on surfaces, since both the electronic and geometric properties of the sample contribute to the STM topographic images. For instance, a conjugated molecule may exhibit its apparent height in STM images higher than a non-conjugated molecule of the same size. Simulated STM images from density functional theory (DFT) may be helpful to understand and interpret the experimental data.

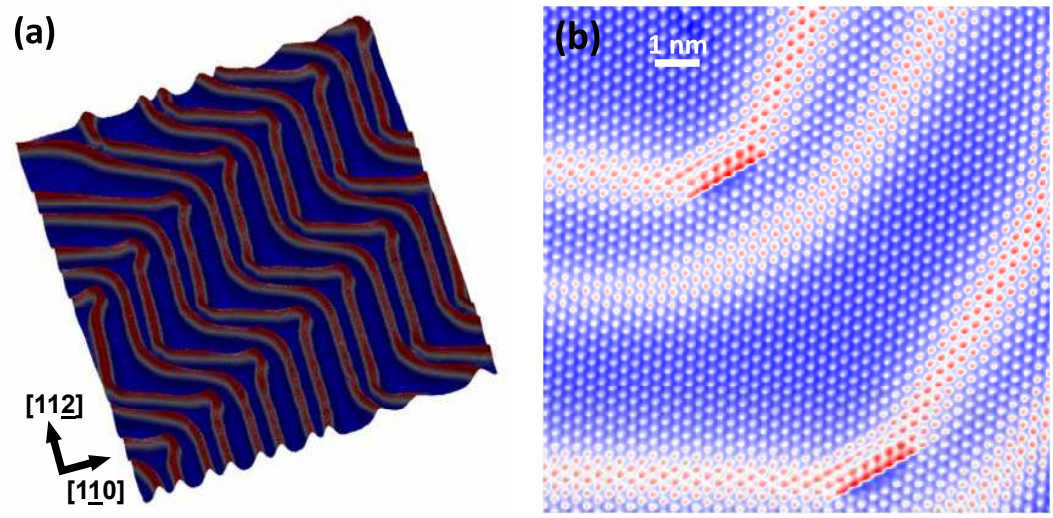

Figure 2.3: STM topographic images of clean Au(111). (a) 3D representation of large field of view showing a surface reconstruction, so-called *herringbone reconstruction*. The periodicity of the surface reconstruction in the [1$\bar{1}$0] direction is ∼63 Å. (b) a close-up image showing atomic resolution of surface gold atoms. Images are pseudo-color coded. Both images were acquired with a constant tunneling current of 100 pA at sample voltage of −1 V.

2.3 STM Spectroscopy: Electronic Structure

In the previous section the tunneling process was described using the Tersoff-Hammann model in the limit of low bias voltage V. At a higher bias voltage V this model can be extended to a tunneling current weighted over a range of energies

$$I \propto \int_0^{eV} \rho_s(E_F+E)\cdot\rho_t(E_F+E-eV)\cdot T(E,eV,d)\cdot[f(E_F+E-eV,T_t)-f(E_F+E,T_s)]\,\mathrm{d}E \tag{2.10}$$

with a transmission coefficient of the tunneling barrier

$$T(E,eV,d) = \exp\left[-d\cdot\sqrt{\frac{4m}{\hbar^2}(\phi_T+\phi_S+eV-2E)}\right], \tag{2.11}$$

where ρ_s is the LDOS of the sample, ρ_t that of the tip, $f(E,T)$ the Fermi functions at energy E and temperature T, and ϕ_T and ϕ_S represent the work functions of tip and sample. For instance, the work function of the tungsten tip and Au(111) surface that mostly used in this thesis are ∼4.5 eV and ∼5.3 eV, respectively.

Schematic diagram of the electron tunneling process in STM measurements as described in Eq. 2.10 is shown in Fig. 2.4 [34]. Here the tip and sample are represented by the left and

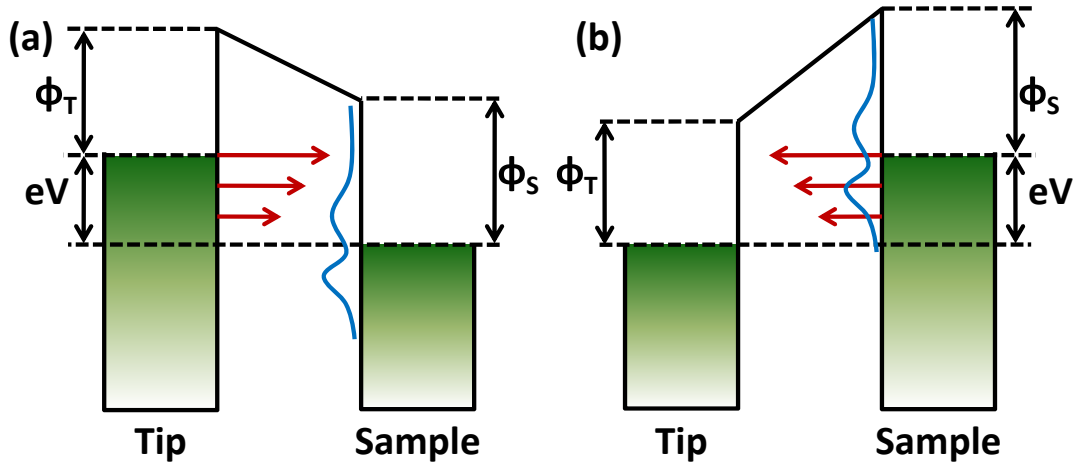

Figure 2.4: Energy level diagram of the STM configuration. (a) Positive sample bias: electrons from occupied states of the tip tunnel into unoccupied states of the sample. (b) Negative sample bias: electrons from occupied states of the sample tunnel into unoccupied states of the tip. ϕ_T and ϕ_S represent the work function of the tip and the sample, respectively.

right electrodes, and the shaded regions indicate the occupied states below the Fermi level E_F. In the equilibrium condition ($V = 0$) the Fermi level of the tip and sample are aligned at the same level and thus the net tunneling current is zero. Applying a bias voltage leads to a shift of the Fermi levels by eV. When $V > 0$ (i.e., positive sample bias), electrons from occupied states of the tip in the energy interval from $E_F - eV$ to E_F tunnel into unoccupied states of the sample [Fig. 2.4(a)]. For $V < 0$ (i.e., negative sample bias) the situation is reversed and electrons from occupied states of the sample tunnel into unoccupied states of the tip [Fig. 2.4(b)]. Note that the current mainly originates from electrons tunneling from the Fermi level E_F since they experience the lowest effective energy barrier.

Assuming ρ_t being constant, differentiation of Eq. 2.10 results in

$$\frac{dI(V)}{dV} = \rho_t(0) \cdot \rho_s(eV) \cdot T(E, eV, d) + \int_0^{eV} \rho_s(E) \cdot \rho_t(eV - E) \cdot \frac{dT(E, eV, d)}{dV} dE. \quad (2.12)$$

Often the second term of Eq. 2.12 can be neglected. Assuming T being a smoothly varying exponential function with V, the differential tunneling conductance dI/dV is a good measure of ρ_s at an energy equal to eV [40].

Figure 2.5 shows a typical dI/dV spectra acquired on clean Au(111) surface, where the well-known Au(111) surface-state onset at $\sim$−0.45 eV is observed. Experimentally, $dI/dV(V)$ is measured by stabilizing the tip above the surface at I_{stab} and V_{stab}. To fix the tip-sample distance (d), the feedback loop is then switched off. While the voltage is

ramped from the initial to a final voltage, the tunneling current is measured. By numerical differentiation of $I(V)$ curves the respective dI/dV signal can be obtained, which typically decrease the signal-to-noise ratio. In this work the lock-in technique was used to determine dI/dV. Here, a small ac modulation is added to the bias voltage at a reference frequency f_{ref} (typically a few hundred Hz), and the respective response in the current signal at f_{ref} is analyzed with a lock-in amplifier. To investigate the electronic structure of a sample with high spatial resolution, dI/dV maps can be obtained. In this case a spectrum is taken at every point (x, y) on the surface. This technique allows us to directly correlate topographic $z(x, y)$ and spectroscopic properties $dI/dV(x, y, eV)$ of the sample.

If only the electronic structure at one particular energy eV_0 is of interest, the acquisition of dI/dV-maps at fixed bias voltage V_0 is a time-saving alternative to full dI/dV spectroscopy maps. In contrast to the full dI/dV spectra, where the feedback loop is switched off during voltage ramping, the dI/dV signal at fixed bias V_0 can be recorded with the feedback loop on. Simultaneously to the topographic measurement, a lock-in technique derives the dI/dV signal at the voltage V_0 while the tip is scanned under constant current conditions.

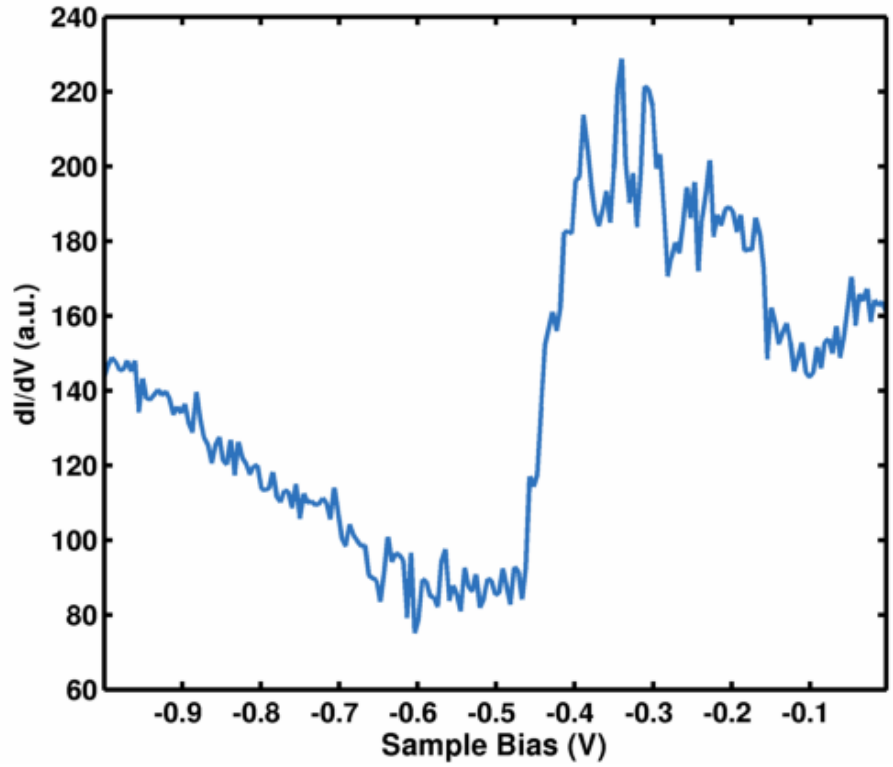

Figure 2.5: A typical dI/dV spectra measured on clean Au(111) showing the surface state onset.

Chapter 3

STM Instrumentation

In the following we will introduce the main parts of the experimental setup used for the measurements presented in this thesis. The STM was designed and built primarily by M. F. Crommie, K. Nagaoka, and M. Comstock. A detailed description of the VT-STM can be found in the Ph.D. thesis of Matt Comstock [35]. Only a brief description of the instrument and some significant modifications are presented here.

3.1 UHV System and Cryostat

To investigate clean and well-defined molecular nanostructures, the instrumental setup has to ensure the cleanliness and repeatability of the experiments. All sample preparation and characterization in UHV conditions ensures the minimal influence of external contaminants and stable experimental conditions, and the observed properties uniquely ascribed to the nanostructure under study.

The experiments presented in this thesis were conducted in a home-built UHV chamber system. It consists of four chambers separated by UHV gate valves: (i) an preparation chamber equipped with a sputter-gun, sample preparation stage, Auger electron spectroscopy (AES), quadrupole mass spectrometer, and low energy electron diffraction (LEED) for sample preparations and sample analysis, (ii) an STM chamber equipped with our home-built STM, (iii) a load-lock with a dedicated pumping system, allowing sample transfer into the system within a few hours, (iv) a dosing chamber for molecular deposition.

An overview of the system is shown in figure 3.1. Samples are transferred between the chambers by a magnetically coupled linear transfer rod (manufactured by Transfer Engineering). A combination of 500 L/s turbo pump and a diaphragm backed 70 L/s turbo pumping station is employed to pump down the system from the atmosphere pressure to high vacuum range. Both preparation and STM chamber are equipped with an ion-pump ($\sim$500 L/s). These large ion pumps along with titanium sublimation pumps can maintain the base pressure below 1×10^{-10} torr.

The whole VT-STM is cooled by a liquid He flow cryostat from Advanced Research Systems (ARS Helitran LT-3B). During operation, cold cryogen (almost exclusively helium)

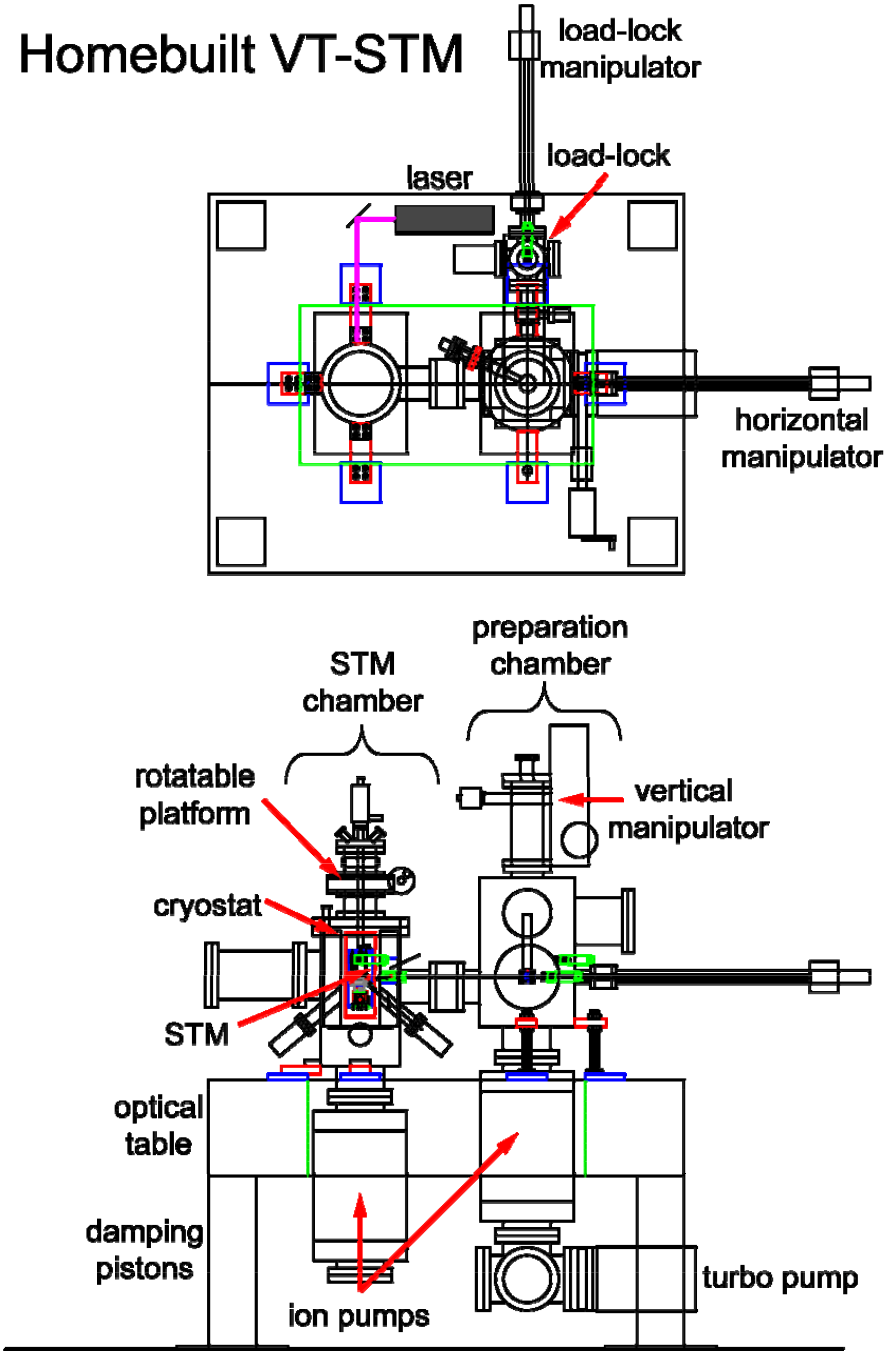

Figure 3.1: Schematic drawings of our home-built STM system

constantly flows through the cryostat. The product and shield flow are controlled by flow

meters at the gas exhaust exits. While the STM is designed to operate in the variable temperature (VT) mode, we usually operate it at the base temperature. The cryogenic setup allows operation at a base temperature of 12K now. Some works presented in this thesis were conducted when the base temperature was 30 K. The base temperature was significantly improved after recent modifications were performed by me and Luis Berbil-Batista in 2008: (i) replacing manganin wires running from room temperature feedthrough to the low temperature sapphire feedthrough with stainless steel coaxial wires, (ii) better thermal anchoring of these wires near the cryostat with more molybdenum clamps, and (iii) attaching the gold-coated copper braid between the cold finger and the STM sample stage to provide the better thermal coupling when STM is left hanging (figure 3.3).

The sample temperature is measured using a Si diode sensor (LakeShore DT-470) fixed to the STM body near the sample holder. While Chromel-Au/Fe (0.07%) thermocouple was used to monitor the sample temperature in the past, we only use the Si diode these days for reliable temperature measurements. Care must be taken to ground the Si diode readouts during STM measurements not to cause electrical noise.

3.2 Variable-temperature STM

Figures 3.2 and 3.3 show the schematic drawing and photograph of our STM, respectively. The main body is made from OFHC copper and serves as the main electrical grounding for STM measurements. Six shear piezo stacks (4 layers each) are glued inside the body cavity in two sets of three (Epotek H20E). Alumina contact pads are glued to the each shear piezo stack top and altogether the stacks hold and move a long polished sapphire prism. Recently, we have modified the piezo stack design to minimize the possibility to electrical connection between the high-voltage wires and the ground wires (or STM body). It also offers better control of the positions of these wires within a tight space due to the compact STM design. The single shear piezo plates and metal shims are stacked and glued together, as shown in figure 3.4.

The STM scanner assembly is mounted at the top of the sapphire prism. Wires from the piezo tube scanner (five total corresponding to $\pm$x, $\pm$y, and z scan directions) pass down through grooves in a sapphire insert in the center bore of the prism and connect to contact plugs at the bottom. The STM scanner consists of a piezo tube scanner, a ceramic cylinder which contains a tip holder, and the STM tip itself. Electrical connection is made to the tip via a 3 mil, bare gold wire expoxied (H20E) on one end to the tip holder and on the other end to a wire feedthrough (PTFE tube for electrical insulation).

One of the main challenges of STM design is a coarse tip approach mechanism which can move the tip towards the sample over a range of a few millimeters all the way down to a few nm without mechanical contact between the tip and the sample. Two of the most reliable coarse approach these days are stick-slip motion (Besocke-beetle type) [36, 37, 38] or Pan-type [39]. Our STM adapts a Pan-type coarse approach design (z direction). In our STM configuration the sample is mounted upside down in the sample holder, and the tip

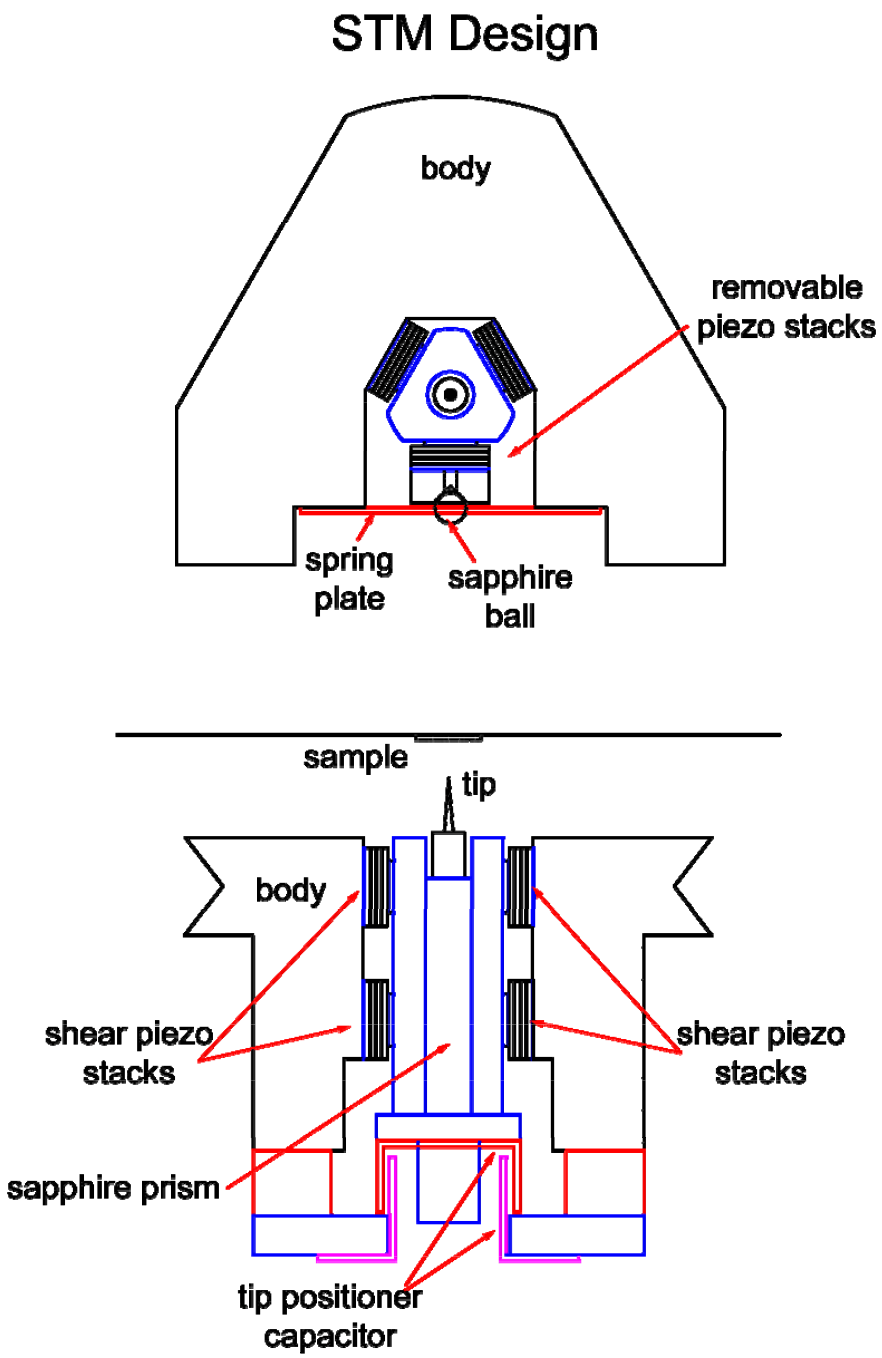

Figure 3.2: Schematic drawing of VT-STM

is approached from the bottom. The Pan coarse approach moves the sapphire prism which holds the STM scanner.

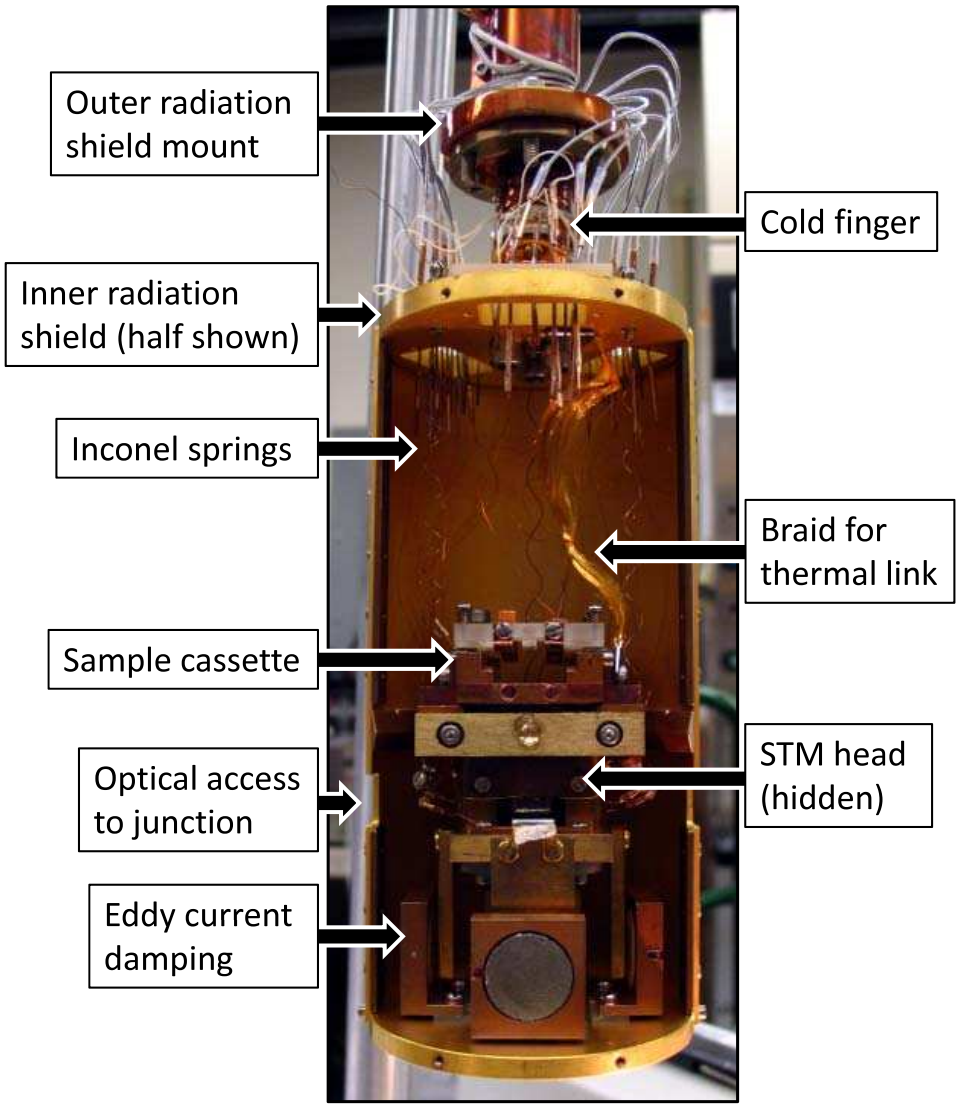

Figure 3.3: A photograph of the home-built VT-STM

The Pan-type coarse approach is well described in Ref. [39]. Only a brief description of the working principle is provided here. First, all the shear piezos simultaneously shear in the same direction. Next, each shear piezo one at a time returns back to its initial position. The motion of only one shear piezo cannot move the prism against the other five, thus after all shear piezos have returned to their initial positions the prism has been left either forward or backward from its initial position. The described scheme offers very reliable coarse approach with reproducible step sizes. One of benefit of Pan-type coarse approach is a capability to approach the same spot after macroscopic tip travel, which is essential for our measurements.

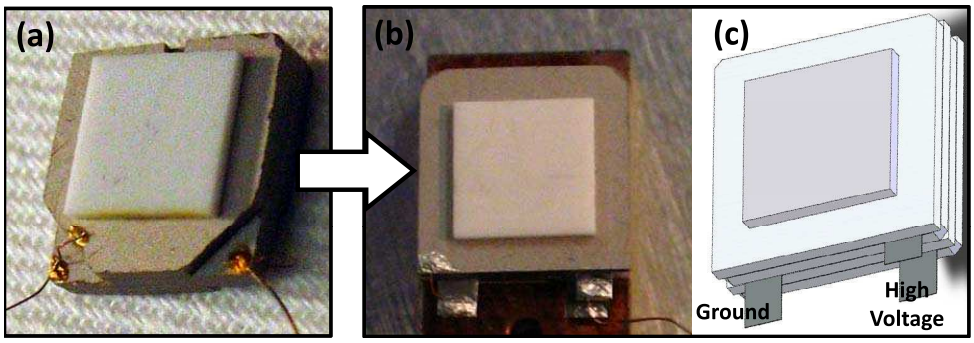

Figure 3.4: Piezo stacks of the home-built VT-STM: (a) photograph of previous piezo stack, (b) current piezo stack, (c) schematic drawing of current piezo stack.

The microscope is suspended by three inconel springs inside the two gold-coated copper cans that serve as radiation shields. Its oscillations are damped by an eddy current damping (figure 3.3). Four copper fins are attached to the bottom of the STM body and aligned parallel and close to magnets.

A commercial current-to-voltage amplifier (FEMTO DLPCA-200) is employed to measure the tunnel currents. Its bandwidth is $\sim$1.2 kHz at 10^9 gain setting. We usually acquire topographic images of molecules on surfaces at very low currents below 50 pA in order not to disturb the molecules. We use a commercial STM control electronics from RHK.

Tip approach to the surface consists of two steps: the coarse approach and fine approach. For the coarse approach we use the walker box, a custom control box built by the UC Berkeley Physics Department Electronics Shop. For the fine approach the walker box takes a TTL trigger input from RHK STM control box and the tunnel current is monitored at every walker step.

3.3 Tip Preparation

The performance of a STM is found to depend to a large extent on the quality of the tip used. While various materials such as tungsten, platinum-iridium, platinum, silver, or gold can be used for an STM tip, the tungsten is widely used because of its great mechanical strength, high melting temperature, and the easy tip fabrication process using an electrochemical etching. The tips used in this thesis are made from a 0.020" polycrystalline tungsten wire from California Fine Wire. The stage of tip preparation includes electrochemical DC etching of the W wire suspended through a hole in a stainless steel plate. The hole is covered by a meniscus of a 5.0 N NaOH solution from Alfa Aesar. During the etching process, the etching current is kept constant at $\approx$10 mA. The process is cut off when the bottom part of the W wire drops. It is caught in a beaker with shaving cream (idea taken from Armen Kirakosian), which prevents the tip from mechanical damage. The tip at the

bottom part of the wire is preferred, since it drops out of the electrochemical etching stage quicker and thus tends to be sharper than the top part. After the etching process, the tip is gently immersed in deionized water to remove any residue of etching solution, and then rinsed in pure methanol. Immersion in a HF solution is often used to remove the surface oxide layer. Note that the STM resolution does not have a direct correlation with the appearance of the tip under the optical microscope or even scanning electron microscope (SEM).

Typically the tip created in this manner needs a further post-process for best results after being introduced into the microscope. We often get the reliable tips after *in-situ* field emission onto the clean metallic surface (typically, a few μA at $\sim$200 V). Controlled collision of the tip with a clean gold surface, thereby transferring gold atoms to the end of the tip, also serves as one of *in-situ* tip treatments while tunneling.

3.4 Surface Preparation

The cleanliness of the surface plays a crucial role in characterizing and identifying the individual molecular structures. Because of its relative inertness and well-characterized surface reconstruction a Au(111) surface is suitable as a substrate for various molecules and serves as the substrate for most experiments described in this thesis. In order to achieve a good clean surface quality for the gold surface we employ the sputter and annealing technique. The Au(111) surface is cleaned by cycles of Ar-ion sputtering and e-beam annealing in UHV at a base pressure of $<1\times10^{-10}$ Torr. Samples that have been exposed to ambient conditions are first annealed to desorb the residual gas contaminating the surface. The subsequent sputtering is performed with Argon at a background pressure of $\sim1\times10^{-5}$ torr and an ion current measured at the sample of ~2 μA. Using high-energy inert gas ions, bombarding the surface provides a good way of removing adsorbed contaminants. The sputtering cycles of 6 min are followed by a 10 min annealing at $\sim500-600$ °C. Following cleaning the sample is quickly moved to the STM chamber where it is cooled down to the base temperature. The low chamber base pressure coupled with the cryo-pumping on the radiation shields allow us to keep clean samples for several weeks without noticeable sample degradation.

In order to achieve a good clean surface quality for the GaAs(110) surface we employ the cleaving technique, that is, fracturing the sample pieces along one of the preferred cleavage planes of the sample. Both n-doped and p-doped GaAs(110) wafers (purchased from Wafer Technology) were cleaved in UHV preparation chamber at room temperature, exposing a clean (110) crystal face. In order to be able to do that, I designed the cleaving stage that is added below the current sample heating stage of the vertical manipulator in the preparation chamber (figures 3.5(a) and (b)). The current magnetically coupled transfer rod located in the preparation chamber is used to transfer the sample holder in and out of the cleaving stage and provide a contact area to break the wafer piece *in situ*. The cleaving stage is equipped with the tungsten filament close to the sample holder, thereby providing sample

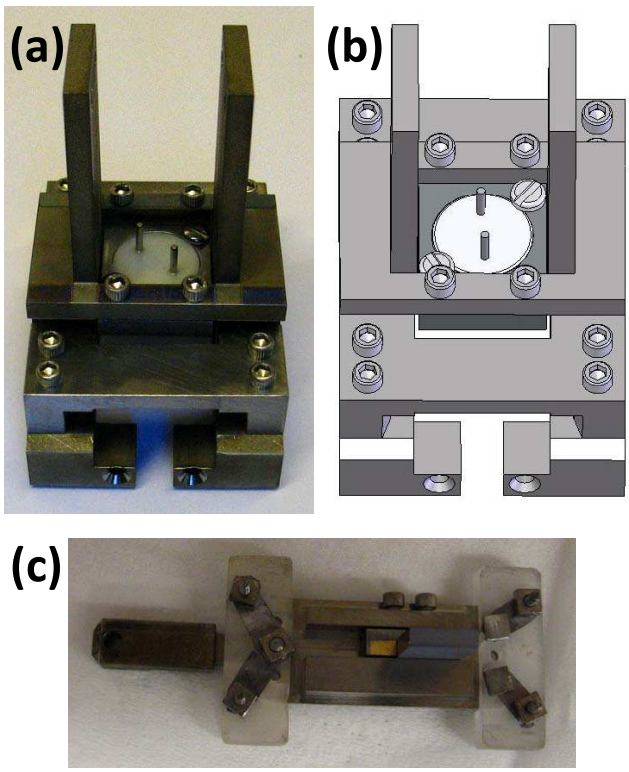

Figure 3.5: GaAs cleaving stage and sample holder: (a) photograph of the cleaving stage, (b) schematic drawing of the cleaving stage, (c) photograph of the sample holder with GaAs mounted.

outgassing capability. The GaAs wafer (3" diameter, 2 mm thick) was diced into small GaAs pieces (10×7 mm) with "U" shape notch across the face of wafer in one direction (performed by American Precision Dicing Inc.). The contacts to the wafer pieces were made with small gold foil (5 mil). The sample holder is also specially designed accordingly, as shown in figure 3.5(c).

In addition to the Au(111) and GaAs(110) surface, we have also successfully prepared Si(111), Si(100), NiAl(110), hydrogen-passivated Si(100), NaCl on Au(111), and Al oxide on NiAl(110).

3.5 Molecular Deposition

Some of the basic questions regarding molecular deposition onto a clean surface include: (i) Do they have high enough vapor pressure at room temperature? (ii) Will the molecules fly intact to the surface? The molecules may lead to a decomposition during the sublimation process. (iii) Is it possible to conduct a mass spectrometer characterization?

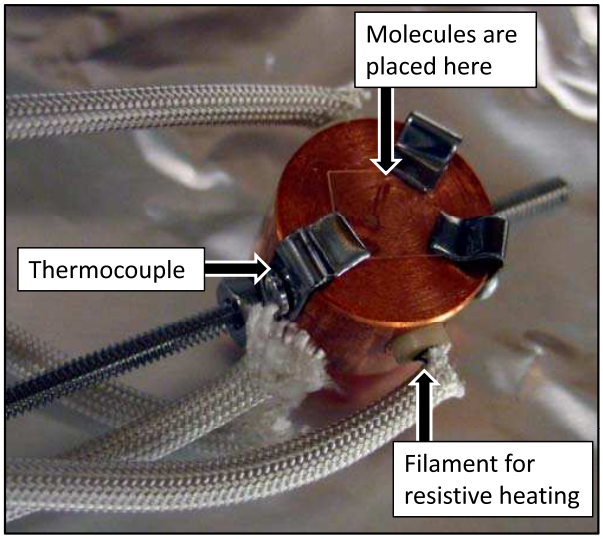

Figure 3.6: A photograph of a home-built molecular evaporator

In case of the molecules (such as TTB-azobenzene) with low vapor pressure at room temperature, thermal sublimation technique is employed to adsorb the molecules onto the surface. Figure 3.6 shows a photograph of our home-built molecular evaporator. Heater is made out of coiled chromel wire inside alumina to provide resistive heating. The 10 mil sapphire plate is placed on top of the copper (or molybdenum) body in order to prevent any reaction with the molecules from taking place. K-type thermocouple is used to monitor the deposition temperature. Note that the molecules have to be thoroughly outgassed prior to the deposition of the molecules to remove loosely adsorbed materials and get very pure sources of molecular beams onto the clean surface.

This way we are able to deposit molecules onto the surface in a very clean manner.

Part II

STM Study of Azobenzene Derivatives at Surfaces

Chapter 4

Self-Assembly Properties of Azobenzene on Au(111)

4.1 Introduction

Engineering the self-assembly and functional characteristics of adsorbed molecules is critical for laying the ground-work of future nanotechnologies. Progress has been made in this direction using molecular classes that exhibit polar functional behavior [40, 41, 42, 43, 44, 45] , chirality [46, 47], "spacer leg" groups [48, 49, 50], and different optical properties [51, 52, 53]. Azobenzene is an important member of this final class because it undergoes a reversible, photoactive *trans-cis* isomerization that may allow it to serve as an optically active device element [13, 54]. This simple molecule consists of two phenyl rings joined by a pair of double-bonded nitrogen atoms [figure 4.1(a) inset]. Some attempts have been made to observe the *trans-cis* isomerization of azobenzene-containing films with scanning tunnel microscopy (STM) [55, 56, 57], but none have clearly resolved intramolecular structure, namely the phenyl rings.

In this chapter, we resolve the intramolecular structure and self-assembly behavior of surface-adsorbed azobenzene molecules. We find that azobenzene molecules deposited onto Au(111) form a surprising variety of molecular structures whose commensurability with the periodicity of the underlying Au(111) herringbone surface reconstruction depends on molecular coverage. At low coverage we observe two commensurate molecular chain phases that can be converted, one to the other, via manipulation with the STM tip. At saturation coverage the azobenzene molecules switch to an incommensurate configuration comprised of two new phases. Commensurability is regained, however, at only slightly lower coverages as molecular vacancies order with the underlying herringbone reconstruction. This behavior arises from a coverage-dependent competition between intermolecular and molecule-substrate interactions for azobenzene on Au(111).

We performed our measurements using the home-built variable-temperature UHV STM (base pressure $<5\times10^{-11}$ Torr). A clean Au(111) substrate was obtained by repeated cycles of Ar-ion sputtering and annealing. Azobenzene molecules were leaked into the vacuum

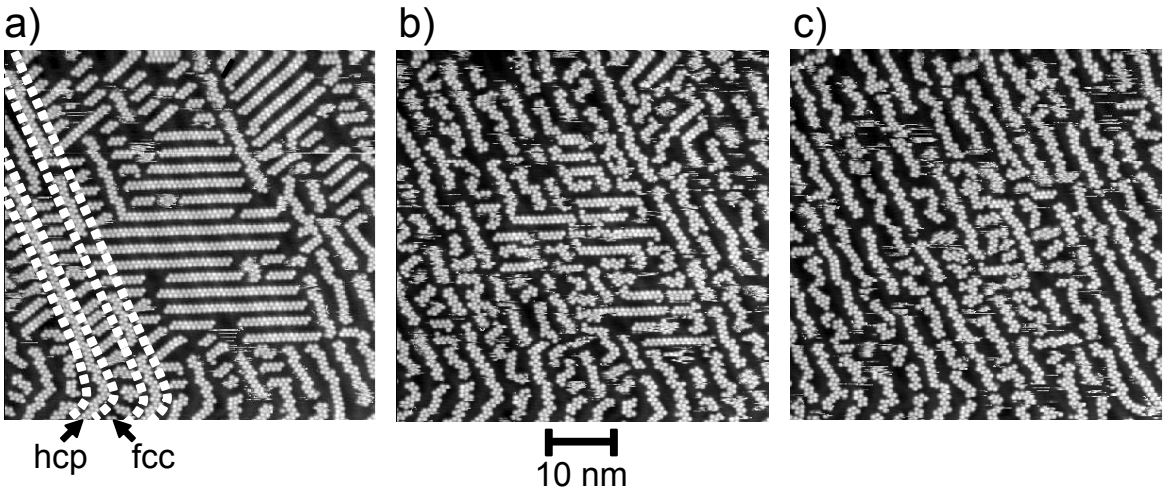

Figure 4.1: STM images of 0.50 ML of azobenzene on Au(111) surface acquired at a typical scan bias of $-1.25V$ (59 × 59 nm, 50 pA, 35 K). The sequence from (a) to (c) shows the tip-induced conversion of the straight phase to the zigzag phase induced by scans at an elevated bias (−1.75 V).

chamber and deposited onto the Au(111) substrate at room temperature. After azobenzene exposure, the sample was transferred to the STM, which was operated between 35 K and room temperature. At room temperature, azobenzene molecules diffuse and are too unstable for STM imaging. At saturation coverage [one monolayer (1 ML)] azobenzene is stable enough for imaging at 90 K, while lower coverage structures ($0.5 - 0.8$ ML) required cooling to 35 K. Tunneling currents were kept below 100 pA for stable imaging.

4.2 Low Coverage: the "Parking Lot" Arrangement

Figure 4.1(a) shows a 0.50 ML coverage of azobenzene on the Au(111) surface. The Au(111) herringbone reconstruction consists of parallel pairs of slightly elevated surface ridges [58]. [outlined by the dashed lines in figure 4.1(a), parallel ridges separated by 6.3 nm] that separate domains of fcc- and hcp-ordered Au surface atoms. We can distinguish two types of azobenzene ordering relative to the herringbone reconstruction. The first, referred to as the "zigzag" phase, consists of long, zigzagging azobenzene chains that lie predominantly within the contours of the hcp regions of the herringbone reconstruction. The second phase, the "straight" phase, consists of straight azobenzene chains that run in the two directions oriented 120° from the ridges of the herringbone domain walls. Parallel straight chains appear to repel each other, having a minimum separation of 0.5 nm. Straight chains occasionally cross the herringbone ridges to form extended domains, as seen in the

center of figure 4.1(a). The straight and zigzag phases alternate over much of the surface, and coexist even when the sample is cooled slowly from room temperature down to 35 K over a period of many hours.

We are able to convert the straight phase into the zigzag phase by imaging the azobenzene-coated surface at increased sample biases. This can be seen in figures 4.1(b) and 4.1(c), which show conversion from the azobenzene straight phase to the azobenzene zigzag phase after repeated STM scans. The straight chain domains of the initial image almost completely convert into zigzag domains filling both the fcc and hcp regions of the herringbone reconstruction. The transformation is irreversible and independent of the scan direction. The onset voltage for the transformation ranges from -1.5 to -2.0 V, and varies with changes to the tip apex. Tip-induced current and electric field perturb the molecules beneath the tip, freeing them to diffuse and rearrange. Limited thermal diffusion at 35 K results in the creation of the locally disordered zigzag phase.

The internal structure of the molecular chains can be more clearly seen in figure 4.2(a), which shows a close-up of a straight phase chain. The chain appears as eight closely spaced protrusions whose center-to-center spacing ($\sim$0.8 nm) in the marked directions is similar to the center-to-center spacing of phenyl rings in crystalline *trans*-state azobenzene (0.63 nm) [59]. Line scans taken across the chain [figure 4.2(b)] show that the depths of the minima between protrusions along the long-chain axis (A-B) are 45% greater than along the short-chain axis (C-D). This suggests that the protrusions along the short-chain axis are bonded differently than along the long-chain axis. We commonly observe chain lengths change spontaneously during scanning, always with pairs of protrusions attaching or detaching from the chain ends (often leading to an odd number of protrusions along the chain length). Hence, we identify adjacent pairs of protrusions along the short chain axis to be individual azobenzene molecules as shown in the figure 4.2(a) overlay. Isolated azobenzene molecules having the same shape as chain members have been observed at even lower coverages. We note that the azobenzene "dumbbell" appearance is similar to the related stilbene molecule that has been observed in films on the Ag/Ge(111)-$\sqrt{}$(3) surface [60] (with a similar center-to-center lobe distance of $\sim$0.76 nm).

4.3 Saturation Coverage: Two Distinct Ordered Arrangements

At higher molecular coverage (1 ML), where the Au(111) surface is saturated with azobenzene, we observe two different molecular orderings [marked I and II in figure 4.3(a)] that are incommensurate with the herringbone reconstruction. Phase I, shown more closely in figure 4.3(b), is a closed-packed structure where the positions of azobenzene phenyl lobes lie on a slightly distorted hcp lattice. The closed-packed arrangement of the phenyl lobes makes it difficult to be certain of the positions and orientations of individual azobenzene molecules within the film. The molecular arrangement sketched in the inset of figure 4.3(b) represents one of many possible arrangements. Phase II, shown more closely in figure 4.3(c),

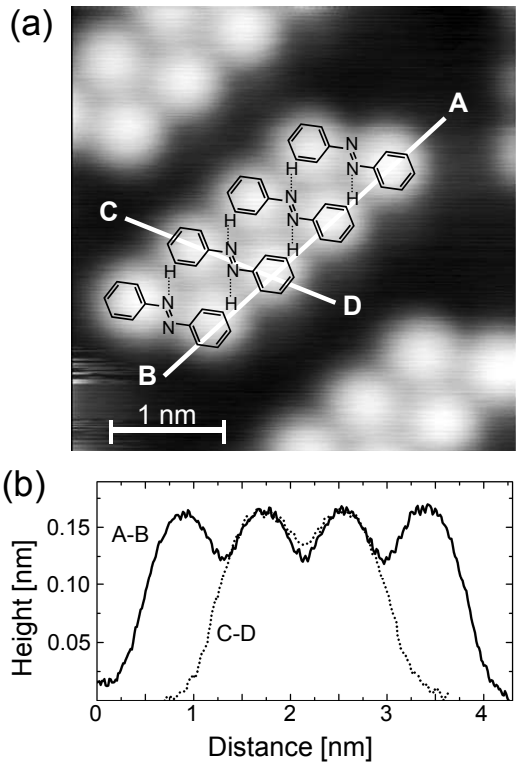

Figure 4.2: (a) Close-up STM image of a short chain of azobenzene molecules confined to the fcc region of the Au(111) herringbone surface reconstruction (5 × 5 nm, −1.25 V, 50 pA, 35 K). Proposed molecular structure indicated by overlay (dotted lines represent hydrogen-like bonds). (b) Cross-sectional topographic line scans along the directions marked in (a).

arranges the azobenzene molecules in a crisscross fashion. Phase II has a lower packing fraction than phase I and is observed less often. Unlike phase I, the positions and orientations of individual azobenzene molecules in phase II are distinguishable [figure 4.3(c) inset].

4.4 Near Saturation Coverage: Ordered Vacancy Arrangement

Commensurability with the herringbone reconstruction is regained at slightly lower coverage (∼20% below the phase I saturation coverage) through an ordered vacancy structure that extends across the molecular layer. This can be seen in figure 4.4 where dark vacancies (typically the size of a single azobenzene molecule) orient themselves in either of the two directions 120° from the herringbone domain walls. The oriented vacancies form domain structures as outlined in the figure 4.4 overview image. Close-up images of the vacancy

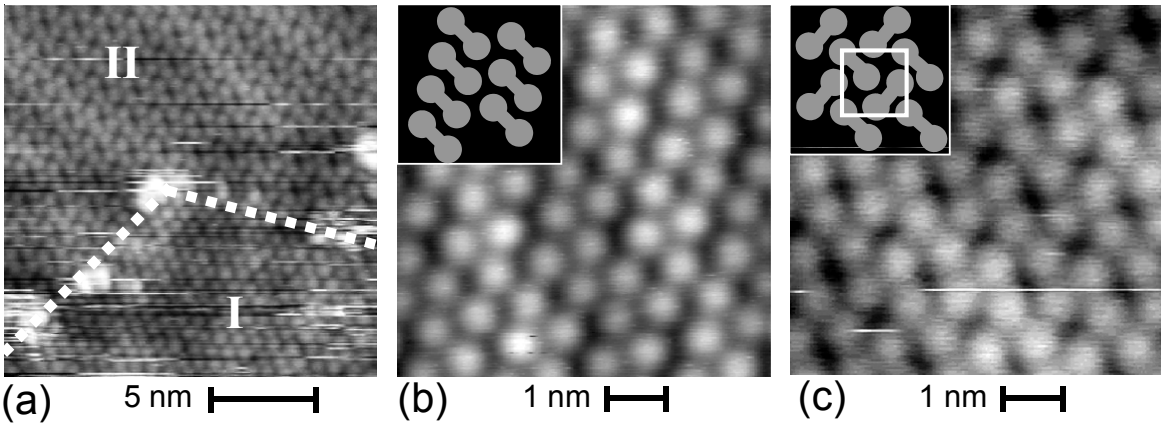

Figure 4.3: STM images of the saturation coverage (∼1 ML) of azobenzene on Au(111) surface (1.5 V, 25 pA, 90 K). (a) Large-scale image (18 × 18 nm) shows coexistence of two incommensurate phases, labeled I and II. The dashed line marks phase boundary. (b) Close-up image of phase I (6 × 6 nm). Inset: a diagram of a possible phase I molecular arrangement. (c) Close-up image of phase II (6 × 6 nm). Inset: the diagram of the phase II molecular arrangement with the unit cell marked by white box overlay.

structure (inset) show that molecular segments four units long exist between the ordered vacancies.

4.5 Molecule-Molecule and Molecule-Surface Interaction

The ordering of azobenzene molecules on the Au(111) surface is determined by the interplay of intermolecular and molecule-surface interactions. At low coverage, intermolecular interactions, which likely arise from a dipole-dipole interaction enhanced by hydrogen-like bonds, dominate short-range order. The hydrogen-like bond is formed between the unshared electron pair of a nitrogen atom of one azobenzene molecule and the net positive hydrogen atoms of the phenyl ring of another molecule [see overlay of figure 4.2(a)]. The ordering of azobenzene molecules on the Au(111) surface is determined by the interplay of intermolecular and molecule-surface interactions. At low coverage, intermolecular interactions, which likely arise from a dipole-dipole interaction enhanced by hydrogen-like bonds, dominate short-range order. The hydrogen-like bond is formed between the unshared electron pair of a nitrogen atom of one azobenzene molecule and the net positive hydrogen atoms of the phenyl ring of another molecule [see overlay of figure 4.2(a)]. Neighboring chains are unable to form these stabilizing hydrogen-like bonds, and are possibly repelled by the positive charge distribution around the outer edges of the azobenzene chains (e.g.,

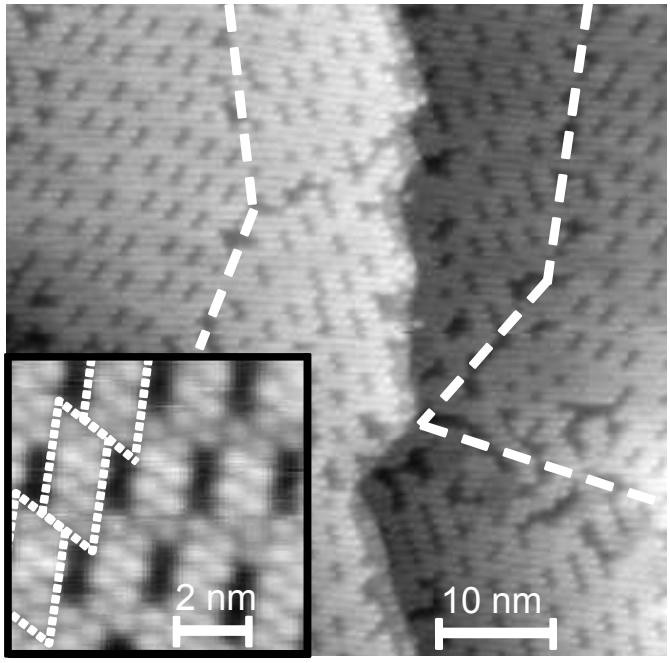

Figure 4.4: STM image of 0.8 ML coverage of azobenzene on Au(111) surface (58 × 58 nm, 1.0 V, 25 pA, 35 K) showing ordered molecular vacancies (dark elongated depressions). The domains of aligned vacancies are separated by boundaries marked with dashed lines. Inset: close-up image (8 × 8 nm) of a vacancy domain showing the short-range molecular ordering of four-molecule-long chains (outlined by the dotted lines).

such a mechanism was suggested for 1-nitronaphthalene chains by Bohringer *et al.*) [42].

Molecule-surface interactions are likely van der Waals in nature and play two roles in the ordering of azobenzene molecules. First, at larger distance scales, molecule-surface interactions induce the azobenzene chains to order with respect to the large scale periodicity of the underlying herringbone surface reconstruction. This commensurability indicates a weak repulsion between azobenzene molecules and the domain boundaries between the fcc and hcp regions of the herringbone reconstruction (the surface ridges). This repulsion is strong enough to retain molecular commensurability even after the azobenzene molecules are converted from the straight phase to the zigzag phase via STM-tip manipulation. The second way in which the molecule-surface interaction influences the molecular ordering is in determining the allowed orientations of the straight azobenzene chains. Straight chains orient only in the three equivalent surface directions following the sixfold symmetry of the Au(111) hcp and fcc lattices.

In the high-coverage saturation regime, where molecules are tightly packed, intermolecular interactions dominate over molecule-substrate forces, and the resulting phases thus do not order with the herringbone reconstruction. Surprisingly, however, the herringbone

reconstruction does exert an influence on the behavior of azobenzene film vacancies. The vacancies appear to repel each other and the combination of mutual repulsion and herringbone surface interaction leads to the ordered structure. Vacancy repulsion might arise from electrostatic charge accumulation at the edges of short adjacent azobenzene chains, in a mechanism similar to straight chain repulsion in the low coverage regime.

4.6 Conclusion

We have observed a variety of ordered azobenzene molecular structures whose commensurability with the underlying Au(111) herringbone reconstruction is governed by a coverage-dependent competition between intermolecular and molecule-surface interactions. In the low coverage regime, intermolecular interactions determine the short-range order, leading to the formation of molecular chain structures. Long-range ordering of the chains, on the other hand, is dominated by the molecule-surface interaction and leads to chain orientations commensurate with the herringbone reconstruction. In the saturation coverage regime, intermolecular interactions determine both short- and long-range order, leading to molecular arrangements that are incommensurate with the herringbone reconstruction. At coverages only slightly below saturation, however, commensurability is recovered for azobenzene vacancies. The coverage dependent structures observed here, in addition to the tip-induced phase conversion behavior, show that azobenzene molecular self-assembly can be controlled at the nanoscale.

Chapter 5

STM Manipulation of Azobenzene on Au(111)

5.1 Introduction

Molecular electronics promises a new generation of devices with potential advantages in speed and functionality [2, 61, 62]. "Bottom-up" fabrication using a STM tip has been pursued as one technique for creating prototype molecular structures and testing their properties. Various structures have been assembled and tested using this technique, including adatom structures [63, 29, 64, 65], porphyrin [66, 49, 67], fullerene [68], and other molecular assemblies [69, 70]. These systems allow electronic, magnetic, and mechanical properties to be tuned at the nanometer scale. Azobenzene molecules are of particular interest for molecular manipulation because they offer the possibility of coupling optical excitations with mechanical degrees of freedom at the single molecule level. This arises from the fact that azobenzene consists of two phenyl rings joined by two double-bonded nitrogen atoms, and is known to transition between metastable *cis* and *trans* configurations when optically excited in solution [71, 13].

Here we demonstrate several different techniques for manipulating azobenzene molecules using an STM tip. The first involves rotational bistable switching of individual molecules anchored at defect sites on a Au(111) surface. The second involves lateral manipulation of individual azobenzene molecules via a tip-controlled sliding mechanism. The third technique involves the creation of stable molecular anchor sites on the surface via voltage pulsing of the STM tip.

We performed our measurements using the home-built variable-temperature ultrahigh vacuum STM (base pressure $<5 \times 10^{-11}$ Torr). All of our experiments were performed on a Au(111) substrate that was cleaned by repeated cycles of Ar-ion sputtering and annealing. Azobenzene molecules were leaked into the vacuum chamber and deposited onto the Au(111) substrate at room temperature. After azobenzene exposure, the sample was transferred to the STM which was operated between 34 K and room temperature. Tunneling currents were kept below 100 pA for stable imaging.

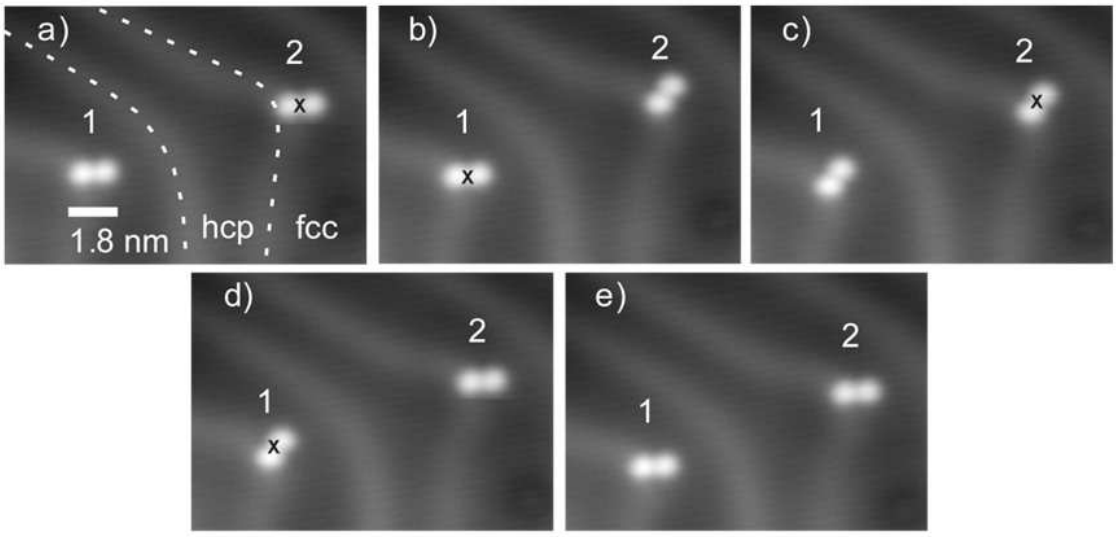

Figure 5.1: A low temperature (T=34 K) STM manipulation sequence: isolated azobenzene molecules on the Au(1111) surface are selectively and reversibly switched by STM tip voltage pulses. An "X" marks the position of the tip above a selected molecule just before a tip voltage pulse causes that molecule to rotate (as seen in each following image). The dotted lines in (a) trace the Au(111) herringbone surface reconstruction domain walls separating hcp and fcc domains. The imaging parameters are −1.25 V, 50 pA.

5.2 Rotating Single Molecule

At low azobenzene coverages (<0.1 ML), we observe individual molecules anchored to "kinks" of the Au(111) reconstruction, as shown in figure 5.1. This is in contrast to the self-assembled parallel chain structures observed at higher azobenzene coverage [72]. The low coverage images in figure 5.1 were taken at a reduced temperature of 34 K to hinder lateral molecular diffusion. Single azobenzene molecules appear as pairs of bright protrusions, marking the phenyl rings of the molecule. The Au(111) herringbone reconstruction can be observed in the background as parallel pairs of slightly elevated surface ridges [traced by dashed lines in figure 5.1(a)]. Single molecules adsorb at the kink site of the herringbone reconstruction and orient outwards from the kink in either of two equivalent directions at ±30° to the direction bisecting the kink.

Using tip-induced voltage pulsing we are able to toggle individual azobenzene molecules between these two orientation states. This process can be seen for two azobenzene molecules (molecules 1 and 2) in figures 5.1(a)−(e). Figure 5.1(b) shows the orientational change of molecule 2 after it has been subjected to a single 1 μs long, −3 V pulse (increased from a −1.5 V sample bias) while the STM tip is positioned above the molecules center. Upon pulsing, molecule 2 rotates counterclockwise by 60. Molecule 1 was unaffected by the nearby

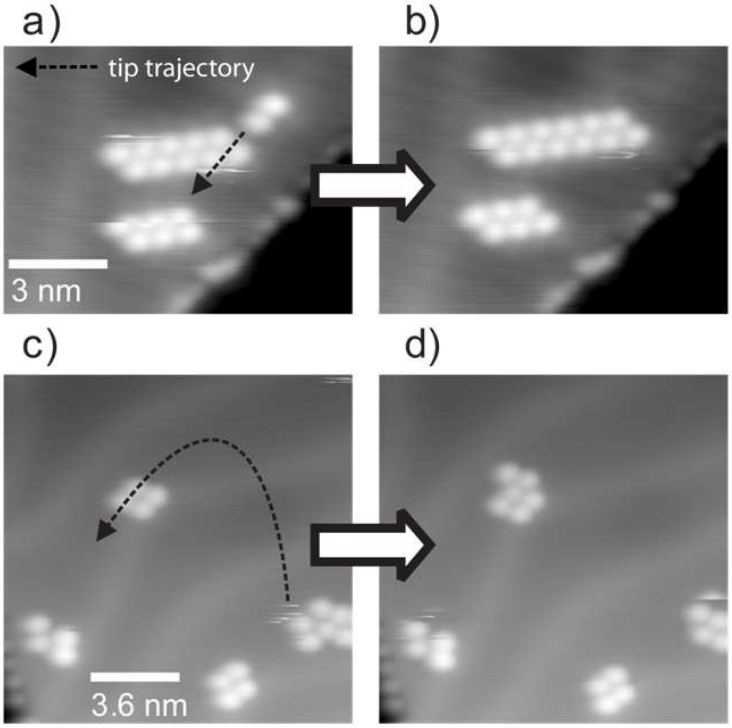

Figure 5.2: Two low temperature (T=36 K) STM sequences demonstrating lateral manipulation of single azobenzene molecules enabling molecular chain construction. Dotted lines indicate path of STM tip during manipulation. (a) and (b) Isolated single molecule is removed from a kink site and attached to the end of a five-member chain. (c) and (d) A single molecule is removed from a three-member chain and attached to the end of a two-member chain. The imaging parameters are −1 V, 50 pA.

voltage pulse to molecule 2. Figure 5.1(c) shows molecule 1 after it has been subjected to the same manipulation procedure, and subsequently has rotated. This manipulation process is completely reversible, as seen in figures 5.1(d) and 5.1(e), which show molecules 1 and 2 returned to their original states after the application of additional identical pulses. The switching success rate per tip voltage pulse depends on the detailed configuration of the STM tip apex. Different tips yielded success rates from 40% to near 100% under similar voltage pulsing conditions. For a given STM tip, the switching success rate did not depend sensitively on either the precise lateral tip position above the molecule or the tip voltage pulse width or amplitude. For most tips, the −3 V, 1 μs voltage pulse amplitude and width used above was found to be optimal within a parameter range of −6 to 7 V and 1 to 1000 μs.

5.3 Constructing Molecular Chain

In addition to rotating azobenzene molecules around anchor-sites, we are also able to slide them laterally across the Au surface using the STM tip. This has been used to change the length of one-dimensional azobenzene chains. Figure 5.2 shows two demonstrations of this ability. In figure 5.2(a), a single azobenzene molecule residing at a kink site is pulled onto the end of a five-member azobenzene chain to create the six-member chain seen in figure 5.2(b). Figure 5.2(c) shows a single azobenzene molecule being detached from one short azobenzene chain and then being reattached to the end of a different small chain [figure 5.2(d)]. The "sliding" technique [28] was employed to achieve both manipulations with typical moving parameters of 50 mV, 600 pA.

Successful manipulation of azobenzene molecules via the sliding technique is hindered by the fact that azobenzene adsorbates bind stably only to surface defects or molecular clusters at the temperature investigated (T=34 K). Events that cause the tip to lose contact with the molecule during manipulation thus free the molecule to instantly diffuse away from the tip towards distant binding sites. We found that the most reliable technique for precisely positioning azobenzene molecules is to move the STM tip (with a captured azobenzene molecule) across fixed molecular chains from one side to the other [as indicated by the dashed lines in figures 5.2(a) and 5.2(c)], thereby allowing the chains to capture the manipulated molecule from the tip.

5.4 Creating Molecular Anchor Site

At higher sample temperatures (T>50 K), azobenzene molecules diffuse freely across the surface and do not bind singly at kink sites or even in the molecular chains of figure 5.2. Figure 5.3(a) shows an image of a Au(111) surface at T =50 K that has a coverage of azobenzene equal to the coverage seen in figure 5.2. However, the Au(111) terrace appears free of azobenzene molecules (although there is some step edge adsorption). Azobenzene molecules on the terrace diffuse too quickly to be observed by the STM tip, but appear as increased "flicker" noise in our images.

We find that it is possible to bind diffusing azobenzene molecules at this temperature to artificial anchor sites positioned on the Au(111) terraces. These anchor sites are created by applying voltage pulses to the STM tip. Figure 5.3(b) shows the results of applying a -6 V, 1 μs long pulse to the location marked "X" in the previously clean region of figure 5.3(a). Two immobilized clusters of azobenzene molecules are subsequently found in that region: a cluster of ten molecules at the precise location of the tip pulse and a smaller satellite cluster of three molecules. A second identical tip voltage pulse applied to the spot marked "X" in figure 5.3(b) creates a new cluster of seven molecules [seen in figure 5.3(c)]. The voltage pulsing parameters of -6 V, 1 μs used above were generally optimal for this manipulation category, although the threshold for manipulation was typically -4 V, 1 μs.

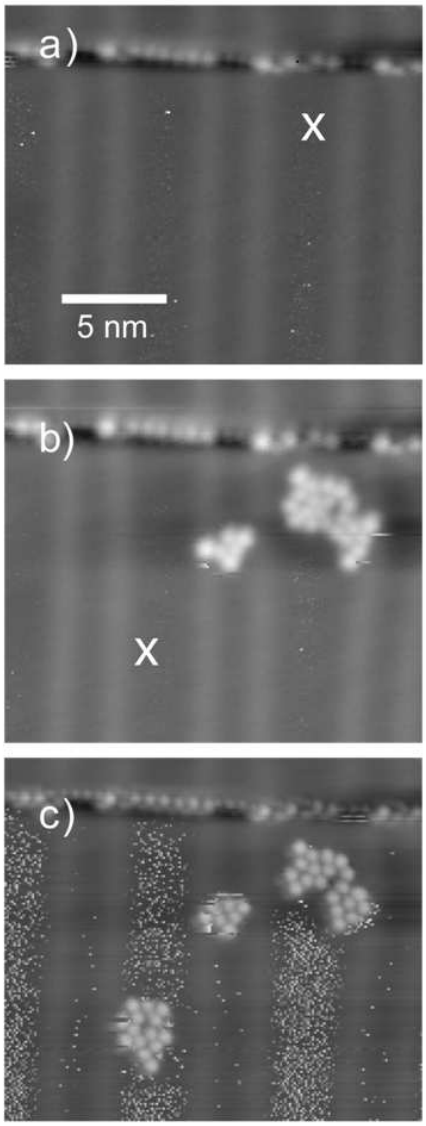

Figure 5.3: The anchor-site creation manipulation at T=50 K. The tip voltage pulse (−6 V, 1 μs) at the position marked by "X" in (a) subsequently creates a region of stably adsorbed molecular clusters as seen in (b). A second pulse indicated by an "X" in (b) creates the additional cluster seen in (c). Differences in image quality are caused by slight tip changes during the manipulation process. The imaging parameters are −1 V, 50 pA.

5.5 STM Manipulation Mechanism of Azobenzene on Au(111)

We now discuss possible physical mechanisms involved in the three azobenzene manipulation modes that we have observed. We begin with the bistable orientational switching. The bistable orientational states of single azobenzene molecules bound to kink sites are clearly influenced by the surface and molecular symmetries. As illustrated in the sketches of figure 5.4(a), the close-packed Au(111) surface atoms and the azobenzene phenyl rings both possess a quasi-sixfold symmetry. The herringbone kink defect breaks this symmetry and induces local minima in two of the six possible configurations. Voltage pulsing above a molecule either reduces the energy barrier between the two orientation configurations, allowing thermal activation between states, or it may directly provide enough energy to the molecule to excite it above the rotational barrier. The latter mechanism has been observed previously in single molecule systems such as acetylene on Cu(100) [69], and *cis*-2-butene on Pd(110) [70].

Our ability to laterally manipulate azobenzene is influenced by the fact that azobenzene molecules bond to each other only in specific configurations, most likely due to a modified hydrogen-bonding mechanism [72, 42]. This causes laterally manipulated azobenzene molecules to "snap" precisely onto the ends of chains in perfect alignment [see figure 5.4(b) sketch]. Molecules cannot be stably positioned on a terrace in the absence of a defect or stationary molecular cluster because the azobenzene diffusion barrier is so low on Au(111) (even at a reduced temperature of T=34 K).

The third manipulation technique, anchor-site creation, is useful in this context because it allows the definition of positions on a metal terrace that can serve as the starting point of an artificial molecular nanostructure. The mechanism of anchor-site creation involves an irreversible change at the gold surface that creates a defect binding site. Because the gold surface near the anchor site appears undamaged, we believe that the creation of the anchor site is due to tip-induced damage to azobenzene molecules diffusing beneath the tip during the voltage pulse. This proposed mechanism is sketched in figure 5.4(c). Here damaged azobenzene molecules bind to the surface beneath the tip, and provide a stationary point for other diffusing molecules to collect. Damage to molecules might include hydrogen atom dissociation or even phenyl ring opening or dissociation. Phenyl ring dissociation is suggested by the frequent observation of clusters made up of *odd* numbers of lobes. This technique is similar to other tip-induced lithography techniques that involve the cracking of a background gas in the junction region beneath the tip to deposit various substances [73, 74]. The difference here is that in our case the reservoir of molecules is a 2D gas diffusing on the surface rather than a 3D gas diffusing through the vacuum chamber.

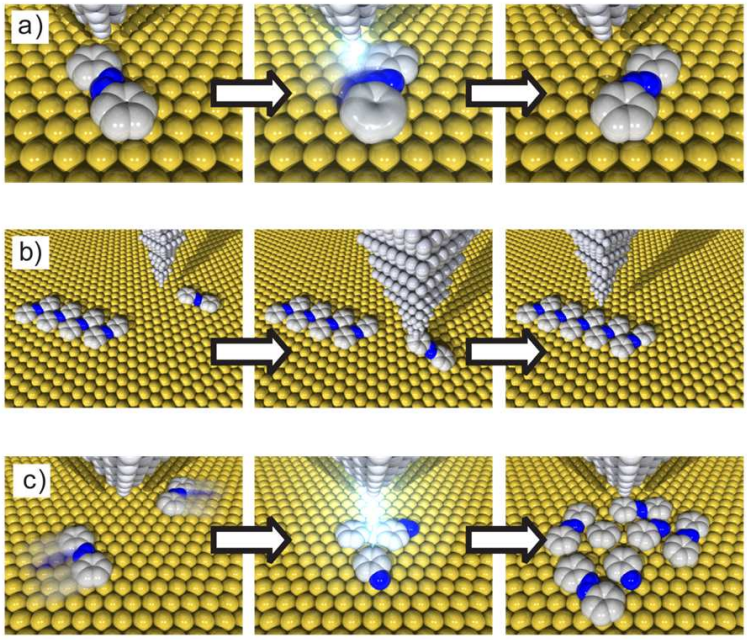

Figure 5.4: Three sketches illustrating azobenzene manipulation techniques. (a) Bistable rotational switching: a single azobenzene molecule is induced by a tip voltage pulse to rotate clockwise by 60°. (b) Lateral translation: an isolated azobenzene molecule is bound to the STM tip and slid to join a four-member azobenzene chain. (c) Anchor-site creation: azobenzene molecules diffusing beneath the STM tip are damaged by a voltage pulse, causing them to bind to the surface and create a stable cluster.

5.6 Conclusion

We show that azobenzene molecules can be manipulated in a number of ways on the Au(111) surface. Single azobenzene molecules adsorbed at herringbone kink sites are bistable and can be reversibly switched between two configurations. Lateral STM manipulation can be used to shuttle single molecules between anchor sites, allowing the construction of molecular structures. At higher temperatures, where azobenzene undergoes strong thermal diffusion, STM tip voltage pulses can be used to create new anchor sites for molecular clustering.

Chapter 6

Reversible Photoswitching of TTB-Azobenzene on Au(111)

6.1 Introduction

The conversion of light to mechanical motion at the molecular level provides exciting possibilities for nanomachine control and characterization, including high frequency and noncontact operation [4, 54]. Progress in this area has occurred through the investigation of solution-based molecular machine ensembles [75], organic polymers capable of light-induced expansion and contraction [14, 13], light-controlled ion channels [15], and other surface-molecule systems [76, 77, 78]. A common motif here is to employ molecular subunits, such as azobenzene, known from ensemble measurements to reversibly transform from one isomeric state (e.g., *trans*) to another (e.g., *cis*) upon absorption of light [12]. A central concern is what strategies might be used to reversibly and optically control the mechanical state of a single, addressable molecule, and how such strategies are influenced by the coupling between a molecule and its environment.

In order to explore this issue, we have used scanning tunneling microscopy (STM) to spatially resolve the features of individual azobenzene molecules on a gold surface before and after reversibly cycling their mechanical structure between *cis* and *trans* states via photoisomerization. This procedure is different from previous STM tip-induced molecular manipulation studies [79, 20, 21, 22] in that it is performed in the absence of an STM tip, it explores a different physical regime (i.e., photomechanical coupling), and it offers the flexible dynamical control inherent to optical processes.

We achieved reversible single-molecule photoisomerization by engineering azobenzene molecules to increase their surface photomechanical activity. While gas- and solution-phase azobenzene molecules readily photoisomerize [12], this process can be quenched at a surface by molecule-surface coupling [17, 53, 80]. We therefore attached *tert*-butyl "legs" (TB: C_4H_9) to an azobenzene scaffold ($C_{12}H_{10}N_2$) to reduce this coupling. When illuminated by UV light, azobenzene molecules made with zero or two TB legs did not photoisomerize when placed on a gold surface, but azobenzene molecules with four attached TB legs

did. Single-molecule photoisomerization was confirmed unambiguously by the reversibility of the photoreaction and by comparing experimentally resolved intramolecular features of single *trans* and *cis* azobenzene molecules with *ab initio* simulations. The "transition" that we observe from quenched to active photomechanical behavior reveals the importance of electromechanical coupling between a molecule and substrate.

We performed our measurements using a home-built variable-temperature ultrahigh vacuum STM. Two-legged 4,4'-di-*tert*-butyl-azobenzene (DTB-AB) and four-legged 3,3',5,5'-tetra-*tert*-butyl-azobenzene (TTB-AB) were synthesized via oxidative coupling reactions of 4-*tert*-butyl-aniline and 3,5-di-*tert*-butyl-aniline, respectively [81]. *Trans* isomers of the molecules were deposited via leak valve and Knudsen cell techniques onto clean Au(111) substrates held at 30 K. Samples were then annealed at room temperature for 10 min in order to achieve ordered molecular arrangements. STM images were acquired in the temperature range of 25 to 30 K using tunnel currents below 50 pA for stable imaging. A cw diode laser at an external viewport provided UV radiation at 375 nm with an average intensity of 90 mW/cm^2 at the sample surface. During UV exposures the STM tip was retracted and the sample temperature was maintained between 28 and 32 K.

6.2 Lifting Azobenzene Derivatives from Au(111)

The STM images in figure 6.1 reveal the differences between adsorbed bare azobenzene (no TB legs), DTB- AB (two TB legs), and TTB-AB (four TB legs). Bare azobenzene molecules [figure 6.1(a)] appear as pairs of closely touching lobes, with each lobe indicating the position of a single phenyl ring [79, 72]. Individual DTB-AB molecules [figure 6.1(b)] similarly appear as a pair of lobes, except that the DTB-AB lobes are separated by a wider gap. Individual TTB-AB molecules [figure 6.1(c)] appear as four-lobed structures [22]. The appearance of DTB-AB and TTB-AB is consistent with their expected TB-leg arrangements [see models in figures 6.1(b) and 6.1(c)]. Constant-current line scans across the azobenzene derivatives [figure 6.1(d)] show that the DTB-AB and TTB-AB molecules are progressively taller than bare azobenzene molecules. Hence, molecular engineering using TB-leg functionalization [66] achieves progressive "lifting" of photomechanical molecules away from a surface.

6.3 Photoisomerization of TTB-AB on Au(111)

The photomechanical activity of this series of azobenzene derivatives was checked by illuminating each type of molecular adsorbate separately with an equal exposure to UV light. Successful UV-induced switching was observed only for the four-legged TTB-AB molecules. Figure 6.2 shows the same island of TTB-AB molecules on Au(111) before and after a 3 h exposure to UV light. Before UV exposure the island is uniformly composed of the *trans* isomer. After UV exposure the emergence of new, bright protrusions can be seen in the island. While *trans*-TTB-AB molecules display four peripheral lobes before UV

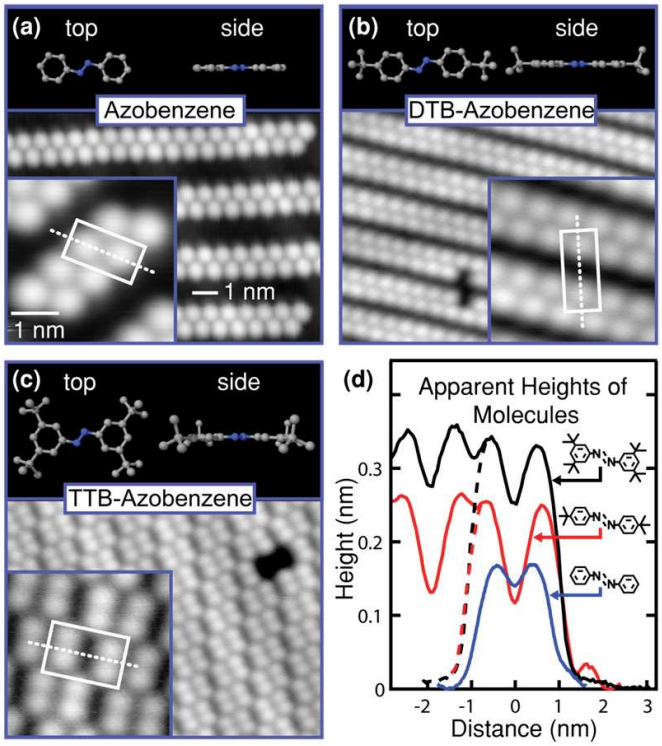

Figure 6.1: STM constant-current images of functionalized azobenzene molecules on Au(111) (T = 30 K, V = -1 V, I = 25 pA, images are scaled identically): (a) bare azobenzene, (b) DTB-AB, (c) TTB-AB. Upper panels show chemical structure of the *trans* isomers of the imaged molecules. Single-molecule images are identified by white boxes in insets [dotted line in each box shows line scan trajectory for (d)]. (d) Line scans across different functionalized molecules show apparent height on Au(111). DTB-AB and TTB-AB line scans were taken at the edge of islands. Dashed part of the line scan provides a guide to the eye for identifying single-molecule width.

illumination, the UV-transformed TTB-AB molecules display only three peripheral lobes along with a new, bright (i.e., "tall") feature near the center of the molecule (figure 6.2 insets and figure 6.3). Approximately 4% of *trans*-TTB-AB molecules photoswitch to the new "three-lobe state" after a 1 h UV exposure at 90 mW/cm^2. For comparison, *trans*-TTB- AB in solution (dilute 24 μM in chloroform) switched to 65% *cis* after exposure to 145 mW/cm^2 of 378 nm UV light for 6 min, yielding an approximate solution-based switching rate of greater than 50 times the surface-based rate.

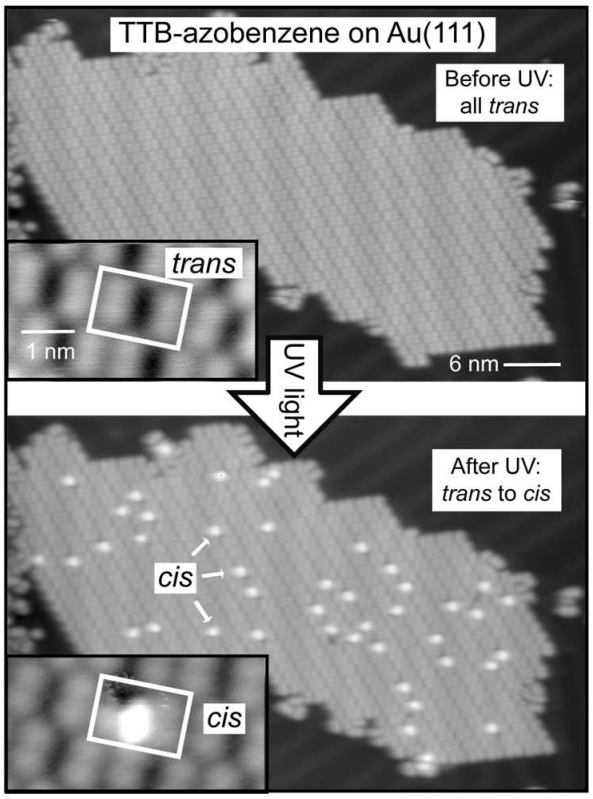

Figure 6.2: Photoisomerization of individual TTB-AB molecules on Au(111) from *trans* to *cis*. Same island of TTB-AB molecules is shown before (upper image) and after (lower image) a 3 h exposure to 90 mW/cm^2 UV irradiation at 375 nm. After UV exposure 45 TTB-AB molecules have switched from the *trans* to the *cis* state. Inset zoom-in images show UV-induced switching (before and after) from *trans* to *cis* for a single molecule (identified by white box).

6.4 Reversible Photoisomerization

The observed photomechanical switching can be optically reversed for single molecules by reexposing the molecules to UV light. Figure 6.3 shows one particular TTB-AB molecule undergoing a complete cycle of reversible photoswitching (*trans* state → three-lobe state → *trans* state). The reversibility of the photoswitching provides strong evidence that the three-lobe state is indeed the *cis* isomer of TTB-AB, since reversibility rules out other possible structural change mechanisms such as photodissociation (STM tip-based molecular manipulation in the absence of photons can also achieve similar structural transformations [22]).

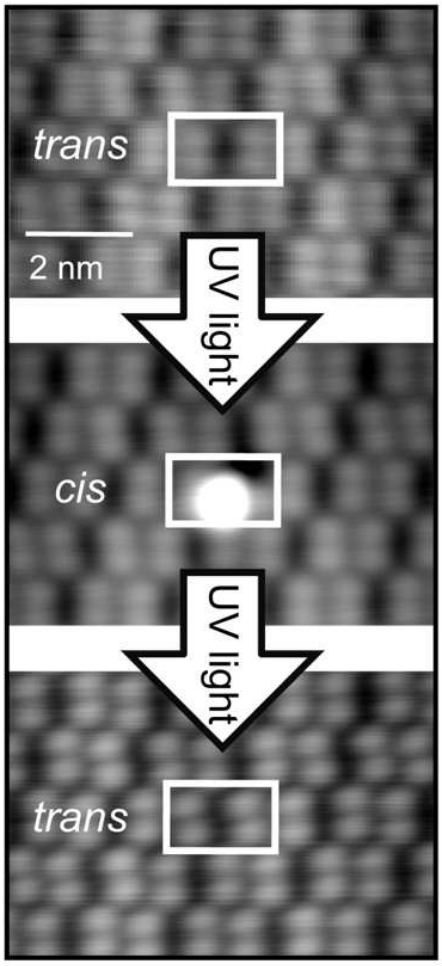

Figure 6.3: Reversible photoinduced switching is observed for a single TTB-AB molecule. The same individual TTB-AB molecule (identified by white boxes in three successive panels) is shown before and after two successive exposures to UV light. The molecule starts out in the *trans* state (top panel), is then switched to the *cis* state after the first exposure to UV light (middle panel), and is then switched back to the *trans* state after a second exposure to UV light (bottom panel).

6.5 DFT Simulation

Ab initio density functional theory (DFT) calculations predict TTB-AB *cis* and *trans* isomer appearances very close to the experimentally observed molecules [figure 6.4]. Local density of states (LDOS) calculations were performed for isolated *trans*- and *cis*-TTB-AB molecules using the SIESTA code [82] (similarly to Ref. [25] but with the generalized-gradient approximation (GGA) [83]). The *trans* and *cis* isomer molecular structures were

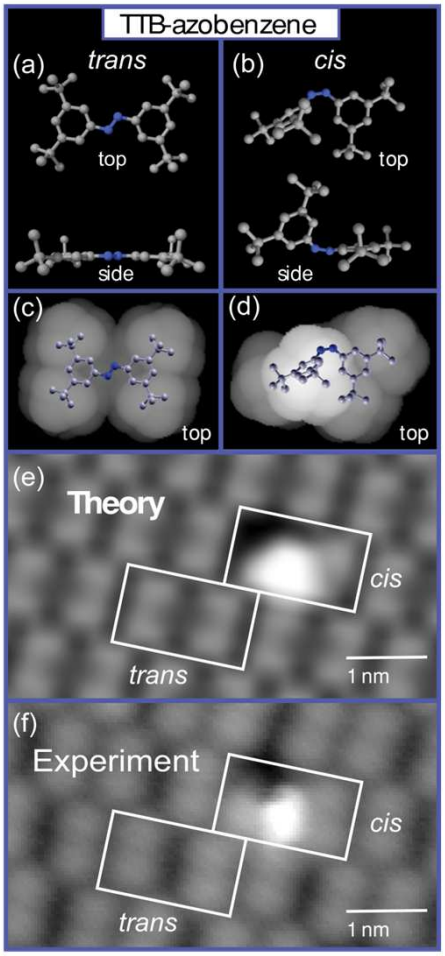

Figure 6.4: Simulated *trans*- and *cis*-TTB-AB structures compared to experiment. (a) Calculated *trans* geometry. (b) Calculated *cis* geometry. (c) Calculated *trans* LDOS integrated from EF to EF−1 eV, at an isosurface about 3 Å away from the nearest atoms. (d) Calculated *cis* LDOS isosurface [same parameters as in (c)]. (e) Simulated STM image of TTB-AB using tiled single-molecule LDOS isosurfaces from (c) and (d) (image has been smoothed using a 0.2 nm width Gaussian blur filter to approximate experimental convolution with the STM tip). (f) Experimental STM image of TTB-AB molecules including one photoisomerized *cis* isomer.

optimized via energy minimization [figures 6.4(a) and 6.4(b), *cis* CNNC and CCNN angles are 11° and 47°, respectively], and isosurfaces of HOMO orbital LDOS were calculated to simulate STM images. The simulated *trans* isomer STM image is dominated by four peripheral lobes at the TB-leg positions [figure 6.4(c)]. The simulated *cis* isomer STM image shows a bright central area due to the upwards rotation of one TB-leg, leaving the three remaining TB legs on the periphery below [figure 6.4(d)]. A simple tiling of the calculated

trans and *cis* isomer simulated images using experimentally observed lattice positions [figure 6.4(e)] shows that the simulated *trans* and *cis*-TTB-AB images match the experimental data [figure 6.4(f)] quite well.

6.6 Photoisomerization Mechanism

All of the azobenzene molecules studied here photoisomerize easily in solution and so it is clear that the change in environment at a surface plays a role in modifying molecular photoswitching behavior. The influence of a surface on molecular photoswitching can be divided into three general mechanisms: (i) *Steric hindrance*: molecules lose the freedom to change conformation if atomic motion is constrained by either the surface or neighboring molecules [12]. (ii) *Electronic lifetime effects*: if the surface-modified lifetime of photoexcited electrons is less than the time it takes for a molecule to complete a conformational change then photoswitching can be quenched [12, 17, 80]. (iii) *Substrate-induced changes in optical absorption*: hybridization between an adsorbed molecule and a surface can change the optical absorption spectrum (and subsequent photoswitching properties) of a molecule [17]. A recent theoretical study proposes that, analogous to the Franck-Condon principle, coupling between molecular and substrate electromechanical degrees of freedom (e.g., dissipative modes such as phonons) can quench the optical absorption necessary for azobenzene *cis* $\leftrightarrow$ *trans* photoswitching [80].

We believe that steric hindrance due to gold surface attachment is not the cause of quenching, as follows: azobenzene bonds weakly to gold (physisorption limit) [79]; we observe similar surface diffusion rates for the different azobenzene derivatives, and STM tip-pulsing experiments show that it is possible to isomerize bare azobenzene on gold using tip-manipulation techniques [21]. Steric hindrance due to molecule-molecule interactions within islands is also not likely to play a dominant role in photoquenching. Molecule-molecule bonding appears weak because we can easily separate azobenzene molecules without damage using STM manipulation and we also measure a very low melting point (approximately 50 K) for islands of all three azobenzene species. Furthermore, molecules at the boundaries of islands (which have fewer nearest neighbors compared to interior molecules) show identical photoswitching to interior molecules.

Our observation of an increase in azobenzene photoswitching rate as the molecule is lifted off the surface is consistent with quenching mechanisms (ii) and (iii). We find these possibilities difficult to distinguish at present. Molecule-substrate electronic state hybridization can lead to both optical absorption shifts and changes in excited state lifetimes [17]. Recent theoretical work, however, predicts that increased hybridization of azobenzene to substrate dissipative modes will cause a sharp transition to completely quenched photoisomerization accompanied by gaps opening in optical absorption bands [80]. Future STM measurements of the dependence of single-molecule photoswitching on the wavelength of light, as well as new optical absorption measurements, will be useful in distinguishing the mechanisms that dominate photoswitching in this hybrid molecule-surface system.

6.7 Conclusion

We have experimentally observed reversible photomechanical switching for individual azobenzene molecules at a metal surface. Our measurements reveal the significance of environmental coupling in determining molecular photoswitching behavior. This effect will likely play an important role in future applications of molecular photoswitching in nanostructured condensed matter systems.

Chapter 7

Wavelength-Dependent Photoswitching of TTB-AB on Au(111)

7.1 Introduction

To eventually implement photomechanical molecules into useful devices, it is critical to determine how their rates for forward and reverse molecular switching depend on optical wavelength and surface environment. Azobenzene molecules in solution typically show a high forward (*trans*-to-*cis*) switching cross section for UV light excitation, which drives a majority of irradiated molecules to the *cis* state. When irradiated with visible light, the reverse (*cis*-to-*trans*) switching cross section typically dominates for molecules in solution, driving them into the *trans* state. The overall photoswitching activity of TTB-AB molecules at a surface has been observed to be substantially reduced compared to switching rates in solution, but the important asymmetry between forward and reverse switching rates for molecules at a surface has not been directly measured [107, 84].

We present direct measurements (based on single-molecule imaging) of both forward and reverse photoswitching cross sections for TTB-AB molecules on gold in response to UV and visible light excitation. We find that forward and reverse switching cross sections are comparable for UV light at 375 nm, a result similar to what is seen for molecules in solution phase at this wavelength. In a surprising departure from solution phase behavior, however, we also observe comparable forward and reverse molecular switching rates for visible light at 444 nm. This behavior has important implications for the design and control of surface-based photoswitching elements at the single molecule level.

Our measurements were performed by using scanning tunneling microscopy (STM) to directly image and precisely determine the number and configuration of photoswitching molecules as a function of optical exposure. The STM is a homebuilt variable-temperature ultrahigh vacuum instrument with optical access to the sample. cw lasers aligned at an external view port provided UV (375 nm) and blue (444 nm) radiations at the sample surface

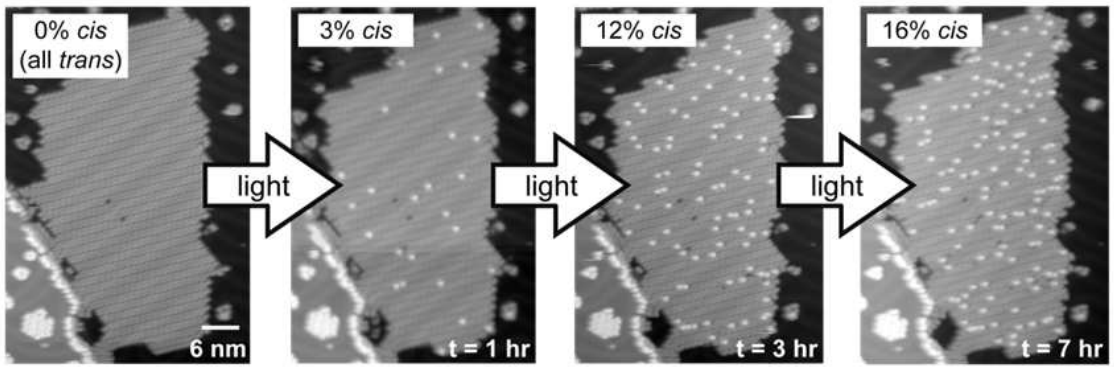

Figure 7.1: Sequential images of a single island of TTB-AB on Au(111) after successive exposures to 375 nm UV light. The first image is the preexposure configuration of uniformly *trans* isomers. The three following images were acquired after 1, 3, and 7 h total exposures to UV light.

with average intensities of 92 and 255 mW/cm^2, respectively. During laser exposures, the STM tip was retracted and the sample temperature was maintained between 28 and 35 K. TTB-AB molecules were synthesized via oxidative coupling reactions of 3,5-di-*tert*-butyl-aniline [81]. 0.1 Monolayer (ML) of the trans isomer of TTB-AB was deposited via Knudsen cell techniques onto clean Au(111) substrates held at 30 K. Samples were then annealed at room temperature for 10 min to achieve ordered monolayer-high islands of trans molecules. STM images were acquired in the temperature range of 30 K to 35 K by using tunnel currents below 50 pA for stable imaging.

7.2 TTB-AB Photoswitching Saturation

The fraction of surface-bound TTB-AB molecules that switch from the *trans* to the *cis* state increases with increased exposure to UV light (375 nm). Figure 7.1 shows a time series of images of the same island of TTB-AB molecules after successive UV light exposures. The first image shows the preexposure starting configuration, where the island is uniformly composed of TTB-AB molecules in the *trans* state. The three following images were acquired after total exposures of 1, 3, and 7 h to UV light. In these images, TTB-AB molecules that have been optically switched to the *cis* state can be clearly identified in the island by the presence of their bright lobes. The spatial distribution of the switched *cis* molecules is random. While the total fraction of molecules in the *cis* state increases with exposure, some individual molecules do reversibly switch from *cis* back to *trans* with continued exposure.

The total fraction of surface-bound molecules in the *cis* state as a function of UV light exposure can be seen in figure 7.2. The data shown are an average over many similar islands of TTB-AB molecules from the same sample that was subjected to the same light

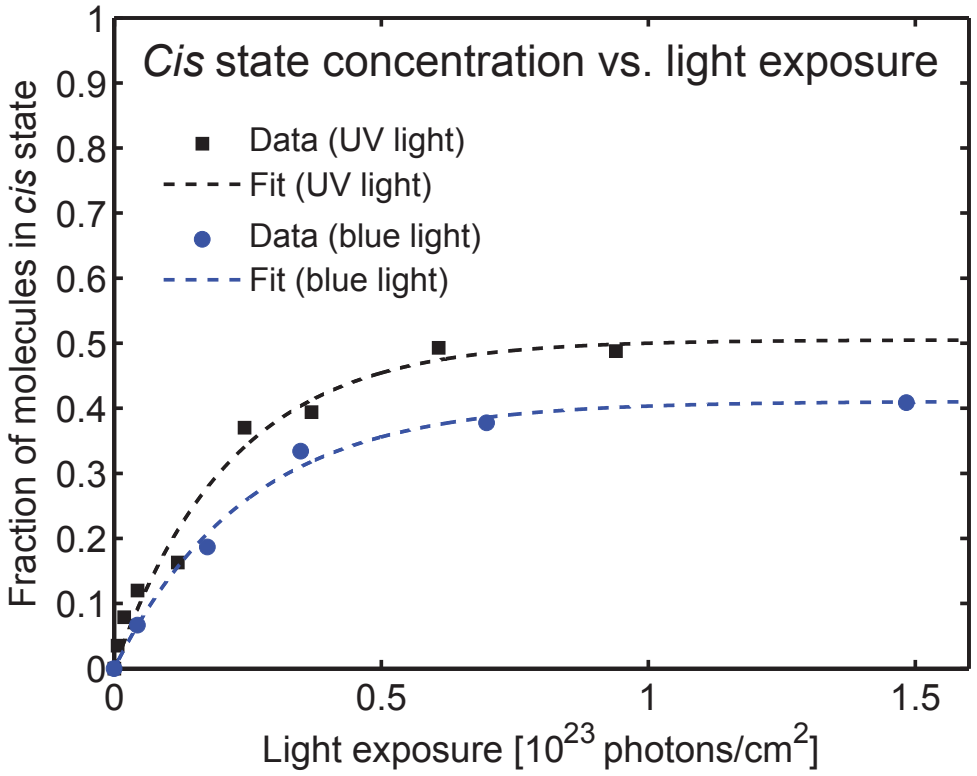

Figure 7.2: Concentration of *cis*-TTB-AB molecules on Au(111) plotted vs total photon exposure for both UV (375 nm) and blue (444 nm) light, revealing photoswitching saturation behavior. The plotted fraction of *cis*-TTB-AB molecules is an average over many similar islands on the same sample (statistical error is smaller than symbol size). Dashed lines are fits to data using the first-order rate equation discussed in the text.

exposure. The fraction of molecules in the *cis* state is seen to saturate to a photostationary condition with sufficient exposure to UV light. This photostationary condition exhibits a *cis* fraction of 50% (i.e., molecules are equally distributed between the *cis* and *trans* states). We performed similar measurements on TTB-AB molecules exposed to visible light (444 nm blue light, figure 7.2). Surface-bound TTB-AB molecules exposed to blue light also switch from *trans* to *cis*, but the blue light photostationary condition was achieved with a net conversion of TTB-AB to 41% *cis* (9% less than the UV saturation). This implies that the blue light is less efficient at switching molecules from *trans* to *cis* than from *cis* to *trans*, but these forward and reverse rates are still quite comparable. This behavior dramatically deviates from what is observed for molecules in solution at this wavelength, in which case forward *trans*-to-*cis* switching is typically diminished by a factor of 10 in comparison with reverse *cis*-to-*trans* switching [12].

Table 7.1: TTB-AB on Au(111) photoisomerization cross sections

	Φ_T (*trans* to *cis*) (cm^2)	Φ_C (*cis* to *trans*) (cm^2)
UV light (375 nm)	2.3×10^{-23}	2.3×10^{-23}
Blue light (444 nm)	1.7×10^{-23}	2.3×10^{-23}

7.3 Determination of Photoswitching Cross Sections

We can quantitatively determine the forward and reverse molecular switching cross sections for both UV and blue light exposures of TTB-AB on gold by using the saturation curves of figure 7.2. The probability of a molecule to be in the *cis* state is most easily described by the first-order rate equation,

$$\dot{C} = \Phi_T \times I \times T - \Phi_C \times I \times C. \tag{7.1}$$

Here, C and T represent the fraction of molecules in the *cis* and *trans* states, respectively, Φ_C and Φ_T represent the *cis*-to-*trans* (reverse) and *trans*-to-*cis* (forward) photoswitching cross sections, respectively, and I represents the photon flux. Eq. (7.1) can be analytically solved to yield the fraction of molecules in the *cis* state C versus photon exposure n (total photons per unit area),

$$C(n) = C(\infty)[1 - \exp^{-(\Phi_T+\Phi_C)n}], \tag{7.2}$$

where $C(\infty)$ is the measured saturation fraction of molecules in the *cis* state. The forward and reverse cross sections Φ_T and Φ_C are related to each other via the *cis* saturation concentration,

$$C(\infty) = \frac{\Phi_T}{\Phi_T + \Phi_C}. \tag{7.3}$$

Equation (7.2) can be fit to our data to determine both Φ_T and Φ_C. The best fits to the UV and blue wavelength data are plotted in figure 7.2. The fits quite nicely follow the experimental data and yield the cross sections, as shown in the Table 7.1. The fact that the fit matches the experimental data well implicitly indicates *cis*-*trans* photoisomerization of TTB-AB on Au(111) is a single-photon process.

7.4 Surface Photoswitching vs. Photoswitching in Solution

The biggest surprise in this data is that the blue light forward and reverse photoswitching cross sections are so similar for TTB-AB molecules on gold, in contrast to the strong difference seen in these cross sections for molecules in solution. Blue light-induced forward and reverse photoswitching cross sections for azobenzenes in solution (including TTB-AB) are typically 1×10^{-19} and 1×10^{-18} cm^2 respectively, differing from each other by an order

of magnitude [12, 107].

The presence of a surface alters molecular photoswitching rates through a number of factors, two of the most important being optical absorption and steric hindrance [12, 17, 80]. Molecules at a surface can hybridize with surface excitations, both electronic and vibrational, leading to changes in the distribution of optical absorption spectral lines and lifetimes [17]. The close proximity of a surface, as well as adjacent molecules, also introduces steric constraints on molecules (including both attractive and repulsive forces, e.g., TB leg surface binding) that can reshape conformational potential energy surfaces and switching dynamics. Molecular photoswitching rates are a product of optical absorption (which changes with shifts in the molecular excitation spectrum) and switching quantum efficiency (which depends on excited state lifetimes and steric hindrance) [12]. Because of this product relationship, STM experiments that measure switching rates are unable to easily distinguish between these different effects. It will, thus, be useful in the future to combine STM experiments with direct optical absorption measurements of *cis*- and *trans*-TTB-AB molecules at a surface to untangle these factors and allow a deeper understanding of local surface molecular photoswitching mechanisms.

7.5 Conclusion

We have directly measured the concentrations of *cis* isomers of TTB-AB on Au(111) that have been conformationally switched from *trans* via calibrated exposure to UV and blue lights. This has enabled us to determine both the forward and reverse photomechanical switching cross sections for each photon wavelength. We find that the visible light does not efficiently reverse the photoreaction for adsorbed molecules, contrary to what is seen for molecules in solution. Placing optically switching molecules on a surface, thus, creates new challenges for efficiently controlling their photomechanical behavior. Overcoming these challenges will require further engineering of photoswitching molecules and their nanoscale environments, as well as a deeper understanding of the dynamics of surface photoswitching.

Chapter 8

Patterned Molecular Photoswitching of TTB-AB on Au(111)

8.1 Introduction

In this section, we investigate how molecular photoswitching properties vary for different two-dimensional structural orderings of photoactive TTB-AB molecules at a gold surface. Scanning tunneling microscopy (STM) was used to image monolayer high islands of TTB-AB molecules having three different geometrical arrangements on Au(111). We find that the photoswitching properties of TTB-AB molecules are dramatically different for each of these three orderings. Molecular photoswitching rates were found to be either uniformly quenched or uniformly robust throughout a particular molecular assembly or to vary periodically in a way that creates self-patterned regions of locally quenched and locally robust photomechanical switching. The photoswitching behavior of a molecule at a surface is seen to depend strongly on its molecule-molecule interactions and its particular molecule-surface configuration. We show experimentally how these interactions lead to a correlation between local electronic structure and photoswitching probability.

We performed our measurements using a home-built variable-temperature ultrahigh vacuum scanning tunneling microscope. 3,3',5,5'-tetra-*tert*-butyl-azobenzene (TTB-AB) molecules were synthesized via oxidative coupling reactions of 3,5-di-tert-butylaniline [81]. *Trans* isomers of the molecules were deposited via Knudsen cell evaporation onto clean Au(111) substrates held at 30 K. Samples were then annealed at room temperature for 10 min. STM images were acquired in the temperature range of 25 K to 30 K using tunnel currents below 50 pA for stable imaging. Scanning tunneling spectroscopy (STS) was also performed on this molecular system, utilizing lock-in detection with a typical modulation frequency of 2 KHz and an amplitude of 20 mV. Point spectra were acquired in an open-loop mode (feedback off), while dI/dV maps were acquired in a closed-loop mode (feedback on). A cw diode laser aligned at an external viewport provided UV radiation at 375 nm with an average intensity of 90 mW/cmi^2 at the sample surface. During UV exposures, the STM tip was retracted and the sample temperature was maintained between 30 and 36 K.

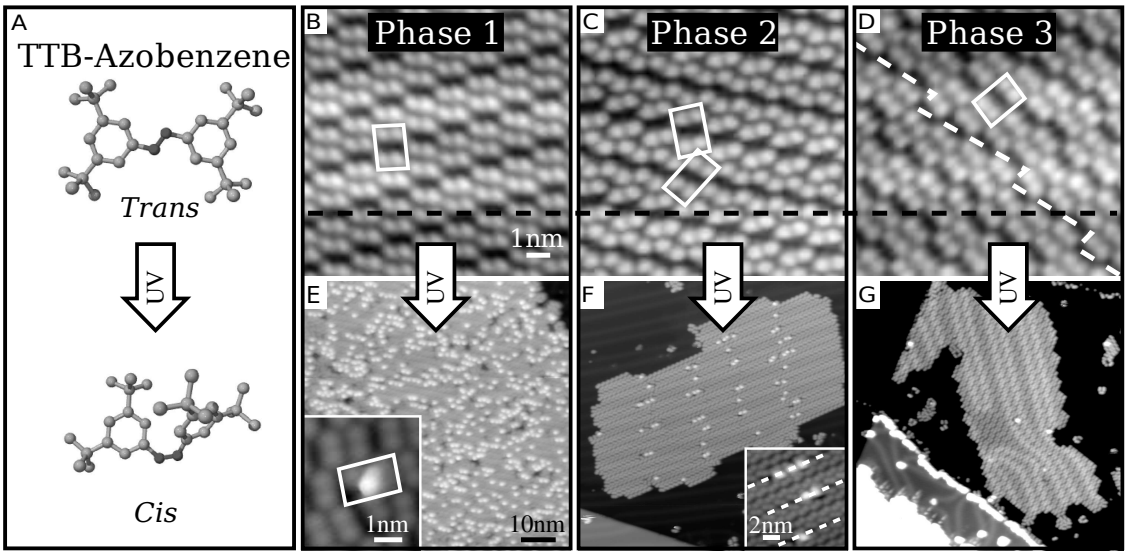

Figure 8.1: (A) Ball-and-stick models of *trans*- and *cis*-TTB-AB (from ab initio DFT calculations [107]). (B-D) Constant-current STM topographs of phase 1, 2, and 3 monolayer islands of *trans*-TTB-AB molecules on Au(111). Each white box surrounds a single molecule. All three images are oriented identically (HB ridges are parallel to dashed black line). Dashed white line in panel D shows phase 3 stacking faults. (E-G) Topographs of phase 1, 2, and 3 islands following 100 h of UV light exposure. *Cis* molecule positions indicated by the appearance of bright protrusions. (E inset) Close-up image of a single *cis* molecule. (F inset) Close-up image of a phase 2 island following UV exposure shows the photoisomerization orientation selectivity. The dashed white lines mark molecular rows having 100° orientation with respect to the local HB ridge orientation.

8.2 Three Structural Orderings

We observe that *trans*-TTB-AB molecules on Au(111) self-assemble into ordered islands having three possible configurations, here denoted as phases 1, 2, and 3 (see figures 8.1(B-D)) with each phase displaying very different photoswitching behavior. All individual molecules appear the same before they are exposed to light, regardless of phase (they appear as a rectangular four-lobe structure with each lobe indicating a tert-butyl (TB) "leg"). The three different island phases vary in their molecule-molecule ordering and in the orientation of molecules with respect to the underlying Au(111) herringbone (HB) surface reconstruction. Phase 1 islands are close-packed and have one molecule per unit cell that is oriented with its long axis tilted 87 ± 3° with respect to the HB ridges (the HB ridge orientation, which is parallel to one of the three equivalent [11$\underline{2}$] crystal directions, is indicated by the black dashed line in figures 8.1(B-D)). Phase 2 islands have a two-molecule unit cell with one molecule tilted 101 ± 4° and the other 49 ± 4° with respect to the HB ridges. Phase 3

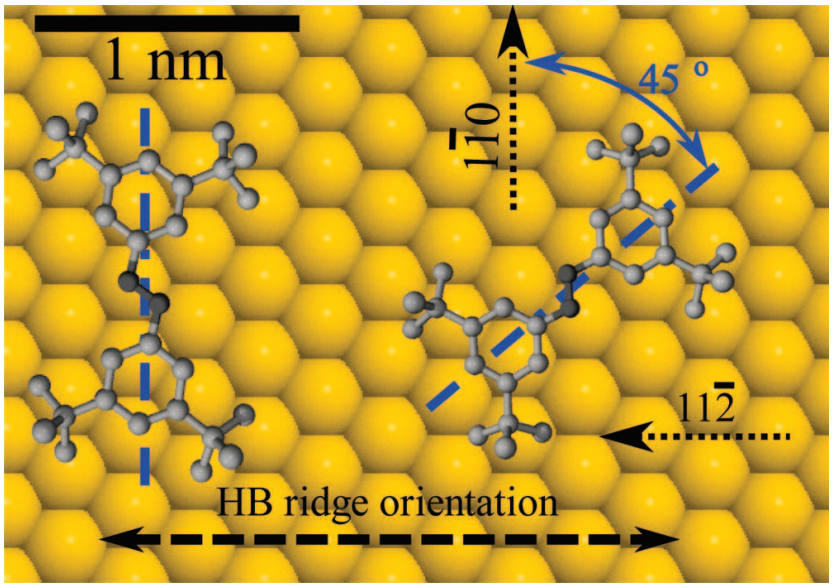

Figure 8.2: Ball-and-stick models of *trans*-TTB-AB on the Au(111) surface showing the two main orientations of molecules relative to the Au surface for phases 1-3 (actual orientations vary by approximately ±10° as described in text).

islands are close packed and have one molecule per unit cell tilted 40 ± 3° with respect to the HB ridges. Phase 3 islands also display quasi-periodic stacking faults (white dashed line in figure 8.1(D)).

Phase 2 and phase 3 islands occur with less frequency than phase 1 islands by about 2 orders of magnitude, which explains why they have not been previously reported [107, 22]. Figure 8.2 shows the different molecular orientations observed with respect to the surface.

8.3 Photoswitching Dependence on Structural Orderings

We examined how different surface orderings of identical molecules affect their photoswitching behavior by exposing all three TTB-AB phases to UV light. Figures 8.1(E-G) shows topographic STM images of phase 1, 2, and 3 islands, respectively, after equal exposures to UV light (approximately 100 h, starting from an all-*trans* initial state). Individual photoswitched molecules in the *cis* state typically appear as a bright protrusion surrounded by three dimmer peripheral lobes (inset of figure 8.1(E) [107, 22]). The quantity and spatial distribution of *cis* molecules are seen to be extremely different between the three phases. Phase 1 islands have a high concentration of *cis* isomers (∼40%) that appear to be randomly distributed spatially (figure 8.1(E)). Photoswitched molecules in phase 2 islands display an

unexpected striped pattern (figure 8.1(F)). The "switching stripes" are oriented nearly perpendicular to the HB ridges and have a pitch that varies from 85 to 115 Å, depending on the island. All photoswitched molecules in these stripes are tilted 100° with respect to the HB ridges (see inset of figure 8.1(F)). Within a stripe, the rate of photoisomerization is approximately the same as in a phase 1 island, but the rate plunges to nearly zero outside of the stripes. Photoisomerization in phase 3 islands (figure 8.1(G)) is highly quenched relative to phase 1 and 2 islands. The phase 3 switching rate is at least 2 orders of magnitude smaller than the phase 1 switching rate (phase 3 switched molecules appear to be randomly distributed spatially). For all three phases, the overall photoswitching rate is independent of whether a molecule is above an facecentered cubic (fcc) or hexagonal close-packed (hcp) region of the reconstructed gold surface.

8.4 Influence of Electronic Structure of Structural Orderings on Photoswitching

We performed STM spectroscopy (STS) measurements to probe the electronic structure of the different TTB-AB island phases in order to better understand the source of the variable photoswitching behavior. dI/dV spectra measured over the bare Au(111) surface between TTBazobenzene islands showed a surface state band-edge at ∼0.5 eV below EF, consistent with previous work [87, 88, 89] (figure 8.3(A)). dI/dV spectra measured over the TTB-AB islands however showed quite different behavior. Spectra measured for all three TTB-AB phases can be grouped into two position-dependent categories, designated as "bright" and "dark"(figure 8.3(A)). Both types of spectra show a steep shoulder near V_{sample} ∼-0.25 V that is similar to the bare Au(111) surface state band-edge but is shifted up in energy by ∼0.2 eV. The main difference between the bright and dark spectra is that the bright spectra have a steeper shoulder exhibiting more spectral weight than dark spectra (see difference spectrum in figure 8.3(A)).

The spatial dependence of the two spectral types (bright and dark) can be seen in constant current dI/dV maps acquired at V_{sample} = -0.27 V (the bias where they show greatest contrast) (figures 8.3(B-D)). All island phases show a spatial modulation in electronic local density of states (LDOS) that runs perpendicular to the HB ridges (the HB ridges are horizontal in figures 8.3(B-D)). The pitch of this modulation exactly matches the HB reconstruction itself. For phase 1 and 3 islands, bright-type spectra are observed in the brighter regions of the islands that lie above the hcp regions of the Au(111) surface, while dark-type spectra are observed over the darker fcc regions. This perpendicular LDOS modulation is similar to HB-induced electronic modulation seen previously in the bare Au(111) surface state [89]. Phase 2 islands are different in that they have an additional spatial modulation running parallel to the HB ridges (figure 8.3(C)) that darkens previously bright hcp regions and that causes dark-type spectra to appear in the newly darkened regions. This behavior is compared to the behavior of phase 1 and phase 3 islands (both of which lack a parallel modulation) in the line scans shown in figure 8.3(E). The phase 2 parallel modulation has

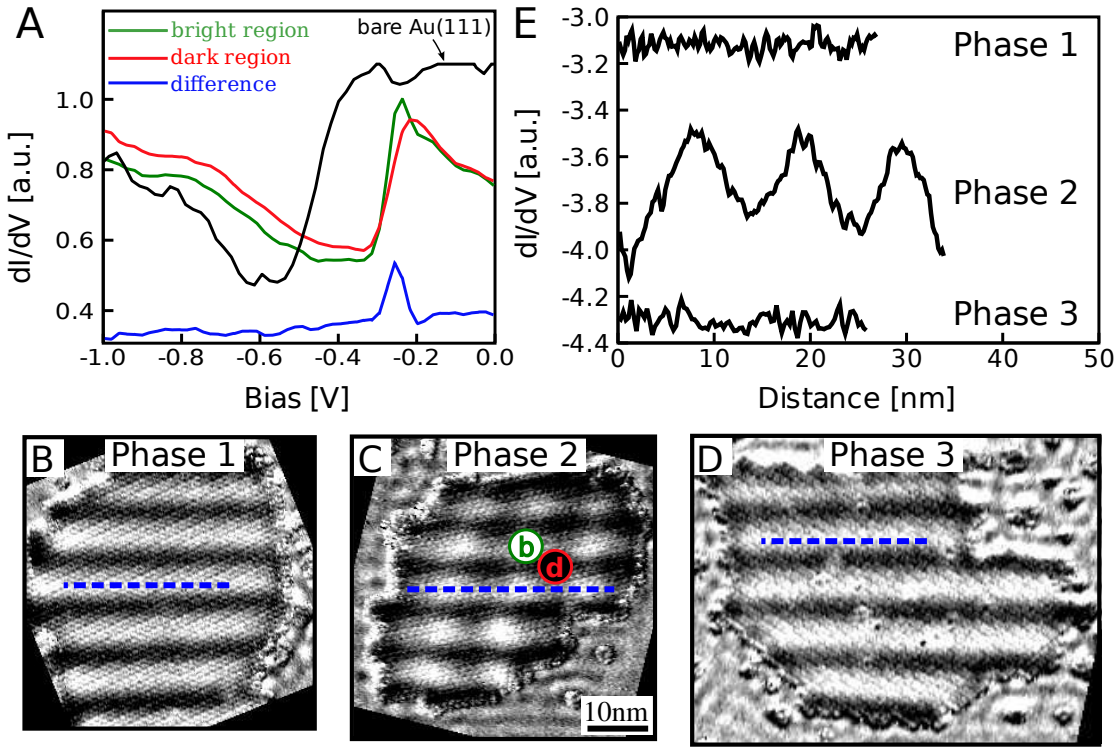

Figure 8.3: (A) Two types of dI/dV spectra are observed for all TTB-AB islands ("bright region" type vs "dark region" type) and are compared here to a dI/dV spectrum measured on bare Au(111) (TTB-AB spectra are spatial averages). Subtracted difference between bright region and dark region spectra is shown (bare Au(111) spectrum and difference spectrum are both shifted vertically for viewing clarity). (B-D) dI/dV maps at $V_{sample} = -0.27$ V of phase 1, 2, and 3 islands (dashed lines mark the positions for line scans shown in panel E). The "bi" and "di" marks in panel C show typical positions for acquiring respective bright and dark point spectra. (E) dI/dV line scans in phases 1, 2, and 3 at V = −0.27 V show unmodulated phase 1 and phase 3 behavior compared to strongly modulated phase 2 behavior (phase 1 and 3 line scans are both shifted vertically for viewing clarity).

a pitch that varies from 85 to 115 Å between islands. No additional LDOS modulations at other biases were observed.

We find that the bright areas of the phase 2 parallel LDOS modulation occur at the same positions as the phase 2 photoswitching stripes. To confirm this connection between local electronic structure and photoswitching probability, we performed topographic and dI/dV imaging of a phase 2 island before and after exposure to UV light. Figure 8.4(A) shows a dI/dV map of an all-*trans* phase 2 island before light exposure, highlighting the typical phase 2 parallel modulations in LDOS. Figure 8.4(B) is an image of the same island after 100 h of exposure to UV light. The positions of the switching stripes containing *cis* isomers

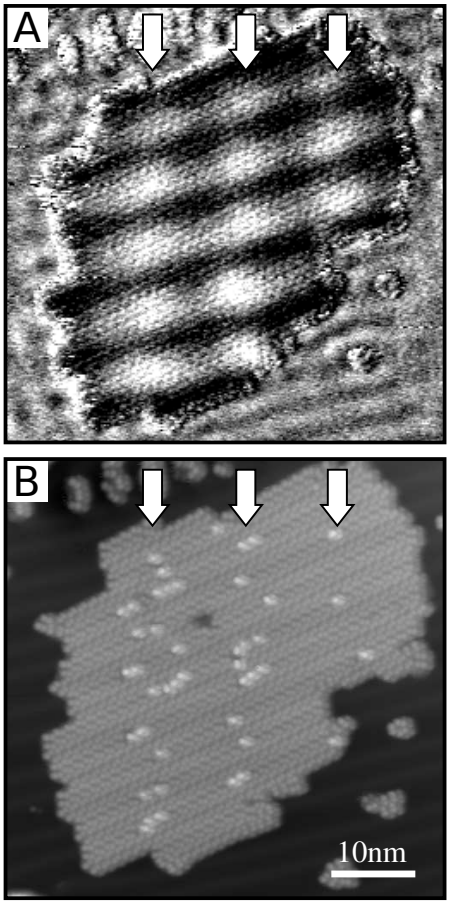

Figure 8.4: (A) dI/dV map taken at $V_{sample} = -0.27$ V for a phase 2 island containing only *trans*-TTB-AB molecules prior to UV exposure. Arrows identify bright regions of parallel LDOS modulation. (B) Constant current STM topograph of the same island after UV exposure. Arrows (same positions as in panel A) identify self-patterned phase 2 photoswitching stripes containing *cis* isomers.

in figure 8.4(B) clearly match the bright regions of the parallel electronic LDOS modulations in figure 8.4(A).

8.5 Influence of TTB-AB Assembly on Photoswitching

This data reveals a strong dependence of TTB-AB surface photoswitching behavior on molecular assembly and orientation on Au(111). We can generalize this behavior into the following two empirical photoswitching "selection rules" for TTB-AB on Au: (1) The orientation of a molecule relative to the underlying crystallographic structure determines whether

that molecule is switching-enabled or switching- quenched. Molecules oriented at 95 ± 10° with respect to the HB ridges are switching-enabled (all phase 1 and half of phase 2 molecules), while those oriented at 45 ± 8° are switching-quenched (all phase 3 and half of phase 2 molecules). (2) Regions of reduced electronic LDOS parallel to the HB ridges in phase 2 islands correlate with additional quenching.

Our challenge is to understand how the TTB-AB molecular surface environment leads to these photoswitching selection rules. In general, the photoswitching properties of molecules are influenced by their electronic excitation and relaxation behavior, optical absorption, and molecular steric hindrance properties (i.e., constraints on atomic motion) [17]. Molecules in phases 1 and 3 have markedly different switching rates and different molecular orientations with respect to the gold substrate, but they share the same nearest neighbor molecule-molecule configuration. We therefore believe that intermolecule-based steric hindrance does not play a significant role in determining the photoswitching rates for these two phases, but that the switching rates are rather determined by orientation-dependent molecule-surface interactions. These likely induce variation in molecular excited-state lifetimes and optical absorption, thus leading to the observed difference in photoswitching rates between phases 1 and 3.

On the other hand, the self-patterned switching stripes observed in phase 2 are more likely due to molecule-molecule interactions. Two questions naturally arise regarding this behavior: (i) What is the cause of the phase 2 parallel electronic LDOS modulation? and (ii) What is the mechanistic link between the phase 2 electronic LDOS modulation and the self-patterned molecular switching stripes? We do not believe that the phase 2 parallel LDOS modulation is related to island-induced size quantization of the underlying two-dimensional Au(111) Shockley surface state [90, 29] since it has neither the correct period nor the correct energy dependence. Rather, we believe that it arises from a strain modulation within phase 2 islands that influences the surface state local potential (thus resulting in the observed variations in dI/dV spectra). This could affect photoswitching through dependence of molecular steric hindrance on stresses arising from the induced strain. Such a strain modulation may be qualitatively described as either a thin film buckling instability [91] or an Asaro-Tiller-Grienfeld instability [92, 93, 94] within continuum elasticity theory. The fact that we do not see clear signs of phase 2 periodic strain in our topographic data does not rule this mechanism out due to limited spatial resolution in our images.

8.6 Conclusion

We find that the photoswitching properties of molecules at a surface depend strongly on molecule-surface and molecule-molecule interactions with the latter inducing self-patterned photoswitching domains. This result has important implications for future photomechanical molecular device engineering at a surface and suggests new opportunities for nanometre-sized photomechanical molecular patterning.

Chapter 9

Surface Photoswitching Dynamical Mechanism of TTB-AB on Au(111)

9.1 Introduction

The internal molecular motions associated with the photoswitching process have been well studied for molecules in solution, where different bond angles have been observed to undergo rotation and inversion at picosecond time scales [10, 96, 97, 98, 99]. Many potential nanotechnology applications, however, require contact between such molecules and a surface, leading to an environment where the molecular potential energy surface and dynamical pathways are not known. While this is an important regime for applications, it is largely unexplored due to the difficulty of performing ultrafast time-resolved optical measurement of adsorbate-coated surfaces. Recently, some investigations have been performed that explore surface-based molecular photoswitching using surface analysis techniques [107, 85, 86], but these measurements reveal little about the actual dynamical motion of molecules as they switch. Here we describe a new technique for extracting dynamical switching information from surface-bound molecules by spatially mapping their chirality state before and after a photoswitching event. This technique is applicable when different dynamical switching pathways transition a molecule between states of well-determined chirality.

We find that this type of situation exists for 3,3',5,5'- tetra-*tert*-butyl-azobenzene (TTB-AB) molecules adsorbed onto Au(111) [107]. While the isolated molecule is not chiral, the adsorbed molecule is chiral due to the breaking of mirror symmetry by the presence of the surface [100, 101, 102, 103]. Using scanning tunneling microscopy (STM) we observe that *trans*-TTB-AB on Au(111) assembles into monolayer-high islands composed uniformly of either right-handed (RH) or left-handed (LH) enantiomers [17]. When these *trans* molecules are illuminated with light, we observe that they can switch into two possible *cis* isomer states ("type 1" and "type 2"). The chirality of the resulting *cis* isomers is not random, but rather follows a chirality-dependent photoswitching selection rule: RH (LH) *trans* isomers on Au(111) almost exclusively switch to either LH (RH) type 1 *cis* isomers or RH (LH) type 2 *cis* isomers (the chirality convention is defined below). Using density-functional

theory we have determined the geometrical structure of the type 1 and type 2 *cis*-TTB-AB isomers. Armed with these structures and the chirality-dependent selection rule, we are able to place symmetry constraints on the possible dynamical pathways involved in *trans*-to-*cis* switching. This provides evidence for a new surface-based dynamical mechanism for *trans*-to- *cis* photomechanical switching of TTB-AB molecules on Au(111).

Our measurements were performed using a home-built variable-temperature ultrahigh vacuum STM with optical access to the sample. TTB-AB molecules were synthesized via oxidative coupling reactions of 3,5-di-tert-butyl-aniline [18]. 0.1 monolayer (ML) of the trans isomer of TTB-AB was deposited via Knudsen cell onto clean Au(111) substrates held at 30 K. Samples were then annealed at room temperature for 10 minutes in order to achieve ordered monolayer-high islands of trans molecules. STM images were acquired in the temperature range of 30 to 35 K using tunnel currents below 50 pA for stable imaging. A cw laser aligned at an external viewport provided UV (375 nm) radiation at the sample surface with an average intensity of 92 mW/cm^2. During laser exposures the STM tip was retracted 0.2 mm away from the surface and the sample temperature was maintained between 28 and 35 K.

9.2 Surface-Induced Chirality

Self-assembly of *trans*-TTB-AB molecules into monolayer-high domains having pure chiral flavor can be seen in the mirror-image lattice chiral domains of figure 9.1. Single *trans*-TTB-AB molecules appear as four lobes arranged at the vertices of a parallelogram (the lobes correspond to the location of the tert-butyl (TB) functional groups, as indicated by the molecular model overlays in figure 9.1(a)]. *Trans*-TTB-AB molecules in RH vs LH domains appear slightly sheared to the right and left, respectively. The difference between molecules in the RH vs LH domains is more clearly observed by averaging the location of the highest point of the TB lobes for molecules within like domains, as shown in figure 9.1(b). The resulting average parallelograms for RH and LH domains are mirror images of each other with the edges of the parallelograms angled by 2° from the horizontal and vertical.

9.3 Chirality-Dependent Photoswitching

When the chiral *trans*-TTB-AB islands are illuminated with UV light, the molecules begin photoswitching into a *cis* isomer structure. High-resolution STM images of the resulting *cis* isomers, as shown in figure 9.2(a), reveal that there are two distinct types of isomers [labeled type 1 and type 2 in figure 9.2(a)]. Each has the appearance of a bright (taller) lobe surrounded by three dimmer (lower) lobes, but the location of the bright lobe with respect to the dim lobes differs between the two types. For type 1 *cis* isomers the bright lobe lies closer to the center line between the two far opposite dim lobes, whereas for type 2 *cis* isomers the bright lobe lies further from this center line and closer to the diagonal point opposite the dim corner lobe (see figure 9.3). Type 1 and type 2 *cis*-TTB-AB are both

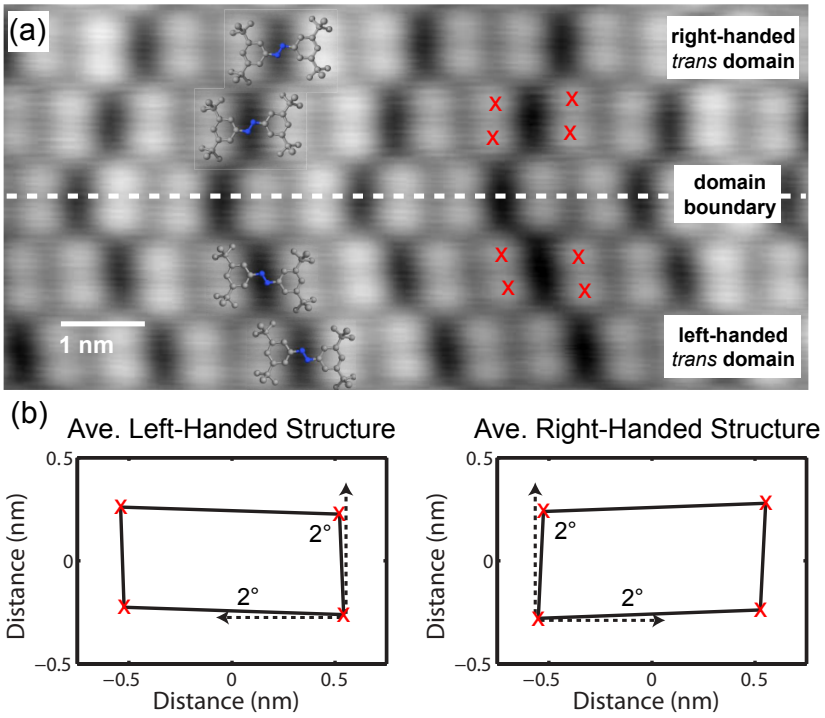

Figure 9.1: (a) Image of *trans*-TTB-AB island composed of two mirror-image chiral domains (domain boundary indicated by dashed white line). *Tans*-TTB-AB single-molecule structural models are superimposed on right-handed and left-handed configurations. Red crosses indicate locations of TB lobe maxima. (b) Average locations of *trans*-TTB-AB TB lobes averaged over 394 left-handed domain molecules (left plot) and 125 right-handed domain molecules (right plot). Left-handed and right-handed domain *trans*-TTB-AB molecules form parallelograms that are angled by 2° from the horizontal and vertical.

chiral, and their RH and LH enantiomers can be seen in the images of figure 9.3 using our chirality convention. The photoreaction yields of type 1 *cis* and type 2 *cis* are not equal: type 1 *cis* occur approximately twice as frequently as type 2 *cis*. Type 1 *cis*-TTB-AB has been previously reported in STM images of molecules switched using light [107] and using tip-based interactions [22, 104, 105], but type 2 *cis* isomers have gone unnoticed until now because they occur less frequently and require exceptional imaging conditions to be distinguished from type 1.

When a *trans*-TTB-AB molecule on Au(111) is photoswitched to a *cis* isomer, the chirality of the final state is not random. This was determined from careful examination of 338 photoswitched *cis* isomers. We find that *trans* isomers in LH domains produce predominantly either RH type 1 or LH type 2 *cis* isomers (with a 9% defect rate), while *trans* isomers in RH domains produce predominantly either LH type 1 or RH type 2 *cis* isomers (with a 5% defect rate). A clear chirality-dependent photoswitching selection rule is thus

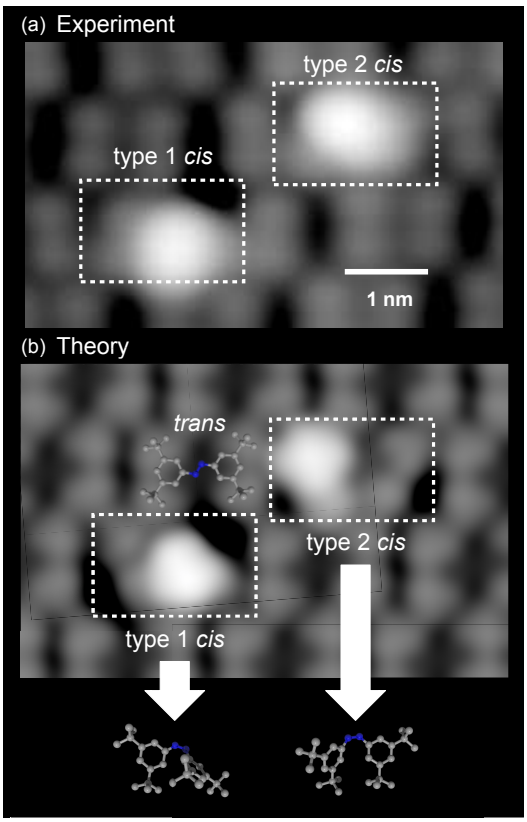

Figure 9.2: (a) High-resolution STM image shows structure of two distinct types of photoswitched *cis*-TTB-AB isomers: a left-handed Type 1 *cis* and a right-handed Type 2 *cis*, contained within dashed white boxes. (b) Ab initio DFT simulated STM image of the two *cis*-TTB-AB types surrounded by trans-TTB-AB molecules, with structural models shown of trans-TTB-AB as well as *cis* type 1 and *cis* type 2 molecules used to calculate simulated STM image.

observed. These results are summarized in Table 9.1.

9.4 DFT Simulation of Chirality-Dependence

In order to determine the specific constraints placed on molecular photoswitching dynamics by the selection rule above, it is critical to determine the geometrical structure of the *cis* and *trans* molecules imaged by our STM. This determination was performed by calculating topographs from the electronic local density of states (LDOS) of different TTB-AB molecular structures by density-functional theory (DFT) and comparing them to our STM images. DFT calculations were performed using the SIESTA code [82] as in Ref. [107]. Structures of isolated molecules of each type were initially relaxed and then assembled into

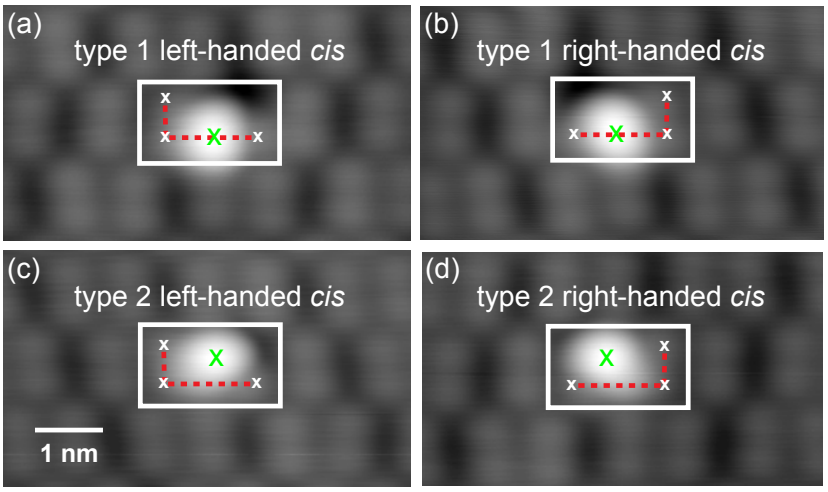

Figure 9.3: STM images showing different chiral states of single *cis*-TTB-AB molecules (within white boxes): (a) *cis* type 1, left-handed (within right-handed trans domain), (b) *cis* type 1, right-handed (within left-handed trans domain), (c) *cis* type 2, left-handed (within left-handed trans domain), and (d) *cis* type 2, right-handed (within right-handed trans domain). Location of single bright lobe indicated by green cross and the locations of three dim peripheral lobes indicated by white crosses. Dotted lines are guides to the eye.

a monolayer of molecules (without surface atoms) according to the experimentally observed surface lattice parameters. The simulated *trans*-TTB-AB molecules (figure 9.2(b)) show four lobes at the corners of a parallelogram angled from the horizontal and vertical by 2°, as observed in the STM images (figure 9.1), confirming the existence of two enantiomers of *trans*-TTB-AB on the surface. We find two local minima in the DFT potential energy surface that produce LDOS topographs corresponding to the *cis*-TTB-AB type 1 and type 2 STM images, thus yielding the underlying molecular structure for these *cis* types [see figure 9.2(b)]. In both *cis* structures the phenyl ring lying on the surface has a CCNN dihedral bond angle $\approx 30°$. The two *cis* types differ in that the CCNN dihedral angle for the lifted ring is 50° for type 1 and −60° for type 2, leading to the different bright lobe positions observed in the STM images. The type 1 *cis* molecular structure has been experimentally

Table 9.1: Correlation of *cis*-TTB-AB type and chirality with initial *trans*-TTB-AB island chirality.

	Final state *cis* Type 1		Final state *cis* Type 2	
	Left-handed	Right-handed	Left-handed	Right-handed
Left-handed *trans* island	2	85	45	11
Right-handed *trans* island	115	0	10	70

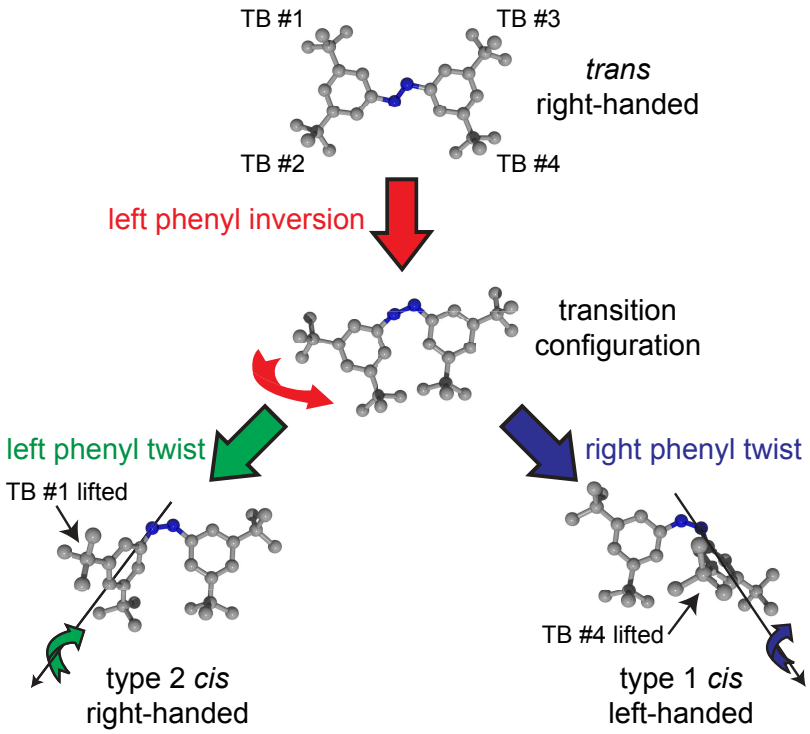

Figure 9.4: Proposed photoisomerization dynamical pathway for TTB-AB on Au(111). A photoexcited right-handed *trans*-TTB-AB molecule (top center, TB legs numbered) begins the isomerization process with an in-plane inversion of the left phenyl ring (middle center). With continuing inversion, steric repulsion due to contact between the phenyl rings forces either: left phenyl to twist out of plane, lifting TB #1 and producing right-handed type 2 cis-TTB-AB (bottom left), or right phenyl to twist out of plane, lifting TB #4 and producing left-handed type 1 cis-TTB-AB (bottom right).

reported in the past [107, 22, 104, 105]. The type 2 molecular structure, however, while suggested by previous theoretical work [25], has never been observed experimentally until now.

9.5 Photoswitching Dynamical Mechanism

We are now in a position to determine the surface dynamical pathways explored by TTB-AB molecules as they photomechanically switch from one isomeric structure to another. While the photoswitching mechanism for molecules in solution remains controversial [10, 96, 97, 98, 99, 25, 106, 23], two commonly considered mechanisms involve (i) pure rotational motion [10, 97, 25, 106, 23], and (ii) concerted inversion [97, 24]. We are able to rule

these mechanisms out for TTB-AB on Au(111) using our experimentally determined chiral selection rule and molecular structures. The rotational pathway, for example, leads to *trans* → *cis* conversion via out-of-plane rotation of a phenyl ring as the CNNC dihedral angle is swept. For a RH (LH) *trans* isomer on a surface this motion always yields a RH (LH) type 1 *cis* isomer. Because this violates our observed chirality-dependent selection rule, we rule it out as a significant dynamical pathway for TTB-AB photoswitching on gold. The concerted inversion pathway, on the other hand, yields *trans* → *cis* conversion through a mechanism involving synchronous inversion of the phenyl rings as the two NNC bond angles are simultaneously swept. Here the TTB-AB molecule goes through a transition state in which the CNNC atoms are nearly collinear, a configuration that by symmetry is expected to lead to either RH or LH *cis* conformations with nearly equal probability. This too violates our chirality-dependent selection rule, and so we rule it out as a significant dynamical pathway for TTB-AB switching on gold.

The question now arises if there exists any reasonable dynamical pathway to convert *trans*-TTB-AB to *cis*-TTB-AB on Au(111) that is consistent with the observed chirality-dependent selection rule. Here an affirmative answer can be made via a new dynamical mechanism that is a variant of the inversion pathway [10, 96, 97, 99, 106]. We propose that isomerization begins with the in-plane inversion of one phenyl ring and proceeds until the moving phenyl ring makes contact with the stationary ring (see figure 9.4 for a sketch of the mechanism starting from RH *trans*-TTB-AB). A branch in the dynamics occurs at this point. In the first branch (lower left-hand side of figure 9.4) the inverting phenyl ring lifts out of the plane starting from the point away from contact, yielding a type 2 *cis* configuration of the proper chirality. In the second branch (lower right-hand side of figure 9.4) the stationary phenyl ring lifts out of plane starting from the point of contact, yielding a type 1 *cis* configuration of the proper chirality. This mechanism is supported by the fact that it should be energetically more favorable for portions of the molecule to slide along the surface (as in inversion) rather than completely unbind and lift off of the surface (as in rotation).

9.6 Conclusion

We have discovered that *trans*-TTB-AB molecules self-assemble into chiral domains on Au(111), and that there are two distinct *cis* isomer structures resulting from TTB-AB *trans* → *cis* surface photoisomerization. Most significantly, we observe a chirality-dependent photoswitching selection rule that imposes a strong correlation between the chirality of initial and final states for photoisomerization of TTB-AB molecules on a surface. This constrains the possible switching dynamics and supports a new inversion-based dynamical pathway for molecular photoswitching on Au(111).

Chapter 10

Surface Anchoring and Dynamics of Thiolated Azobenzene on Au(111)

10.1 Introduction

Azobenzene derivatives are a class of simple organic photoactive molecules that have potential for nanoscale optomechanical applications. This derives from the fact that they can be reversibly actuated between two conformational states in solution under UV and blue light illumination (*cis-trans* photoisomerization) [13, 71]. Utilization of such molecules in future device geometries requires that their behavior be better controlled at surfaces, including both switching and anchoring. Some recent progress has been made in the area of molecular switching. For example, reversibly photoswitching azobenzene derivatives at the surface of gold were imaged with subnanometer resolution using scanning tunneling microscopy (STM) [107, 108]. Azobenzene molecules tethered to self-assembled monolayers (SAMs) have also been observed to photoswitch [86]. Controllable molecular anchoring and self-assembly remain a challenge for this class of molecule.

Thiol functional groups have been used extensively in the past to anchor a wide variety of molecules to gold structures [109, 110, 62, 111, 112, 113] and are thus a candidate to bond azobenzene molecules to gold surfaces and electrodes. Many SAMs of thiols have been investigated to date (see, e.g., Ref. [114] and references therein) and molecular ordering is found to depend to a large extent on parameters such as surface reconstruction, temperature, and

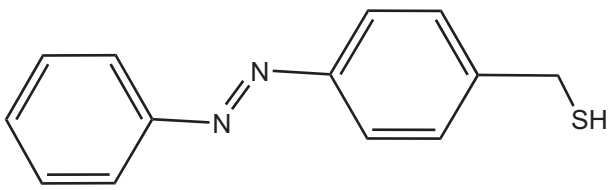

Figure 10.1: Thiol-AB molecule (*trans* isomer)

molecular coverage [115]. The role of surface reconstruction, thereby influencing molecule-surface interaction, has attracted attention recently [116, 117]. However, there have been relatively few studies of aromatic thiolated adsorbates in the low coverage (<0.4 monolayer (ML)) or single molecule regime [118]. The precise nature of the chemical bonding between a thiol group and a gold surface remains unclear. In order to understand thiol-mediated surface anchoring in the context of photomechanically active molecules we have performed a STM study of thiolated azobenzene (thiol-AB) (figure 10.1) adsorbed onto Au(111) in the single-molecule and submonolayer regimes.

We find that thiol functionalization of azobenzene results in enhanced surface anchoring and strong alteration of azobenzene self-assembly behavior. We also find that significant dimer formation occurs when molecules are deposited at room temperature. Single molecules and dimers observed at lower temperature (T=28 K) appear to group in disorganized "wormlike" assemblies. As temperature is elevated from 28 to 60 K, isolated molecules begin spinning in place. By measuring the number density of spinning molecules as a function of temperature we are able to estimate the dynamical parameters of this hindered rotation behavior. The precise surface configuration of the spinning thiol-AB molecules is not clear, but a structural model is proposed based on our STM measurements.

Unlike other experiments in this thesis, our measurements were performed using a commercial variable temperature combined STM/AFM (Omicron VT-AFM/STM) in an ultrahigh vacuum chamber. Clean Au(111) substrates were prepared by repeated cycles of argon-ion sputtering and annealing. Thiol-AB molecules were synthesized and deposited onto clean Au(111) substrates at room temperature via thermal evaporation. Sample temperature was carefully calibrated using diode thermometers and controlled by a liquid-helium flow cryostat and electrical heating. Due to surface diffusion of the molecules above 100 K, the sample temperature was maintained below 75 K for stable imaging (at T<75 K the molecules are stable). Tunnel currents were kept below 50 pA to prevent interaction between the STM tip and molecules.

10.2 Diverse Surface Morphology at Low Temperatures

The low coverage (0.35 ML) behavior of thiol-AB molecules can be seen in the low-temperature (T=28 K) STM images of figure 10.2. Four predominant molecular species are found within the disordered molecular clustering observed on the Au(111) surface. We describe these molecules as "short-straight" [figure 10.2(b)], "short-bent" [figure 10.2(c)], "long-straight" [figure 10.2(d)], and "long-bent" [figure 10.2(e)]. The short-straight species, shown in figure 10.2(b), appears as three collinear lobes with two adjacent identical lobes and a dissimilar third lobe separated by a faint node. The short-bent species, shown in figure 10.2(c), appears as three noncollinear lobes with two circular lobes attached to a larger central oval lobe. The long-straight species, shown in figure 10.2(d), appears as six collinear lobes. The long-bent species, shown in figure 10.2(e), appears as five lobes arranged

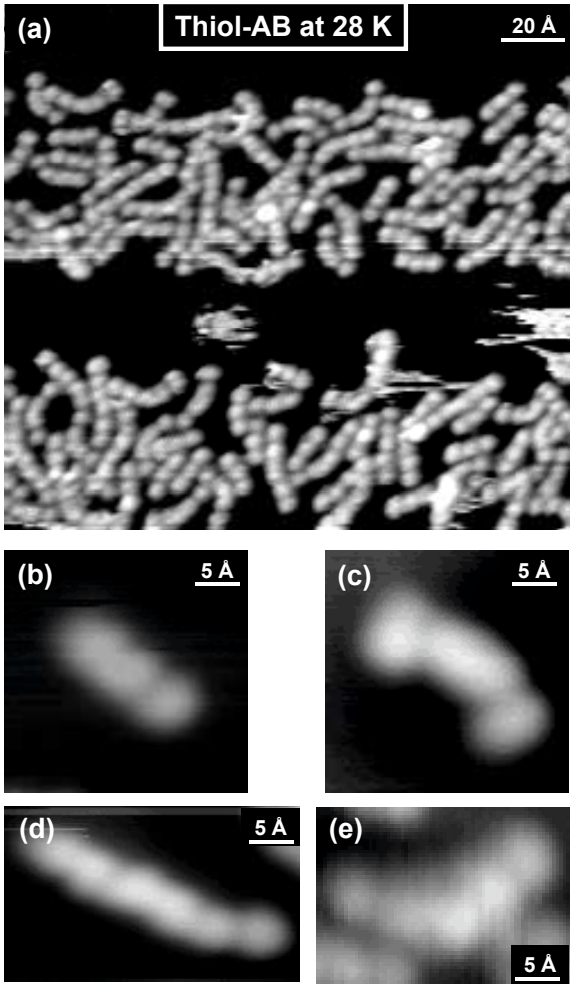

Figure 10.2: STM topographic images of thiol-AB molecules on Au(111) at T=28 K (−2 V, 50 pA): (a) a typical large-scale image and [(b)-(e)] closeup images of four predominant molecular species. (b) Short-straight, (c) short-bent, (d) long-straight, (e) long-bent species are shown. No significant difference between filled and empty state images is observed.

in a symmetrical "V" shape. Both the long-straight and long-bent species are approximately twice the length of the short-straight species. Population percentages of the short-straight, short-bent, long-straight, and long-bent species are 47%, 25%, 13%, and 15%, respectively, at 28 K.

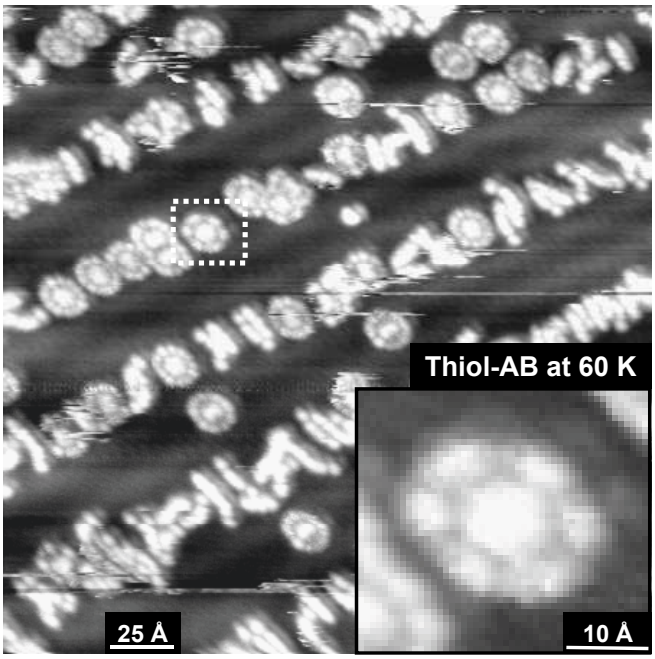

Figure 10.3: STM topographic image of thiol-AB molecules on Au(111) at T=60 K (−2 V, 25 pA). A lrge number of flower-shaped species are observed. The inset shows a closeup view of area outlined by a dashed line.

10.3 Spinning Molecular Species at Elevated Temperatures

At elevated sample temperatures, a large number of new "flower-shaped" species appeared on the surface (figure 10.3, T=60 K). These appear typically as composed of six small satellite lobes around a larger central lobe (see figure 10.3 inset) and have a diameter of ∼22 Å. A complete cooling-warming cycle is shown for one flower-shaped molecule in figures 10.4(a)-10.4(c). Here the flower-shaped molecule observed at 55 K [figure 10.4(a)] is seen to transform into a short-bent molecule upon lowering the temperature to 34 K [figure 10.4(b)]. When the temperature is raised back up to 50 K, the short-bent molecule transforms back into a flower-shaped morphology [figure 10.4(c)]. Thus we identify the flower-shaped species as the time-averaged image of anchored short-bent molecules that rotate on the surface [119].

In order to extract the dynamical parameters describing this molecular motion we counted the number of flower-shaped molecules at different sample temperatures. Figure 10.4(d) shows the areal number density of flower-shaped molecules as a function of temperature. Three different thiol-AB/Au(111) sample preparations were measured, and temperature sweeps between 28 and 60 K were performed for each sample. At each temper-

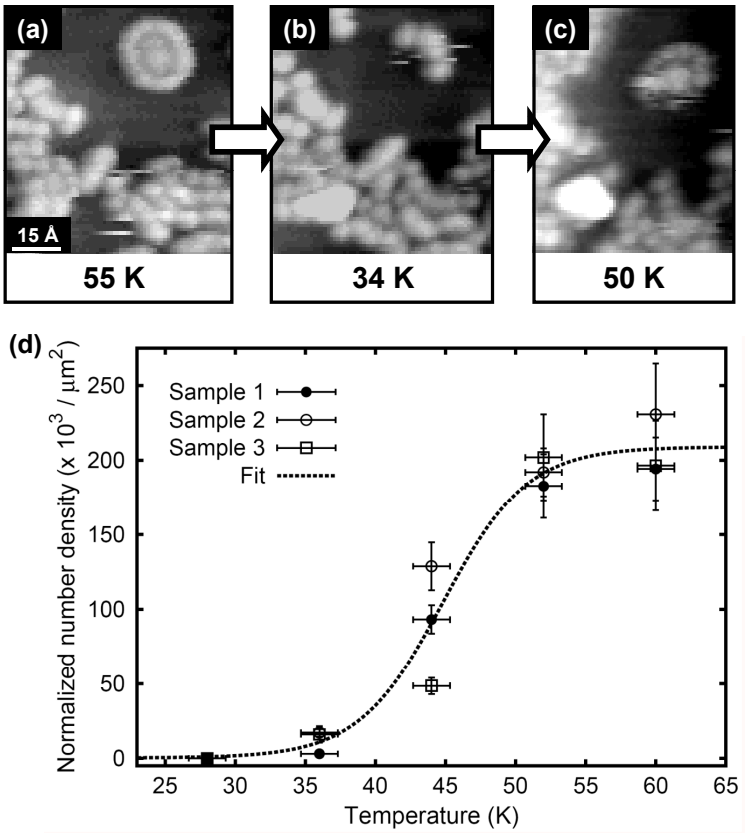

Figure 10.4: A sequence of images showing change in a flower-shaped molecule as temperature is varied. Images taken at (a) 55, (b) 34, and (c) 50 K, respectively, with all other imaging conditions the same (−2 V, 25 pA). (d) Total number of flower-shaped molecules observed at different temperature normalized by total observation area and sample coverage. A sigmoid fit is also shown as a dashed line (see text).

ature the sample was allowed to come to thermal equilibrium and ten different 800×800 Å^2 image areas were analyzed. The number of flower-shaped molecules in each image area was counted and normalized by the total observation area and molecular coverage.

10.4 Surface Anchoring Properties at Low Coverage

The introduction of a thiol group onto the azobenzene molecule strongly changes its adsorption properties on Au(111). This is seen first by the fact that thiol-AB is much more stable and well anchored than nonthiol-AB on gold. For example, stable isolated thiol-AB molecules can be observed on defect-free Au(111) terraces at temperatures of 25 K<T<35 K, whereas bare azobenzene molecules diffuse freely in such regions at these temperatures [79]. Even at higher temperatures of 45 K<T<75 K, thiolated molecules do not diffuse freely, but

a fraction of them are observed to spin in place. Thiol-AB molecules additionally form more disordered structures on Au(111) than the well-ordered assemblies seen for bare azobenzene [72]. This is further evidence of the stronger molecule-surface interaction displayed by thiol-AB. The molecules strongly favor face centered cubic (fcc) over hexagonal close packed (hcp) regions of the Au(111) reconstruction, consistent with a predicted increase in binding energy ($\sim$0.24 eV) for thiols at fcc versus hcp sites [120]. However, we do not observe that the Au(111) reconstruction is lifted upon adsorption under our measurement conditions of low coverage (<0.4 ML) and temperature range (<75 K), unlike decanethiolate on Au(111) where a much stronger molecule-surface interaction is indicated [116].

Thiol-AB exhibits four different molecular species on Au(111), compared to the single molecular structure observed for bare azobenzene. This behavior stems from an interplay between the bonding of thiol groups to the gold surface and the bonding of thiol groups between adjacent molecules. Figure 10.5 shows the proposed structural models for each of the four morphologies observed for thiol-AB on Au(111) [figures 10.2(b)-10.2(e)]. The proposed structure for the short-straight species is a single *trans*-thiol-AB molecule [figure 10.5(a)]. This has the correct shape and size, as seen by the correctly scaled ball-and-stick model superimposed in figure 10.5(a) (we expect the *trans* isomer configuration to be more energetically favorable than the *cis* isomer) [79, 72]. The proposed structure for the long-straight species and long-bent species involves "dimers" of *trans*-thiol-AB molecules [figures 10.5(c) and 10.5(d)]. The observed molecular widths and lengths are correct for these identifications. The dimer linkage here is likely to be either a covalent SS bond or a result from a dipole-dipole interaction between the two thiol functional groups, as illustrated in figure 10.5(e). Currently our measurements cannot distinguish between these two possible modes of association of two thiol-AB molecules.

Identifying the structure of the short-bent species is more difficult. This molecule is symmetric about its center and is longer than the short-straight species by $\sim$40%. A single *cis*-thiol-AB molecule could not display such features, and is thus ruled out as the identity of the short-bent species. Another possibility is that the short-bent species might be composed of fragments of thiol-AB molecules. To test this idea we performed separate STM measurements of both benzyl mercaptan (C_7H_8S) and its disulfide ($C_{14}H_{14}S_2$) on Au(111), but we observed entirely different adsorbate species, and so this explanation is deemed unlikely.

We believe that the most likely structure for the short-bent species involves two pi-stacked thiol-AB molecules [figures 10.5(b) and 10.5(f)]. In this configuration two thiol-AB molecules are joined by stacking their bare phenyl rings [121]. Such a configuration would have approximately the size and symmetry observed in our STM images of the short-bent species. Furthermore, phenyl rings are known to energetically favor such stacking [121]. The central part of the molecule where we expect the stacking to occur does not show a significant height increase in our topographs (apparent height of $\sim$2 Å, as measured at $\sim$2 V sample bias and 25 pA tunneling current): it is only 10% greater than the average height of the short-straight species, but this may be caused by strong molecule-surface hybridization.

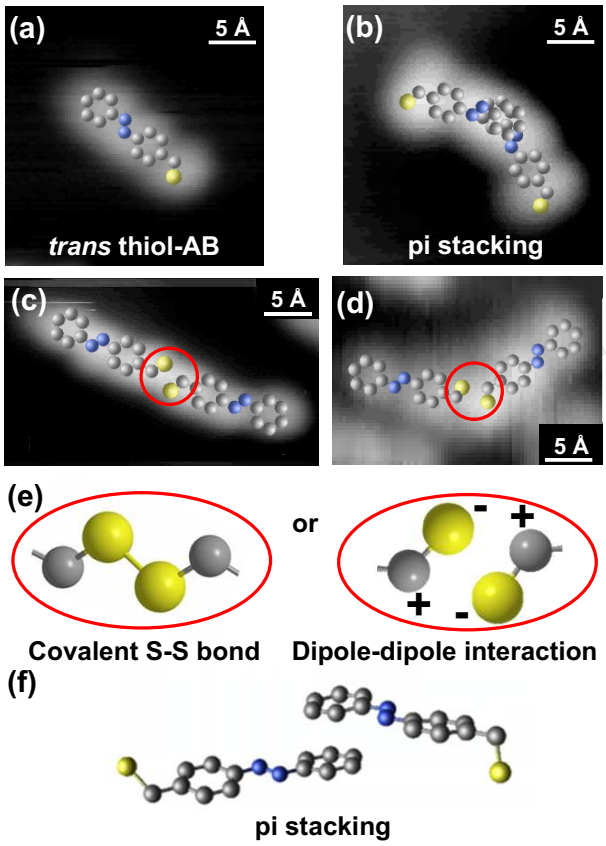

Figure 10.5: Proposed structural models for observed thiol-AB species are superimposed on measured STM images previously shown in figure 10.2: (a) short-straight, (b) short-bent, (c) long-straight, and (d) long-bent species. (e) Two possible bonding configurations for long-straight and long-bent species. (f) Sketch of possible pi-stacking configuration for short-bent morphology.

10.5 Dynamical Temperature-Dependent Behavior

The vast majority of the flower-shaped species observed in our measurements were found to have sixfold symmetry, as shown in the inset of figure 10.3. This can be understood by considering that the time-averaged appearance of a molecule rotating on a surface in a STM image reflects the potential energy profile for that motion [122, 123]. This implies that the short-bent species shown in figure 10.2(c) undergoes hindered rotation about its center through a circumferential potential energy profile having a $\pi/3$ period. Similar rotational features have been observed for different molecular systems [112, 123, 124, 125].

One method for characterizing temperature-dependent molecular rotation is to assume an Arrhenius hopping rate

$$\nu = \nu_0 \exp(-E_r/k_B T), \tag{10.1}$$

where E_r is a rotational energy barrier and ν_0 is an attempt frequency (k_B and T are Boltzmanns constant and the temperature) [126]. Here ν is the rate at which the molecule performs rotational hops of $\pi/3$. In order to quantitatively extract E_r and ν_0 from our experiments, we first assume a sinusoidal potential along the circular rotation path with $\pi/3$ period,

$$V(\theta) = \frac{1}{2}E_r(1 - cos(6\theta)). \tag{10.2}$$

By expanding this around θ=0 for small θ we can equate the resultant potential to a one-dimensional simple harmonic oscillator $V(\theta) = m(2\pi\nu_0)^2 l^2\theta^2/2$ (m and l are the characteristic mass and length of the molecule). This allows us to estimate ν_0,

$$\nu_0 = \frac{1}{2\pi}\sqrt{\frac{E_r}{2m}\left(\frac{6}{l}\right)^2}. \tag{10.3}$$

From the Arrhenius rate equation, (10.1), we then obtain

$$\nu = \frac{1}{2\pi}\sqrt{\frac{E_r}{2m}\left(\frac{6}{l}\right)^2}\exp\left(-\frac{E_r}{k_B T}\right). \tag{10.4}$$

We are able to extract E_r from our data using (10.4) by first finding T_C, the critical temperature at which our scan rate ν_C matches the molecular rotation rate (since m and l are already known). At temperatures significantly below T_C molecular rotation is frozen out, and at temperatures significantly above T_C the density of flower-shaped species is saturated. We thus experimentally determine T_C from the inflection point of a Boltzmann sigmoid function

$$N(T) = \frac{A_1 - A_2}{\exp((T - T_C)/A_3) + 1} + A_2,$$

fitted to the normalized temperature-dependent number density of flower-shaped molecules. The dashed line in figure 10.4(d) shows the best such fit to our data, which yields T_C=45±1 K. For this study our scan rate was kept fixed so that the time to scan a molecule was 5.63±0.26 s, leading to ν_C=0.18±0.01 Hz. Finally, using T_C and ν_C combined with (10.4), we are able to extract E_r. This leads to an energy barrier 102±3 meV and an associated attempt frequency ν_0=110±2 GHz [from (10.3)]. The relatively small error of our extracted rotational barrier (and associated attempt frequency) comes from the relatively low uncertainty in T_C and ν_C and how they are related to E_r through (10.4). ν_C has relatively low uncertainty because it is set by the computer scan rate. T_C also has relatively low uncertainty because the normalized density of flower-shaped species exhibits strong suppression significantly below T_C and collapses the data onto a universal curve that depends exponentially on T_C.

The extracted rotational energy barrier of thiol-AB on Au(111) is lower than that of other thiolated molecules on Cu(111) surfaces reported in previous studies [118], and our attempt frequency is significantly higher. This must arise from different bonding interactions

between molecules on Cu(111) and Au(111), respectively. Our extracted attempt frequency is an order of magnitude smaller than the frequency value of $k_BT/h \approx 6{\times}10^{12}$ Hz (where h is the Plank constant) expected from transition-state theory. This may be related to the molecular steric hindrance properties at the surface. Our rotational energy barrier is also much higher than the calculated value for a different molecule CH_3SH on Au(111) ($\sim$4 meV) [123], presumably due to the higher inertia of thiol-AB as reflected in (10.3).

10.6 Conclusion

We have characterized the surface anchoring, structural diversity, and dynamical behavior of thiol-AB molecules on Au(111) using a variable temperature STM. This overall behavior originates from a combination of molecule-surface and molecule-molecule bonding configurations for thiol-AB which we model based on our STM measurements. Our data reveal thermally induced rotation of thiol-AB molecules on Au(111), from which we have quantitatively extracted dynamical single molecule parameters such as rotational energy barrier and attempt frequency using a simple Arrhenius model.

Chapter 11

Surface Adsorption and Photoswitching Capability of Various Azobenzene Derivatives on Au(111)

11.1 Introduction

Azobenzene molecules have attracted much attention due to their reversible and robust *cis-trans* photoisomerization [12]. Isomerization in gas and solution phase has been studied for both bare molecules as well as molecules with different substitutional groups to tune the isomerization wavelength. Recently, some investigations have been conducted that explore surface-bound azobenzene derivatives [128, 129, 130, 131, 132, 133], and reversible photoswitching of azobenzene molecules functionalized with bulky groups have been reported [107, 84]. However, the position-specific role of bulky space groups in the azobenzene self-assembly and photoswitching properties has not been thoroughly investigated to the best of our knowledge.

Designing molecular nanoscale structures in reduced dimensions is a versatile approach toward the development of larger scale functional devices on the molecular level. Supramolecular engineering on solid surfaces offers exciting possibilities for positioning, interfacing, and controlling the mechanical, electronic, and structural properties of functional molecules [134, 135, 1, 136].

We have used cryogenic scanning tunneling microscope to investigate surface adsorption properties and photoswitching capabilities of azobenzene molecules functionalized with bulky space groups. We find that 2,2',5,5'-tetra-*tert*-butyl-azobenzene (canted-TTB-AB) and 4,4'-dicyano-2,2',5,5'-tetra-*tert*-butyl-azobenzene (cyano-canted-TTB-AB) molecules adsorbed on Au(111) self-assemble into two-dimensional molecular islands in the submonolayer regime. The molecule-molecule interaction that drives the self-organized pattern is attributed to a weak van der Waals interaction between *tert*-butyl (TB) spacer groups for canted-TTB-AB and the C$-$H$\cdots$N$-$C hydrogen bond for cyano-canted-TTB-AB, respectively. In contrast to the behavior of these molecules in solution, they do not undergo

photoswitching on Au(111). Even though the gold surface reconstruction appears to be transparent through the monolayer-high molecular films, thus suggesting a weak molecule-surface interaction, the presence of a metallic surface still prohibits photoswitching from taking place.

Our measurements were performed using a home-built variable-temperature ultrahigh vacuum STM (base pressure $<5\times10^{-11}$ Torr). A clean Au(111) substrate was prepared by repeated cycles of argon-ion sputtering and annealing. Azobenzene derivatives were synthesized and deposited onto clean Au(111) surface held at 30 K via thermal evaporation. Samples were then checked and further annealed at room temperature for 10 min to achieve ordered molecular arrangements. STM images were acquired in the temperature range of 25 to 30 K using tunnel currents below 50 pA to prevent interaction between the STM tip and molecules. A cw diode laser at an external viewport provided UV radiation at 375 nm with an average intensity of 92 mW/cm^2 at the sample surface. During UV exposures the STM tip was retracted and the sample temperature was maintained between 28 and 32 K.

11.2 2,2',5,5'-tetra-tert-butyl-azobenzene on Au(111)

3,3',5,5'-tetra-tert-butyl-azobenzene (TTB-AB) molecules have been experimentally observed to photoswitch on Au(111) [107, 84] in spite of the fact that this molecule has inherent steric limitations due to the relatively restricted space between the meta TB legs. In order to make the azobenzene π unit more versatile for further functionalization and integration into larger scale molecular nanostructures, we have synthesized azobenzene derivatives with TB legs at the 2,2',5,5' positions of the azobenzene scaffold (figure 11.1(a)).

Figure 11.2 shows the STM topographic images of such canted-TTB-AB molecules ad-

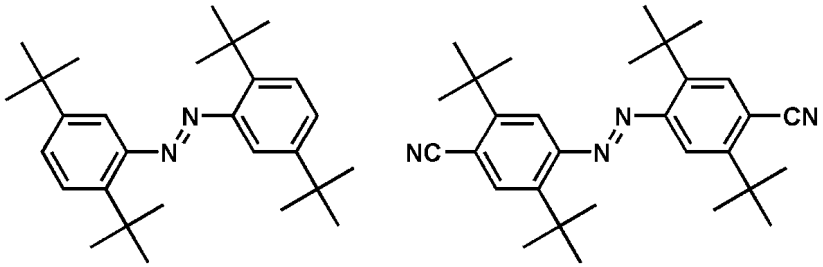

Figure 11.1: Schematic diagrams of functionalized azobenzene molecules (*trans* isomer). (a) 2,2',5,5'-tetra-*tert*-butyl-azobenzene (canted-TTB-AB), (b) 4,4'-dicyano-2,2',5,5'-tetra-*tert*-butyl-azobenzene (cyano-canted-TTB-AB).

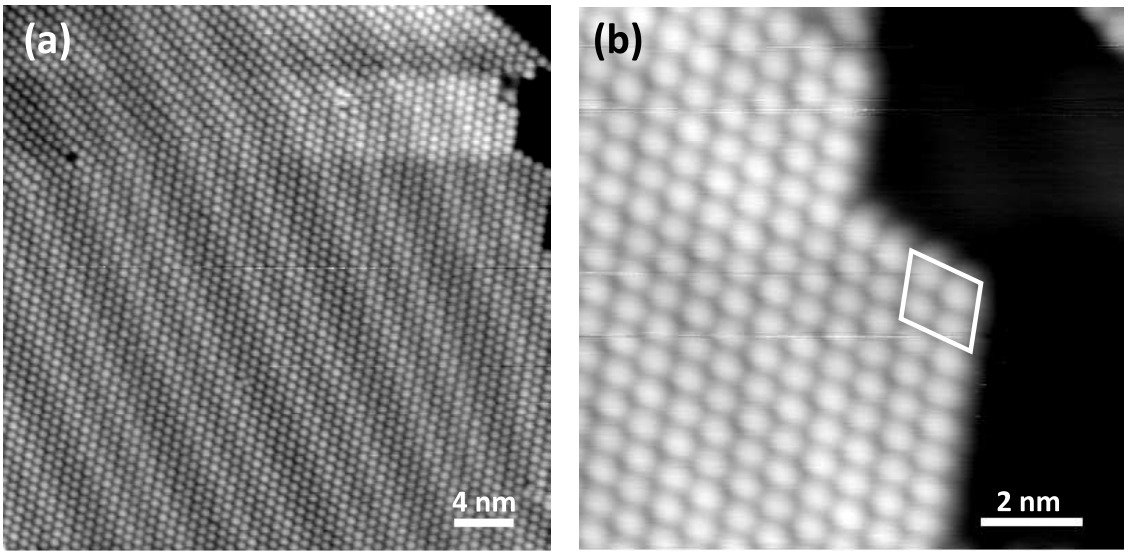

Figure 11.2: STM topographic images of canted-TTB-AB on Au(111). (a) A large field of view. (b) A closeup view of a molecular island. A single molecule is identified by white box.

sorbed on a Au(111) surface. Upon adsorption, the molecules exhibit a close-packed arrangement forming two-dimensional molecular islands (figure 11.2(a)). Individual molecules appear as four bright lobes in a diamond shape indicating the positions of the four coplanar TB legs (figure 11.2(b)).

11.3 4,4'-dicyano-2,2',5,5'-tetra-tert-butyl-azobenzene on Au(111)

Further functionalization of canted-TTB-AB with a cyano (CN) group at the 4,4' position is expected to link adjacent molecules in head-to-tail fashion due to directional hydrogen bonding (figure 11.1(b)). Such a synthetic approach to self-assembly is appealing in that it may allow the exploration of collective photoswitching of azobenzene along the one-dimensional molecular chain.

Figure 11.3 shows the STM topographic images of such cyano-canted-TTB-AB molecules adsorbed on a Au(111) surface. Upon adsorption on Au(111), these molecules favor two-dimensional close-packed molecular islands (figure 11.3(a)). Single molecules are identified by the repeated unit cell in the STM topographic image (figure 11.3(b)) and appear as four bright lobes in a parallelogram, indicating the positions of the four coplanar TB legs. Local disorder is observed near the edges of molecular islands as shown in figure 11.3(a).

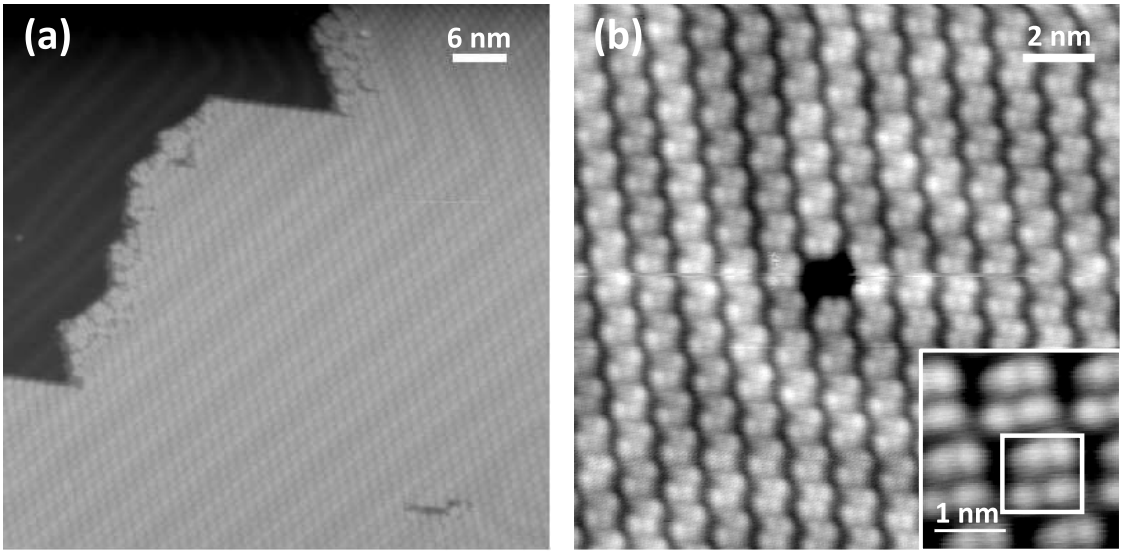

Figure 11.3: STM topographic images of cyano-canted-TTB-AB on Au(111). (a) A large field of view. (b) A closeup view of a molecular island. A single molecule is identified by white box.

11.4 Self-Assembly Properties

Figure 11.4(a) shows a closeup image of a molecular island. While bare azobenzene molecules display a repulsive molecule-molecule interaction at low coverage (<0.5 ML) due to the hydrogen bond [72, 137], the non-conjugated TB legs of the canted-TTB-AB molecules disturbs the hydrogen bond network. The weak van der Waals interaction between the TB legs might be the dominant molecule-molecule interaction, which drives the close-packed molecular island formation.

However, the CN group of the cyano-canted-TTB-AB molecules participates in a selective directional hydrogen bond with adjacent molecules as seen in figure 11.5. Organic molecules functionalized with a CN group self-assemble in the antiparallel configuration as has been seen in other molecular systems [40].

In both cases surface reconstruction of the Au(111) surface is transparent through the monolayer-high molecular island and appear to be unperturbed, suggesting weak surface-molecule interaction.

11.5 Photoswitching Capability

The role of TB groups in both azobenzene derivatives increases the distance between molecules and surface, thereby serving as spacers to electronically decouple the molecules from the surface with minimal modification of the electronic properties of the azobenzene

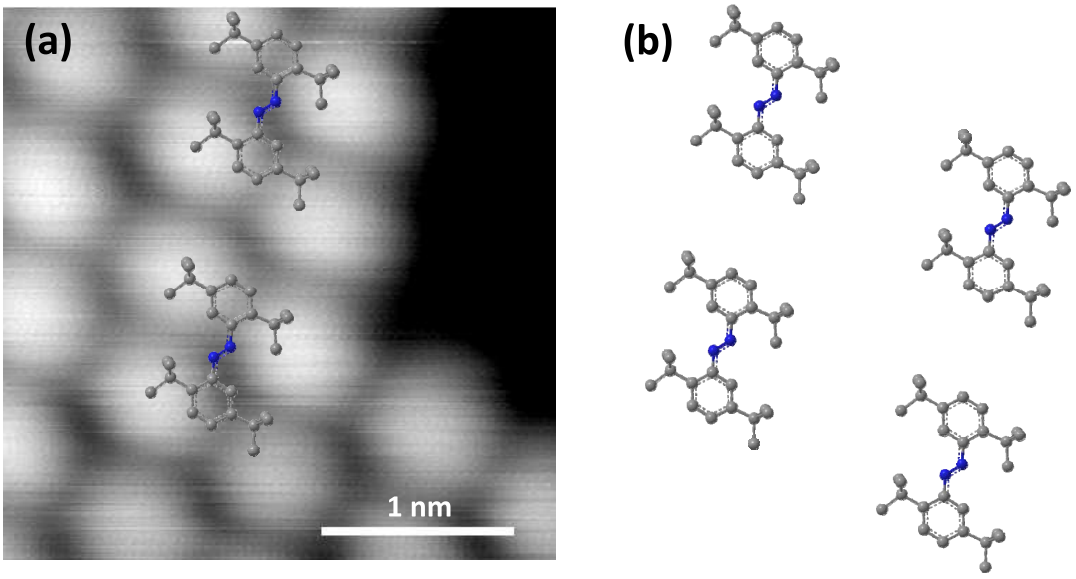

Figure 11.4: STM topographic image and structural model of canted-TTB-AB on Au(111) (a) High-resolution STM image with ball-and-stick model superimposed. (b) Proposed structural models for observed molecules.

unit [104]. TTB-AB on Au(111) photoswitches and the photoswitching of both canted-TTB-AB and cyano-canted-TTB-AB molecules in solution has been confirmed. However, we do not observe any conformational changes upon UV (375 nm) or blue (444 nm) light exposure for the canted molecules on Au(111). This indicates that photomechanical switching is suppressed when these molecules are adsorbed onto Au(111). The reason for the suppressed photoisomerization is not clear, but both steric hindrance and quenching of the excited states is expected to play a major role here.

Motivated by tip-induced isomerization of azobenzene derivatives on Au(111) [20, 21], we have attempted the STM-tip-induced manipulation in order to examine the tip-induced switching capability. No conformational change could be observed for tip-sample voltage up to 3 V, above which the molecules were found to dissociate or desorb.

11.6 Conclusion

We have investigated the self-assembly and photoswitching capabilities of canted azobenzene derivatives on Au(111). We find that functionalization of azobenzene molecules leads to significant alteration of molecular self-assembly properties compared to bare azobenzene, which creates new opportunity for tuning the molecule-molecule interaction. This strategy may allow us to connect functional molecular building blocks to make predesigned structures in the future, but new switching molecule/surface combinations must be found.

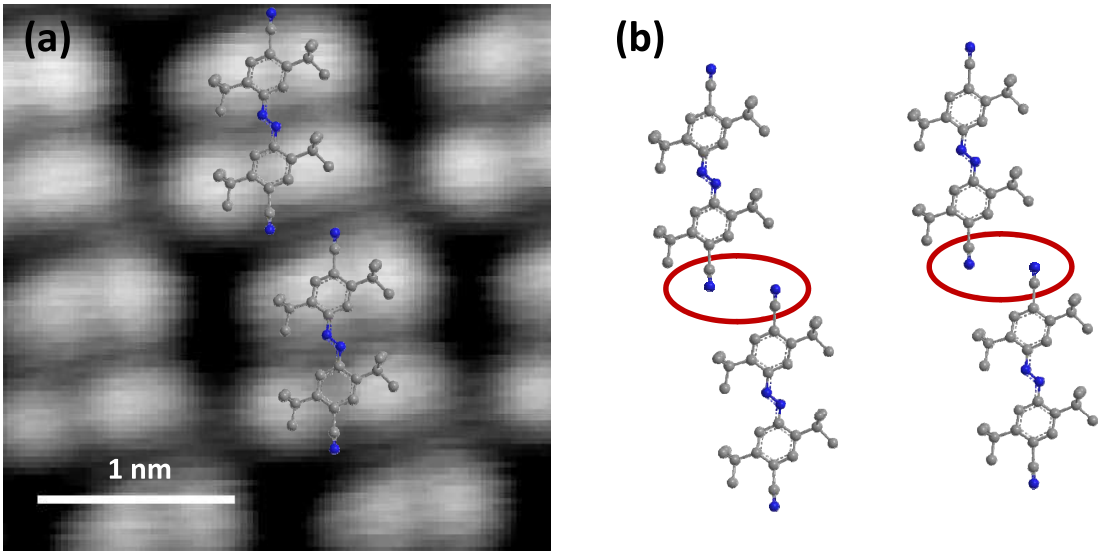

Figure 11.5: STM topographic image and structural model of cyano-canted-TTB-AB on Au(111) (a) High-resolution STM image with ball-and-stick model superimposed. (b) Proposed structural models for observed molecules.

Chapter 12

Photoswitching Capability and Self-Assembly of Azobenzene Derivatives on Semiconductor Surfaces: TTB-AB on GaAs(110)

12.1 Introduction

Using light to control the nanomechanical properties of molecules on surfaces is an attractive strategy for practical applications in molecular machines, and new functional surfaces. This approach presents exciting opportunities for reversible, remote, and ultrafast operation of molecular devices. The challenge here is coupling the light excitation efficiently to the surface-bound molecules without substantial reduction of its photomechanical switching efficiency.

Azobenzene derivatives have been used to construct photoswitchable devices for many years. They readily and reversibly photoswitch in solution without any appreciable fluorescence or phosphorescence. The azobenzene photoisomerization is indeed one of the cleanest and simple photoreactions known and has been intensively investigated from both an experimental and a theoretical perspective [12].

The studies of 3,3',5,5'-tetra-*tert*-butyl-azobenzene (TTB-AB) molecules adsorbed onto Au(111) previously presented in Chapters 6-9 indicate that the presence of a metallic surface reduces the photoswitching activity of the molecules compared to that of the molecules in solution environment. Semiconductor surfaces are expected to induce different molecular switching behavior due to the presence of a band gap, potentially resulting in longer excited-state lifetimes and enhanced control of photomechanical properties.

Unlike other semiconducting surfaces, such as Si(111)7×7 or Si(111)2×1, which are dominated by surface states, the (110) surface of GaAs does not have dangling bond states within the semiconductor band gap (∼1.5 eV) [138]. As such, GaAs(110) is a candidate to reduce electronic coupling between the molecules and the surface. While intensive surface

science studies have been reported on nanoscale defects in GaAs(110) [139, 140], there have been relatively few studies of adsorbed molecules on GaAs(110) [141, 142].

Here we present our exploration of single-molecule-resolved self-assembly and photomechanical switching properties of azobenzene derivatives on a semiconducting GaAs(110) surface using variable temperature scanning tunneling microscopy. We find that the molecules lie planar on GaAs(110) and self-assemble into close-packed molecular islands. Upon UV exposure the adsorbed molecules exhibit conformational changes, which we attribute to the *cis-trans* photoisomerization.

Our measurements were performed using a home-built variable-temperature ultrahigh vacuum STM (base pressure $<5\times10^{-11}$ Torr). Both n-doped and p-doped GaAs(110) wafers (purchased from Wafer Technology) were cleaved in UHV at room temperature, exposing a clean (110) crystal face. Four-legged TTB-AB molecules were synthesized via oxidative coupling reactions of 3,5-di-*tert*-butyl-aniline [81]. *Trans* isomers of the molecule were deposited via Knudsen cell techniques onto freshly cleaved GaAs(110) substrates held at 12 K. Samples were then annealed at room temperature for 30 min in order to achieve ordered molecular arrangements. STM images were acquired in the temperature range of 11 to 13 K using tunnel currents below 50 pA for stable imaging. A cw diode laser at an external viewport provided UV radiation at 375 nm with an average intensity of 92 mW/cm^2 at the sample surface. During UV exposures the STM tip was retracted and the sample temperature was maintained between 11 and 13 K.

12.2 Self-Assembly of TTB-AB on GaAs(110)

After deposition onto clean GaAs(110), TTB-AB molecules were found to self-assemble into densely packed molecular islands as shown in figure 12.1(a). The islands characteristically consist of undulating rows parallel to each other running at either $\sim$37° or $\sim$112° with respect to the [1 $\underline{1}$ 0] direction.

Single molecules are identified based on the fact that all molecules have the same appearance, except for their orientation with respect to the surface crystallographic direction (figure 12.1(b)). All molecules have a planar configuration, suggesting that they adsorb in the *trans* state. The *trans* isomer configuration is expected to be more energetically favorable than the *cis* isomer [12]. Single TTB-AB molecules appear as a four-lobed structure. By comparing the dimensions of the features in the STM image with the expected molecular size, we find that each lobe corresponds to the position of one of the four *tert*-butyl legs of a *trans*-TTB-AB molecule. Individual molecules at low coverage are easily dragged by the STM tip while scanning at I<30 pA, suggesting a relative weak interaction between TTB-AB molecules and the GaAs(110) surface.

Molecule-surface interactions play a key role in the self-assembly properties of TTB-AB molecules on this surface. Determination of the exact detailed bonding configuration remains a challenge, but our STM images provide insight into many basic structural aspects. For example, we are able to identify the molecular adsorption configuration by achieving

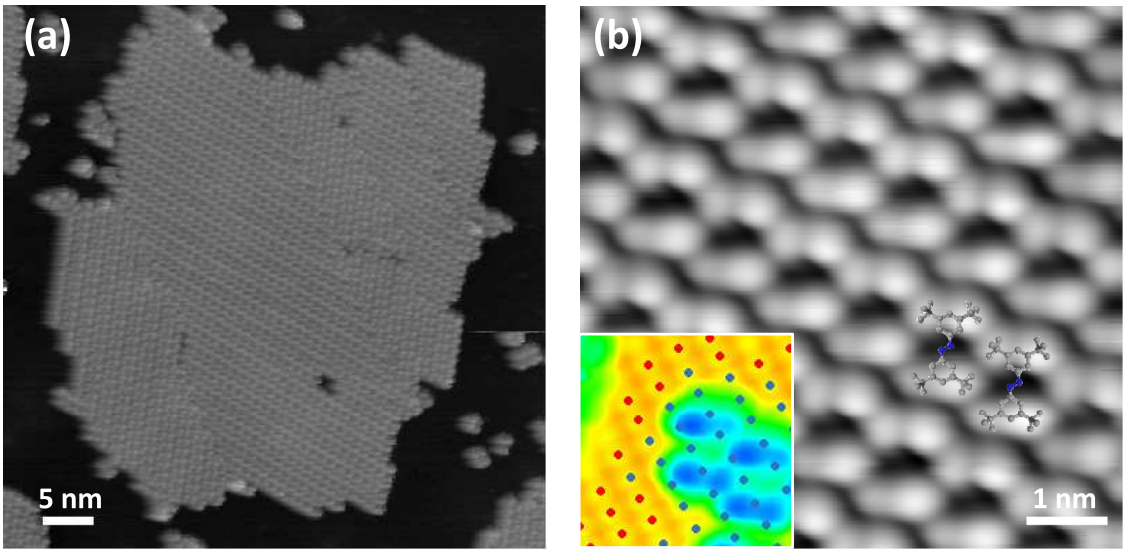

Figure 12.1: STM topographic images of TTB-AB on Zn-doped (p-doped) GaAs(110). (a) A large field of view. (b) A closeup view of a molecular island. A single molecule is identified superimposed with chemical structure. Inset shows the the adsorption configuration, where As atoms were denoted as dots (red: bare GaAs(110), blue: interpolated). Images were acquired with I=20 pA at V=−2 V.

atomic resolution of the GaAs surface while simultaneously imaging the molecules. Figure 12.1 inset shows the the adsorption configuration (here the surface As atoms are denoted as dots). Note that the single-molecule appearance is similar to what is seen for TTB-AB on Au(111) [107, 22]. Two lobes along the long axis of the unit cell appear slightly higher than the other two. This is likely caused by an intrinsic slight buckling of the surface Ga and As atoms of GaAs(110) [143].

12.3 Light-induced Conformational Change of TTB-AB on GaAs(110)

Upon exposure to UV light, the TTB-AB molecules exhibit a photo-induced conformational change. Figure 12.2 shows the same molecular island before and after an 18 hr exposure of UV light (375 nm, 92 mW/cm^2). After UV exposure, the emergence of new protrusions are seen in the island. We believe the UV-induced conformational changes are *cis-trans* photoisomerization, based on the fact that apparent height of the new features is uniform. The new features appear concentrated near the edge and along the domain boundary of the molecular islands. This suggests that the conformational change might be nucleated from the edge of the molecular island, further facilitating the structural change

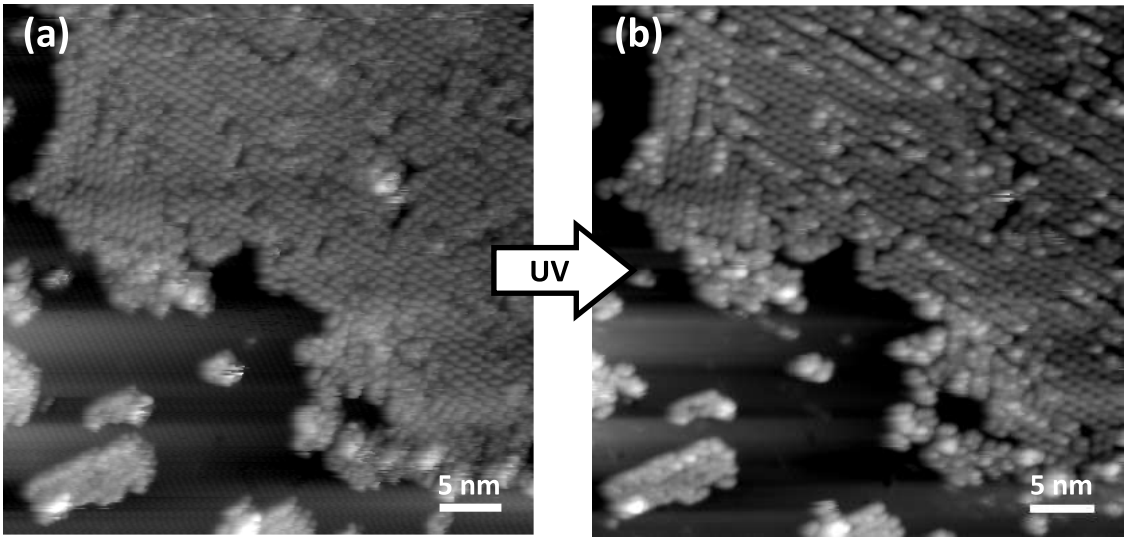

Figure 12.2: STM topographic images of of the same TTB-AB island on p-doped GaAs(110) (a) before and (b) after 8hr of UV 375 nm exposure at 92 mW/cm^2. Images were acquired with I=30 pA at V=−2 V.

of adjacent molecules and propagating through the molecular island.

12.4 Conclusion

We have performed preliminary investigations into the adsorption and photoswitching properties of TTB-AB molecules on the GaAs(110) surface. We find that the molecules form densely packed molecular islands and exhibit pronounced asymmetric topographic features compared to molecules on Au(111). The surface adsorption configuration is identified and explained in terms of surface atom buckling. Upon UV exposure the molecules undergo conformational change, which we believe is *cis-trans* photoisomerization. Further investigation will be required to fully understand the photoswitching properties of molecules adsorbed onto this semiconducting surface.

Bibliography

[1] J. V. Barth, G. Costantini, and K. Kern. Engineering atomic and molecular nanostructures at surfaces. *Nature*, 437(7059):671-679, 2005.

[2] A. Aviram and M. Ratner. Molecular rectifiers. *Chemical Physics Letters*, 29(2):277-283, 1974.

[3] C. Joachim, J. K. Gimzewski, and A. Aviram. Electronics using hybrid-molecular and mono-molecular devices. *Nature*,408(6812):541-548, 2000.

[4] V. Balzani, A. Credi, F. M. Raymo, and J. F. Stoddart. Artificial molecular machines. *Angewandte Chemie-International Edition*, 39(19):3348-3391 (2000).

[5] W. R. Browne and B. L. Feringa. Making molecular machines work. *Nature Nanotechnology*, 1(1):25-35, 2006.

[6] W. Gärtner. The light shall show the way-or: the conformational changes of the retinal chromophore in rhodopsin upon light activation. *Angewandte Chemie-International Edition*, 40(16):2977-2981, 2001.

[7] B. L. Feringa. *Molecular Switches*. Wiley-VCH, Weinheim, 2001.

[8] S. J. van der Molen and P. Liljeroth. Charge transport through molecular switches. *Journal of Physics: Condensed Matter*, 22(13):133001, 2010.

[9] M. Irie. Photochromism: Memories and switches - Introduction. *Chemical Reviews*, 100(5):1683-1683.

[10] N. Tamai and H. Miyasaka. Ultrafast dynamics of photochromic systems. *Chemical Reviews*, 100(5):1875-1890, 2000.

[11] E. R. Talaty and J. C. Fargo. Thermal cis-trans-isomerization of substituted azobenzenes: a correction of the literature. *Chemical Communications*, 2:65-66, 1967.

[12] H. Rau. *in Photochromism: Molecules and Systems*, edited by H. Durr and H. Bouas-Laurent, Elsevier, Amsterdam, 1990.

[13] T. Hugel, N. B. Holland, A. Cattani, L. Moroder, M. Seitz, and H. E. Gaub. Single-molecule optomechanical cycle. *Science*, 296(5570):1103-1106, 2002.

[14] K. Ichimura, S.-K. Oh, and M. Nakagawa. Light-driven motion of liquids on a photoresponsive surface. *Science*, 288(5471):1624-1626, 2000.

[15] M. Banghart, K. Borges, E. Isacoff, D. Trauner, and R. H. Kramer. Light-activated ion channels for remote control of neuronal firing. *Nature Neuroscience*, 7(12):1381-1386, 2004.

[16] D. Dulic, S. J. van der Molen, T. Kudernac, H. T. Jonkman, J. J. D. de Jong, T. N. Bowden, J. van Esch, B. L. Feringa, and B. J. van Wees. One-way optoelectronic switching of photochromic molecules on gold. *Physical Review Letters*, 91(20):207402, 2003.

[17] X.-L. Zhou, X.-Y. Zhu, and J. M. White. Phtochemistry at adsorbate/metal interfaces. *Surface Science Reports*, 13(3-6):73-220, 1991.

[18] S. Hagen, P. Kate, F. Leyssner, D. Nandi, M. Wolf, and P. Tegeder. Excitation mechanism in the photoisomerization of a surface-bound azobenzene derivative: Role of the metallic substrate. *Journal of Chemical Physics*, 129(16):164102, 2008.

[19] M. Wolf and P. Tegeder. Reversible molecular switching at a metal surface: a case study of tetra-tert-butyl-azobenzene on Au(111). *Surface Science*, 603(10-12):1506-1517, 2009.

[20] J. Henzl, M. Mehlhorn, H. Gawronski, K.-H. Rieder, and K. Morgenstern. Reversible cis-trans isomerization of a single azobenzene molecule. *Angewandte Chemie-International Edition*, 45(4):603-606, 2006.

[21] B.-Y. Choi, S.-J. Kahng, S. Kim, H. Kim, H. W. Kim, Y. J. Song, J. Ihm, and Y. Kuk. Conformational molecular switch of the azobenzene molecule: a scanning tunneling microscopy study. *Physical Review Letters*, 96(15):156106, 2006.

[22] M. Alemani, M. V. Peters, S. Hecht, K. -H. Rieder, F. Moresco, and L. Grill. Electric field-induced isomerization of azobenzene by STM. *Journal of the American Chemical Society*, 128(45):14446-14447, 2006.

[23] C. R. Crecca and A. E. Roitberg. Theoretical study of the isomerization mechanism of azobenzene and disubstituted azobenzene derivatives. *Journal of Physical Chemistry A*, 110(26):8188-8203, 2006.

[24] E. W. G. Diau. A new trans-to-cis photoisomerization mechanism of azobenzene on the S_1 (n,π^*) surface. *Journal of Physical Chemistry A*, 108(6):950-956, 2004.

[25] M. L. Tiago, S. Ismail-Beigi, and S. G. Louie. Photoisomerization of azobenzene from first-principles constrained density-functional calculations. *Journal of Chemical Physics*, 122(9):094311, 2005.

[26] G. Binnig, H. Rohrer, Ch. Gerber, and E. Weibel. Surface studies by scanning tunneling microscopy. *Physical Review Letters*, 49(1):57-61, 1982.

[27] R. J. Hammers, R. M. Tromp, and J. E. Demuth. Surface electronic structure of Si(111)-(7×7) resolved in real space. *Physical Review Letters*, 56(18):1972-1975, 1986.

[28] J. A. Stroscio and D. M. Eigler. Atomic and molecular manipulation with the scanning tunneling microscope. *Science*, 254(5036):1319-1326, 1991.

[29] M. F. Crommie, C. P. Lutz, and D. M. Eigler. Confinement of electrons to quantum corrals on a metal surface. *Science*, 262(5131):218-220, 1993.

[30] S.-W. Hla. Scanning tunneling microscopy single atom/molecule manipulation and its application to nanoscience and technology. *Journal of Vacuum Science and Technology B*, 23(4):1351-1360 (2005).

[31] J. Bardeen. Tunneling from a many-particle point of view. *Physics Review Letters*, 6(2):57-59, 1961.

[32] J. Tersoff and D. R. Hamann. Theory and application for the scanning tunneling microscope. *Physical Review Letters*, 50(25):1998-2001, 1983.

[33] J. Tersoff and D. R. Hamann. Theory of the scanning tunneling microscope. *Physical Review B*, 31(2):805-813, 1985.

[34] R. J. Hamers. Atomic-resolution surface spectroscopy with the scanning tunneling microscope. *Annual Review of Physical Chemistry*, 40:531-559, 1989.

[35] Matthew Comstock. *Photomechanical Switching of Individual Molecules on a Surface.* PhD thesis, UC Berkeley, 2008.

[36] K. Besocke. An easily operable scanning tunneling microscope. *Surface Science*, 181(1-2):145-153, 1987.

[37] J. Frohn, J. Wolf, K. Besocke, and M. Teske. Coarse tip distance adjustment and positioner for a scanning tunneling microscope. *Review of Scientific Instruments*, 60(6):1200-1201, 1989.

[38] B. C. Stipe, M. A. Rezaei, and W. Ho. A variable-temperature scanning tunneling microscope capable of single-molecule vibrational spectroscopy. *Review of Scientific Instruments*, 70(1):137-143, 1999.

[39] S. H. Pan, E. W. Hudson, and J. C. Davis. He-3 refrigerator based very low temperature scanning tunneling microscope. *Review of Scientific Instruments*, 70(2):1459-1463, 1999.

[40] T. Yokoyama, S. Yokoyama, T. Kamikado, Y. Okuno, and S. Mashiko. Selective assembly on a surface of supramolecular aggregates with controlled size and shape. *Nature*, 413(6856):619-621, 2001.

[41] J. A. Theobald, N. S. Oxtoby, M. A. Phillips, N. R. Champness, and P. H. Beton. Controlling molecular deposition and layer structure with supramolecular surface assemblies. *Nature*, 424(6952):1029-1031, 2003.

[42] M. Bohringer, K. Morgenstern, W. D. Schneider, R. Berndt, F. Mauri, A. De Vita, and R. Car. Two-dimensional self-assembly of supramolecular clusters and chains. *Physical Review Letters*, 83(2):324-327, 1999.

[43] M. Bohringer, K. Morgenstern, W. D. Schneider, M. Wuhn, C. Woll, and R. Berndt. Self-assembly of 1-nitronaphthalene on Au(111). *Surface Science*, 444(1-3), 199-210, 2000.

[44] S. Berner, M. de Wild, L. Ramoino, S. Ivan, A. Baratoff, H. J. Guntherodt, H. Suzuki, D. Schlettwein, and T. A. Jung. Adsorption and two-dimensional phases of a larg polar molecule: sub-phthalocyanine on Ag(111). *Physical Review B*, 68(11):115427 (2003).

[45] J. V. Barth, J. Weckesser, N. Lin, A. Dmitriev, and K. Kern. Supramolecular architectures and nanostructures at metal surfaces. *Applied Physics A*, 76(5):645-652, 2003.

[46] D. M. Walba, F. Stevens, N. A. Clark, and D. C. Parks. Detecting molecular chirality by scanning tunneling microscopy. *Accounts of Chemical Research*, 29(12):591-597, 1996.

[47] M. Taniguchi, H. Nakagawa, A. Yamagishi, and K. Yamada. Molecular chirality on a solid surface: thiaheterohelicene monolayer on gold imaged by STM. *Surface Science*, 454:1005-1009, 2000.

[48] T. A. Jung, R. R. Schlittler, and J. K. Gimzewski. Conformational identification of individual adsorbed molecules with the STM. *Nature*, 386(6626):696-698, 1997.

[49] F. Moresco, G. Meyer, K. H. Rieder, H. Tang, A. Gourdon, and C. Joachim. Conformational changes of single molecules induced by scanning tunneling microscopy manipulation: a route to molecular switching. *Physical Review Letters*, 86(4):672-675, 2001.

[50] M. Schunack, F. Rosei, Y. Naitoh, P. Jiang, A. Gourdon, E. Laegsgaard, I. Stensgaard, C. Joachim, and F. Besenbacher. Adsorption behavior of Lander molecules on Cu(110) studied by scanning tunneling microscopy. *Journal of Chemical Physics*, 117(13):6259-6265, 2002.

[51] S. M. Nie and S. R. Emery. Probing single molecules and single nanoparticles by surface-enhanced Raman scattering. *Science*, 275(5303):1102-1106, 1997.

[52] G. Hoffmann, L. Libioulle, and R. Berndt. Tunneling-induced luminescence from adsorbed organic molecules with submolecular lateral resolution. *Physical Review B*, 65(21):212107, 2002.

[53] X. H. Qiu, G.V. Nazin, and W. Ho. Vibrationally resolved fluorescence excited with submolecular precision. *Science*, 299(5606):542-546, 2003.

[54] C. Zhang, M.-H. Du, H.-P. Cheng, X.-G. Zhang, A. E. Roitberg, and J. L. Krause. Coherent electron transport through an azobenzene molecule: a light-driven molecular switch. *Physical Review Letters*, 92(15):158301-158304, 2004.

[55] T. Umemoto, K. Ishikawa, H. Takezoe, A. Fukuda, T. Sasaki, and T. Ikeda. Photoisomerization observed by means of scanning tunneling microscopy. *Japanese Journal of Applied Physics, Part 2-Letters*, 32(7A):L936-L939, 1993.

[56] C. L. Feng, Y. J. Zhang, J. Jin, Y. L. Song, L. Y. Xie, G. R. Qu, L. Jiang, and D. B. Zhu. Completely interfacial photoisomerization of 4-hydroxy-3'-trifluoromethylazobenzene studied by STM on HOPG. *Surface Science*, 513(1):111-118, 2002.

[57] S. Yasuda, T. Nakamura, M. Matsumoto, and H. Shigekawa. Phase switching of a single isomeric molecule and associated characteristic rectification. *Journal of the American Chemical Society*, 125(52):16430-16433, 2003.

[58] J. V. Barth, H. Brune, G. Ertl, and R. J. Behm. Scanning tunneling microscopy observations on the reconstructed Au(111) surface - atomic-structure, long-range superstructure, rotational domains, and surface-defects. *Physical Review B*, 42(15):9307-9318, 1990.

[59] C. J. Brown. A refinement of crystal structure of azobenzene. *Acta Crystallographica*, 21:146, 1966.

[60] C. S. Tsai, C. Su, J. K. Wang, and J. C. Lin. STM study of trans-stilbene self-organized on the Ag/Ge(111)-($\sqrt{3} \times \sqrt{3}$)R30 degrees surface. *Langmuir*, 19(3):822-829, 2003.

[61] C. P. Collier, E. W. Wong, M. Belohradsky, F. M. Raymo, J. F. Stoddart, P. J. Kuekes, R. S. Williams, and J. R. Heath. Electronically configurable molecular-based logic gates. *Science*, 285(5426):391-394, 1999.

[62] Z. J. Donhauser, B. A. Mantooth, K. F. Kelly, L. A. Bumm, J. D. Monnell, J. J. Stapleton, D. W. Price, A. M. Rawlett, D. L. Allara, J. M. Tour, and P. S. Weiss. Conductance switching in single molecules through conformational changes. *Science*, 292(5525):2303-2307, 2001.

[63] D. M. Eigler and E. K. Schweizer. Positioning single atoms with a scanning tunneling microscope. *Nature*, 344(6266):524-526, 1990.

[64] W. Chen, T. Jamneala, V. Madhavan, and M. F. Crommie. Disappearance of the Kondo resonance for atomically fabricated cobalt dimers. *Physical Review B*, 60(12):R8529-R8532, 1999.

[65] G. V. Nazin, X. H. Qiu, and W. Ho. Visualization and spectroscopy of a metal-molecule-metal bridge. *Science*, 302(5642):77-81, 2003.

[66] T. A. Jung, R. R. Schlittler, J. K. Gimzewski, H. Tang, and C. Joachim. Controlled room-temperature positioning of individual molecules: molecular flexture and motion. *Science*, 271(5246):181-184, 1996.

[67] C. Loppacher, M. Guggisberg, O. Pfeiffer, E. Meyer, M. Bammerlin, R. Luthi, R. Schlittler, J. K. Gimzewski, H. Tang, and C. Joachim. Direct determination of the energy required to operate a single molecule switch. *Physical Review Letters*, 90(6):066107-066110, 2003.

[68] R. Yamachika, M. Grobis, A. Wachowiak, and M. F. Crommie. Controlled atomic doping of a single C_{60} molecule. *Science*, 304(5668):281-284, 2004.

[69] B. C. Stipe, M. A. Rezaei, and W. Ho. Coupling of vibrational excitation to the rotational motion of a single adsorbed molecule. *Physcal Review Letters*, 81(6):1263-1266, 1998.

[70] Y. Sainoo, Y. Kim, T. Komeda, M. Kawai, and H. Shigekawa. Observation of cis-2-butene molecule on Pd(110) by cryogenic STM: site determination using tunneling-current-induced rotation. *Surface Science Letteers*, 536(1-3):L403-L407, 2003.

[71] P. P. Birnbaum and D. W. G. Style. The photoisomerization of some azobenzene derivatives. *Transactions of the Faraday Society*, 50:1192-1196, 1954.

[72] A. Kirakosian, M. J. Comstock, Jongweon Cho, and M. F. Crommie. Molecular commensurability with a surface reconstruction: STM study of azobenzene on Au(111). *Physical Review B*, 71(11):113409, 2005.

[73] R. M. Silver, E. E. Ehrichs, and A. L. Delozanne. Direct writing of submicron metallic features with a scanning tunneling microscpe. *Applied Physics Letters*, 51(4):247-249, 1987.

[74] U. R. Schoffel, H. Rauscher, and R. J. Behm. Nanostructure formation by localized decomposition of $Mo(CO)_6$ on Si(111)-(7×7) surfaces. *Journal of Applied Physics*, 91(5):2853-2858, 2002.

[75] N. Koumura, R. W. J. Zijlstra, R. A. van Delden, N. Harada, B. L. Feringa. Light-driven monodirectional molecular rotor. *Nature*, 401(6749):152-155, 1999.

[76] G. P. Jiang, J. C. Polanyi, and D. Rogers. Electron and photon irradiation of benzene and chlorobenzene on Si(111)-(7×7). *Surface Science*, 544(2-3):147-161, 2003.

[77] L. Bartels, F. Wang, D. Möller, E. Knoesel, and T. F. Heinz. Real-space observation of molecular motion induced by femtosecond laser pulses. *Science*, 305(5684):648-651, 2004.

[78] C.-S. Tsai, J.-K. Wang, R. T. Skodje, and J.-C. Lin. A single molecule view of bistilbene photoisomerization on a surface using scanning tunneling microscopy. *Journal of the American Chemical Society*, 127(31):10788-10789, 2005.

[79] M. J. Comstock, Jongweon Cho, A. Kirakosian, and M. F. Crommie. Manipulation of azobenzene molecules on Au(111) using scanning tunneling microscopy. *Physical Review B*, 72(15):153414, 2005.

[80] C.-Q. Wu, J.-X. Li, and D.-H. Lee. Switching and nonswitching phases of photomechanical molecules in dissipative environments. *Physical Review Letters*, 99(3):038302, 2007.

[81] N. Pozhidaeva, M. E. Cormier, A. Chaudhari, and G. A. Woolley. Reversible photocontrol of peptide helix content: Adjusting thermal stability of the cis state. *Bioconjugate Chemistry*, 15(6):1297-1303, 2004.

[82] D. Sanchez-Portal, P. Ordejon, E. Artacho, and J. M. Soler. Density-functional method for very large systems with LCAO basis sets. *International Journal of Quantum Chemistry*, 65(5):453-461, 1997.

[83] J. P. Perdew, K. Burke, and M. Ernzerhof. Generalized gradient approximation made simple. *Physical Review Letters*, 77(18):3865-3868, 1996.

[84] S. Hagen, F. Leyssner, D. Nandi, M. Wolf, and P. Tegeder. Reversible switching of tetra-tert-butyl-azobenzene on a Au(111) surface induced by light and thermal activation. *Chemical Physics Letters*, 444(1-3):85-90, 2007.

[85] L. Óvári, M. Wolf, and P. Tegeder. Reversible changes in the vibrational structure of tetra-tert-butyl azobenzene on a Au(111) surface induced by light and thermal activation. *Journal of Physical Chemistry C*, 111(42):15370-15374, 2007.

[86] A. S. Kumar, T. Ye, T. Takami, B. C. Yu, A. K. Flatt, J. M. Tour, and P. S. Weiss. Reversible photo-switching of single azobenzene molecules in controlled nanoscale environments. *Nano Letters*, 8(6):1644-1648, 2008.

[87] P. Heimann and H. Neddermeyer, *Journal of Physics F: Metal Physics*, **7**, L37 (1977).

[88] Y. Hasegawa and Ph. Avouris. Direct observation of standing wave formation at surface steps using scanning tunneling spectroscopy. *Physical Review Letters*, 71(7):1071-1074, 1993.

[89] W. Chen, V. Madhavan, T. Jamneala, and M. F. Crommie. Scanning tunneling microscopy observation of an electronic supperlattice at the surface of clean gold. *Physical Review Letters*, 80(7):1469-1472, 1998.

[90] S. D. Kevan and R. H. Gaylord. High-resoultion photoemission study of the electronic structure of the noble-metal (111) surfaces. *Physical Review B*, 36(11):5809-5818, 1987.

[91] K. G. Kornev and D. J. Srolovitz. Surface stress-driven instabilities of a free film. *Applied Physics Letters*, 85(13):2487-2489, 2004.

[92] M. A. Grienfeld, *Soviet Physicsr-Doklady*, **31**, 831 (1986).

[93] R. J. Asaro and W. A. Tiller. Interface morphology development during stress-corrosion cracking .1. via surface diffusion. *Metallurgical and Materials Transactions B*, 3(7):1789, 1972.

[94] B. J. Spencer, P. W. Voorhees, and S. H. Davis. *Journal of Applied Physics*, 73(10):4955-4970, 1993.

[95] C. Zhang, Y. He, H. -P. Cheng, Y. Xue, M. A. Ratner, X. G. Zhang, and P. Krstic. Current-voltage characteristics through a single light-sensitive molecule. *Physical Review B*, 73(12):125445, 2006.

[96] T. Fujino, S. Y. Arzhantsev, and T. Tahara. Femtosecond time-resolved fluorescence study of photoisomerization of trans-azobenzene. *Journal of Physical Chemistry A*, 105(35):8123-8129, 2001.

[97] C. W. Chang, Y. C. Lu, T. T. Wang, and E. W. G. Diau. Photoisomerization dynamics of azobenzene in solution with S_1 excitation: a femtosecond fluorescence anisotropy study. *Journal of the American Chemical Society*, 126(32):10109-10118, 2004.

[98] I. K. Lednev, T. -Q. Ye, L. C. Abbott, R. E. Hester, and J. N. Moore. Photoisomerization of a capped azobenzene in solution probed by ultrafast time-resolved electronic absorption spectroscopy. *Journal of Physical Chemistry A*, 102(46):9161, 1998.

[99] C. M. Stuart, R. R. Frontiera, and R. A. Mathies. Excited-state structure and dynamics of cis- and trans-azobenzene from resonance Raman intensity analysis. *Journal of Physical Chemistry A*, 111(48):12072-12080, 2007.

[100] S. M. Barlow and R. Raval. Complex oragnic molecules at metal surfaces: bonding, organization and chirality. *Surface Science Reports*, 50(6-8):201-341, 2003.

[101] C. J. Eckhardt, N. M. Peachey, D. R. Swanson, J. M. Takacs, M. A. Khan, X. Gong, J. H. Kim, J. Wang, and R. A. Uphaus. Separation of chiral phases in monolayer crystals of racemic amphiphiles. *Nature*, 362(6421):614-616, 1993.

[102] G. P. Lopinski, D. J. Moffatt, D. D. Wayner, and R. A. Wolkow. Determination of the absolute chirality of individual adsorbed molecules using the scanning tunneling microscope. *Nature*, 392(6679):909-911, 1998.

[103] K. -H. Ernst. Supramolecular surface chirality. *Topics in Current Chemistry*, 265:209-252, 2006.

[104] M. Alemani, S. Selvanathan, F. Ample, M. V. Peters, K. -H. Rieder, F. Moresco, C. Joachim, S. Hecht, and L. Grill. Adsorption and switching properties of azobenzene derivatives on different noble metal surfaces: Au(111), Cu(111), and Au(100). *Journal of Physical Chemistry C*, 112(28):10509-10514, 2008.

[105] C. Dri, M. V. Peters, J. Schwarz, S. Hecht, and L. Grill. Spatial periodicity in molecular switching. *Nature Nanotechnology*, 3(11):649-653, 2008.

[106] H. Rau and E. Luddecke. On the rotation-inversion controversy on photoisomerization of azobenzene - experimental proof of inversion. *Journal of the American Chemical Society*, 104(6):1616-1620, 1982.

[107] M. J. Comstock, N. Levy, A. Kirakosian, Jongweon Cho, F. Lauterwasser, J. H. Harvey, D. A. Strubbe, J. M. J. Fréchet, D. Trauner, S. G. Louie, and M. F. Crommie. Reversible photomechanical switching of individual engineered molecules at a metallic surface. *Physical Review Letters*, 99(3):038301, 2007.

[108] M. J. Comstock, N. Levy, Jongweon Cho, L. Berbil-Bautista, M. F. Crommie,D. A. Poulsen, and J. M. J. Fréchet. Measuring reversible photomechanical switching rates for a molecule at at surface. *Applied Physics Letters*, 92(12):123107, 2008.

[109] M. A. Reed, C. Zhou, C. J. Muller, T. P. Burgin, and J. M. Tour. Conductance of a molecular junction. *Science*, 278(5336):252-254, 1997.

[110] B. Xu and N. J. Tao. Measurement of single-molecule resistance by repeated formation of molecular junctions. *Science*, 301(5637):1221-1223, 2003.

[111] C. P. Collier, G. Mattersteig, E. W. Wong, Y. Luo, K. Beverly, J. Sampaio, F. M. Raymo, J. F. Stoddart, and J. R. Heath. A [2]catenane-based solid state electronically reconfigurable switch. *Science*, 289(5482):1172-1175, 2000.

[112] A. E. Baber, H. L. Tierney, and E. C. H. Sykes. A quantitative single-molecule study of thioether molecular rotors. *ACS Nano*, 2(11):2385-2391, 2008.

[113] Y. S. Obeng, M. E. Laing, A. C. Friedli, H. C. Yang, D. N. Wang, E. W. Thulstrup, A. J. Bard, and J. Michl. Self-assembled monolayers of parent and derivatized [N]Staffane-3,3(N-1)- dithiols on polycrystalline gold electrondes. *Journal of the American Chemical Society*, 114(25):9943-9952, 1992.

[114] J. C. Love, L. A. Estroff, J. K. Kriebel, R. G. Nuzzo, and G. M. Whitesides. Self-assembled monolayers of thiolates on metals as a form of nanotechnology. *Chemical Reviews*, 105(4):1103-1169, 2005.

[115] A. Ulman, *An Introduction to Ultrathin Organic Films: From Langmuir-Blodgett to Self-Assembly*, Academic, New York, 1991.

[116] W. P. Fitts, J. M. White, and G. E. Poirier. Low-coverage decanethiolate structure on Au(111): substrate effects. *Langmuir*, 18(5):1561-1566, 2002.

[117] P. Maksymovych, D. C. Sorescu, and J. T. Yates. Gold-adatom-mediated bonding in self-assembled short-chain alkanethiolate species on the Au(111) surface. *Physical Review Letters*, 97(14):146103, 2006.

[118] K. L. Wong, K. Y. Kwon, and L. Bartels. Surface dynamics of benzenethiol molecules on Cu(111). *Applied Physics Letters*, 88(18):183106, 2006.

[119] J. K. Gimzewski, C. Joachim, R. R. Schlittler, V. Langlais, H. Tang, and I. Johannsen. Rotation of a single molecule within a supramolecular bearing. *Science*, 281(5376):531-533, 1998.

[120] H. Grönbeck, A. Curioni, and W. Andreoni. Thiols and disulfides on the Au(111) surface: the headgroup-gold interaction. *Journal of the American Chemical Society*, 122(16):3839-3842, 2000.

[121] E. A. Meyer, R. K. Castellano, and F. Diederich. Interactions with aromatic rings in chemical and biological recognition. *Angewandte Chemie-International Edition*, 42(11):1210-1250, 2003.

[122] B. C. Stipe, M. A. Rezaei, and W. Ho. Inducing and viewing the rotational motion of a single molecule. *Science*, 279(5358):1907-1909, 1998.

[123] P. Maksymovych, D. C. Sorescu, D. Dougherty, and J. T. Yates. Surface bonding and dynamical behavior of the CH_3SH molecule on Au(111). *Journal of Physical Chemistry B*, 109(47):22463-22468, 2005.

[124] L. Gao, Q. Liu, Y. Y. Zhang, N. Jiang, H. G. Zhang, Z. H. Cheng, W. F. Qiu, S. X. Du, Y. Q. Liu, W. A. Hofer, and H.-J. Gao. Constructing an array of anchored single-molecule rotors on gold surfaces. *Physical Review Letters*, 101(19):197209, 2008.

[125] B. V. Rao, K. Y. Kwon, A. W. Liu, and L. Bartels. 2,5-dichlorothiophenol on Cu(111): initial adsorption site and scanning tunneling microscope-based abstraction of hydrogen at high intramolecular sensitivity. *Journal of Chemical Physics*, 119(20):10879-10884, 2003.

[126] L. J. Lauhon and W. Ho. Single molecule thermal rotation and diffusion: acetylene on Cu(001). *Journal of Chemical Physics*, 111(13):5633-5636, 1999.

[127] Jongweon Cho, N. Levy, A. Kirakosian, M. J. Comstock, F. Lauterwasser, J. M. Fréchet, and M. F. Crommie. Surface anchoring and dynamics of thiolated azobenzene molecules on Au(111). *Journal of Chemical Physics*, 131(3):034707, 2009.

[128] J. Henzl, T. Bredow, and K. Morgenstern. Irreversible isomerization of the azobenzene derivate Methyl Orange on Au(111). *Chemical Physics Letters*, 435(4-6):278-282, 2007.

[129] S. Selvanathan, M. V. Peters, J. Schwarz, S. Hecht, and L. Grill. Formation and manipulation of discrete supramolecular azobenzene assemblies. *Applied Physics A*, 93(2):247-252, 2008.

[130] N. Henningsen, R. Rurali, K. J. Franke, I. Fernández-Torrente, and J. I. Pascual, Trans to cis isomerization of an azobenzene derivative on a Cu(100) surface. *Applied Physics A*, 93(2):241-246, 2008.

[131] S. Wagner, F. Leyssner, C. Kördel, S. Zarwell, R. Schmidt, M. Weinelt, K. Rück-Braun, M. Wolf, and P. Tegeder. Reversible photosiomerization of an azobenzene-functionalized self-assembled monolayer probed by sum-frequency generation vibrational spectroscopy. *Physical Chemistry Chemical Physics*, 11:6242-6248, 2009.

[132] J. Henzl, M. Mehlhorn, and K. Morgenstern. Amino-nitro-azobenzene dimers as a prototype for a molecular-level machine. *Nanotechnology*, 18:495502, 2007.

[133] N. Henningsen, K. J. Franke, G. Schulze, I. Fernández-Torrente, B. Priewisch, K. Rück-Braun, and J. I. Pascual. Active intramolecular conformational dynamics controlling the assembly of azobenzene derivatives at surfaces. *ChemPhysChem*, 9(1):71-73, 2008.

[134] J.-M. Lehn. Toward Self-Organization and Complex Matter. *Science*, 295(5564):2400-2403, 2002.

[135] J. V. Barth, J. Weckesser, C. Cai, P. Günter, L. Bürgi, O. Jeandupeux, and K. Kern. Building supramolecular nanostructures at surfaces by hydrogen bonding. *Angewandte Chemie-International Edition*, 39(7):1230-1234, 2000.

[136] L. Grill, M. Dyer, L. Lafferent, M. Persson, M. V. Peters, and S. Hecht. Nano-architectures by covalent assembly of molecular building blocks. *Nature Nanotechnology*, 2(11):687-691, 2007.

[137] Y. Wang, X. Ge, G. Schull, R. Berndt, C. Bornholdt, F. Koehler, and R. Herges. Azo supramolecules on Au(111) with controlled size and shape. *Journal of the American Chemical Society*, 130(13):4218-4219, 2008.

[138] R. M. Feenstra, G. Meyer, F. Morescro, and K. H. Rieder. Low-temperature scanning tunneling spectroscopy of n-type GaAs(110) surfaces. *Physical Review B*, 66(16):165204, 2002.

[139] P. Ebert. Nano-scale properties of defects in compound semiconductor surfaces. *Surface Science Reports*, 33(4-8):121-303, 1999.

[140] D. Kitchen, A. Richardella, J. M. Tang, M. E. Flatte, and A. Yazdani. Atom-by-atom substitution of Mn in GaAs and visualization of their hole-mediated interactions. *Nature*, 442(7101):436-439, 2006.

[141] Y. Z. Li, J. C. Patrin, M. Chander, J. H. Weaver, L. P. F. Chibante, and R. E. Smalley. Ordered overlayers of C_{60} on GaAs(110) studied with scanning tunneling microscopy. *Science*, 252(5005):547-548, 1991.

[142] Y. Z. Li, M. Chander, J. C. Patrin, J. H. Weaver, L. P. F. Chibante, and R. E. Smalley. Order and disorder in C_{60} and K_xC_{60} multilayers: direct imaging with scanning tunneling microscopy. *Science*, 253(5018):429-433, 1991.

[143] R. M. Feenstra, J. A. Stroscio, J. Tersoff, and A. P. Fein. Atom-Selective Imaging of the GaAs(110) Surface. *Physical Review Letters*, 58(12):1192-1195, 1987.